

EFFECT OF ORGANOMETALLIC CATALYSTS ON COAL LIQUEFACTION AND PRODUCT DISTRIBUTION

Ram K. Sharma and Gary Moffett

Department of Physical Sciences, Eastern New Mexico University,
Portales, New Mexico 88130

INTRODUCTION

Coal hydrogenation remains an attractive and potentially useful source of liquid fuels. There have been a number of studies on the comparative effectiveness of various catalysts and the results have been reviewed from time to time (1-5). A significant finding which has emerged from such studies is the importance of catalyst distribution. For example, in the hydrogenation of Rock Springs coal, nickelous chloride was found to be an ineffective catalyst when added as a powder, however, it was quite effective when it was impregnated on coal (6).

Because of their compatibility with the pasting oil which is used to slurry coal in hydrogenation studies, organometallic compounds would seem to be able to disperse better and therefore might be expected to be more effective catalysts.

Coal can be regarded as a highly cross linked "polymer" in which condensed aromatic rings are linked to one another through hydroaromatic or heteroatom linkages (7,8). On heating, weak bonds break leading to free radicals which can be stabilized by transfer of hydrogen to give soluble products or they may recombine to form insoluble chars (9). The hydrogen which is transferred to the radical could come from coal itself, donor solvent or molecular hydrogen. It is possible that some organometallics might be able to generate an intermediate under liquefaction conditions which might be an effective hydrogen transfer agent (10).

A few reports on the use of organometallics in coal liquefaction have been published. It appears that at temperatures less than 350°C such catalysts are ineffective (11). However, at higher temperatures some organometallics were found to aid coal liquefaction (12). Metal naphthenates of molybdenum, nickel, tin, iron and cobalt produced conversions exceeding 80 percent at 500°C, zero time at temperature (4).

In the present study we have assayed the catalytic activity of a variety of organometallic compounds in the liquefaction of two New Mexico coals. We have also examined their effect on the proportion of asphaltene and oil produced.

EXPERIMENTAL

Parr 4022 pressure reactor with 1 liter T316 stainless steel bomb, 2250 watt heater and 0-600°C automatic temperature controller was used in all hydrogenation experiments. In order to avoid catalyst memory effects, the reactants were placed in a glass vessel (liner) which fitted snugly inside the bomb.

A sub-bituminous coal from Navajo Mine (South Barber Seam 8) and a bituminous high volatile coal from York Canyon seam in Raton Formation were used in our studies. Ultimate analysis of the coals is given in Table 1.

Into the glass container 15g of -60 mesh coal, catalyst (1% of maf coal) and 45g tetrahydronaphthalene (THN) were placed. The container was put in the steel bomb and the bomb was pressurized with hydrogen to 1500 psi after flushing to remove air. It was then heated to the designated temperature and kept at that temperature for the selected reaction time. The reactants were kept mixed by the rocking motion of the pressure reactor. After the reaction, the bomb was cooled to room temperature and contents flushed with benzene and filtered. The filter-cake was extracted in a soxhlet extractor for 24 hours, dried and weighed to obtain the weight of unreacted coal and ash. After distilling off benzene from the filtrate and the soxhlet extract, pentane was added to precipitate asphaltene which was filtered and dried to a constant weight at 50°C at 3mm in a vacuum oven.

After distilling pentane from the filtrate through a vigreux column, as much of THN as possible was removed by distillation under vacuum (16mm) and an oil bath temperature of 120°C. A weighed amount of methyl naphthalene (MNI) was added to the residue which was thinned with chloroform and analyzed by gas liquid chromatography.

From the areas of the peaks of THN and MN the amount of THN present was calculated using a correction factor determined previously from a mixture of known amounts of THN and MN. Difference in the weight of the vacuum distillation residue and the amount of THN gave the amount of oil present.

The results were calculated as follows:

Percent Conversion = (maf coal - unreacted coal) X 100 / maf coal

Percent yield asphaltene = wt. of asphaltene X 100 / coal converted

Percent yield oil = wt. of oil X 100 / coal converted

Percent conversion asphaltene = wt. of asphaltene X 100 / maf coal originally present

Percent conversion oil = wt. of oil X 100 / maf coal originally present

RESULTS AND DISCUSSION

Effect of Catalysts on Coal Conversion: For the Navajo Mine coal (Table 2) organometallic compounds of palladium, rhenium, iridium, molybdenum, rhodium, iron, cobalt, tin and nickel were found to be effective catalysts. Organometallic compounds of germanium, tungsten, gallium, arsenic had moderate catalytic activity whereas the organometallic compounds of copper, lead, zinc and manganese had marginal or no catalytic activity.

For the York Canyon Mine coal (Table 3) organometallic compounds of iridium, rhodium, molybdenum and nickel showed good catalytic activity. Organometallic compounds of germanium, nickel, gallium and antimony were found to be moderately active whereas compounds of arsenic, copper, lead, manganese, chromium and zinc had no or marginal catalytic activity.

Of the other catalysts tested, stannous chloride was found to be an excellent catalyst in agreement with other reports in literature and was used as a standard of comparison. Ammonium molybdate on the other hand was found to have marginal catalytic activity.

Effect of Catalysts on Product Distribution: Hydroliquefaction of coal is the net result of a complex series of parallel or sequential reactions including hydrogenation, thermal fragmentation, disproportionation and stabilization of free radicals etc. It was thought that different catalysts would affect many of the above reactions to varying degrees and thus change the proportion of asphaltene, oil and gas produced.

In our experiments the product of liquefaction was partitioned into asphaltene and oil and the amount of each was determined by the procedures described in the experimental section. Percent of the product found as asphaltene and oil are shown in Table 4.

In uncatalyzed hydrogenation of York Canyon Mine coal the ratio of asphaltene to oil produced is 1.7 whereas for most of the active catalysts the ratio is 1.8-2.5. Thus many of the catalysts produce slightly more asphaltene than the uncatalyzed hydrogenation. Also the sum of asphaltene and oil yield is nearly 100 percent. This indicates that very little gaseous products are formed in hydrogenations at 380°C for 6 hours.

These results can be accommodated in the free radical mechanism of coal liquefaction. At high temperature coal substance fragments into free radicals which are stabilized by transfer of hydrogen to yield asphaltene, oil and gaseous products. In the absence of a catalyst some of these radicals may combine to produce insoluble char. In the presence of a catalyst, more of these radicals are stabilized by hydrogen transfer to produce soluble products.

Effect of Reaction Time and Temperature: York Canyon Mine coal was hydrogenated for various lengths of time in the absence and also in the presence of molybdenum hexacarbonyl as a catalyst. The results show (Fig. 1) that the amount of asphaltene increases, reaches a maximum and then decreases with time. The increase in asphaltene in the initial stages of the reaction and its decrease in the later stages is faster in the catalyzed than in the uncatalyzed hydrogenation. Thus a catalyst not only helps to liquefy coal, it also helps to convert asphaltene into oil.

Paralleling above results, the amount of oil produced (Fig. 1) also increases with time and the increase is faster in the presence of a catalyst than in its absence.

The effect of temperature on the product distribution in some catalyzed and

uncatalyzed hydrogenations is shown in Fig. 2. As noted before, more asphaltene is produced in the early stages of the reaction in the catalyzed than in the uncatalyzed process. In the later stages of the reaction asphaltene is converted faster into oil and gaseous products in the catalyzed than in the uncatalyzed reactions. Molybdenum hexacarbonyl appears to be a better catalyst in this respect than stannous chloride.

The sum of the percent of product found to be asphaltene and oil (Table 5) decreases with time and with increase in temperature. This indicates that asphaltene and oil are being converted into gaseous products at higher temperatures and longer reaction times. Comparison of the catalyzed with the uncatalyzed hydrogenations shows that more gaseous products are formed in the former than in the latter case, and again molybdenum hexacarbonyl is more effective in this respect than stannous chloride.

ACKNOWLEDGEMENT

We are grateful for the support of this work from the New Mexico Energy and Minerals Department and the New Mexico Energy Institute at The University of New Mexico.

REFERENCES

1. T.E. Warren, K.W. Bowles and R.E. Gilmore, *Ind. Eng. Chem., Anal. Ed.* 11, 415 (1939).
2. S. Weller, M.G. Pelipetz, S. Friedman and H.H. Storch, *Ind. Eng. Chem.*, 42, 330 (1950).
3. S. Weller, In "Catalysis"; Emmet, P.H., Ed.; Reinhold Publishing Corporation, New York, 1956; Vol. IV, Chapter 7.
4. C.O. Hawk and R.W. Hiteshue, *U.S. Bur. Mines. Bull.* 622 (1965).
5. W.R.K. Wu and H.H. Storch, *U.S. Bur. Mines. Bull.* 633 (1968).
6. S. Weller and M.G. Pelipetz, *Ind. Eng. Chem.*, 43, 1243 (1951).
7. P.H. Given, *Fuel*, 31, 147 (1960).
8. D.D. Whitehurst, T.O. Mitchell and M. Farcasiu, "Coal Liquefaction", Academic Press, New York, 1980, p. 20.
9. W.H. Wiser, G.R. Hill and N.J. Kertamus, *Ind. Eng. Chem., Process, Design and Development*, 6, 133 (1967).
10. S. Friedman, S. Metlin, A. Svedi, and I. Wender, *J. Org. Chem.*, 24, 1287 (1959).
11. N. Holy, T. Nalesnik and S. McClanahan, *Fuel*, 56, 47 (1977).
12. M.V. McCabe and M. Orchin, *Fuel*, 55, 266 (1976).

TABLE 1 Ultimate Analysis of Coals
Navajo Mine (South Barber Seam #) Coal

	wt%
Moisture	8.62
Carbon	57.00
Hydrogen	3.07
Nitrogen	1.17
Sulfur	0.74
Ash	15.77
Oxygen (diff.)	<u>13.65</u>
	100.00

York Canyon Mine Coal

	wt%
Moisture	1.57
Carbon	63.89
Hydrogen	4.42
Nitrogen	1.35
Sulfur	0.44
Ash	22.30
Oxygen (diff.)	<u>6.05</u>
	100.00

TABLE 2 Effectiveness of Catalysts in the Hydrogenation of Navajo Mine Coal
Hydrogen pressure initial (cold): 1500 psi; Catalyst: 1% maf coal;
Time: 6 hours; Solvent: Tetrahydronaphthalene; Temperature: 350°C.

No. Catalyst	Percent Conversion
1. None	61
2. $(C_2H_5)_2Ni$	68
3. $Co(C_2H_5O)_2$	74
4. $CoCl_2 \cdot 6H_2O$	73
5. $Cu(C_2H_5O)_2$	67
6. $Fe(C_2H_5O)_2$	75
7. $FeCl_3 \cdot 6H_2O$	67
8. $Ga(C_2H_5O)_2$	69
9. $(C_2H_5)_2Fe$	69
10. $[Ir(CO)_2Cl]_x$	83
11. $Mn(C_2H_5O)_2$	63
12. $Mo(CO)_6$	79
13. $(Ni)_6O_{10} \cdot 2H_2O$	66
14. $Ni(C_2H_5O)_2$	73
15. $NiCl_2 \cdot 6H_2O$	67
16. $Pb(C_2H_5O)_2$	66
17. $(C_2H_5)_4Pb$	63
18. $Pd(C_2H_5O)_2$	84
19. $Re_2(CO)_{10}$	84
20. $Rh(C_2H_5O)_2$	82
21. $SnCl_2 \cdot 2H_2O$	75
22. $(C_2H_5)_2Sn$	73
23. $(C_2H_5)_3SnH$	67
24. $W(CO)_6$	68
25. $Zn(C_2H_5O)_2$	64
26. $ZnCl_2$	65

TABLE 3 Effectiveness of Catalysts in the Hydrogenation of York Canyon Mine Coal

Hydrogen pressure initial: 1500 psi; Catalyst: 1% maf coal; Solvent: Tetrahydrofuran; Temperature: 350°C; Time: 6 hours

No.	Catalyst	Percent Conversion
1.	None	44
2.	$\text{SnCl}_2 \cdot 2\text{H}_2\text{O}$	72
3.	$(\text{C}_6\text{H}_5)_3\text{As}$	53
4.	$\text{Co}(\text{C}_5\text{H}_5)_2$	63
5.	$\text{Co}_2(\text{CO})_8$	74
6.	$\text{Cu}(\text{C}_6\text{H}_5)_2(\text{C}_6\text{H}_5\text{COO})_2$	53
7.	$\text{Cr}(\text{C}_6\text{H}_5)_2\text{O}_2$	47
8.	$\text{Cr}(\text{CO})_6$	48
9.	$\text{Fe}(\text{C}_5\text{H}_5)_2$	54
10.	$\text{Fe}(\text{C}_5\text{H}_5)_2 \cdot \text{I}_2 \cdot \text{I}_2(0.5\%)$	76
11.	$\text{Fe}(\text{CO})_5$	58
12.	$\text{Ga}(\text{C}_5\text{H}_5)_2$	61
13.	$\text{Ge}(\text{C}_6\text{H}_5)_4$	64
14.	$\text{I}_2(0.5\%)$	72
15.	$\text{In}(\text{C}_5\text{H}_5)_2$	59
16.	$\text{Ir}(\text{CO})_3\text{Cl}$	77
17.	$\text{Mn}(\text{C}_6\text{H}_5)(\text{C}_6\text{H}_5\text{COO})_2$	47
18.	$\text{Ni}_2\text{Nb}_2\text{O}_7 \cdot 2\text{H}_2\text{O}$	46
19.	$\text{Mo}(\text{CO})_6$	73
20.	$\text{Mo}(\text{CO})_6 \cdot \text{I}_2(0.5\%)$	80
21.	$\text{Ni}(\text{C}_6\text{H}_5)_2\text{O}_2$	67
22.	$\text{Pd}(\text{C}_6\text{H}_5)_2(\text{COO})_2$	49
23.	$\text{Pd}(\text{C}_5\text{H}_5)_2$	72
24.	$\text{Re}_2(\text{CO})_{10}$	74
25.	$\text{Rh}(\text{C}_5\text{H}_5)_2$	75
26.	$\text{Ru}_3(\text{CO})_{12}$	46
27.	$\text{Sb}(\text{C}_6\text{H}_5)_3$	58
28.	$\text{Sn}(\text{C}_6\text{H}_5)_4$	74
29.	$\text{W}(\text{CO})_6$	43
30.	$\text{Zn}(\text{C}_6\text{H}_5)_2$	43

TABLE 4 Effect of Catalysts on the Percent Yield of Asphaltene and Oil from York Canyon Mine Coal.

No.	Catalyst	%Conversion	%Yield Asph.	%Yield Oil	%Yield Asph-Oil	%Asph. Oil
1.	None	48	64	58	102	1.7
2.	$\text{Co}_2(\text{CO})_8$	74	69	29	98	2.4
3.	$\text{Cr}(\text{C}_6\text{H}_5)_2\text{O}_2$	50	41	59*	---	0.7
4.	$\text{Fe}(\text{C}_6\text{H}_5)_2\text{O}_2$	48	66	53	99	2.0
5.	$\text{Fe}(\text{C}_6\text{H}_5)_2\text{O}_2 \cdot \text{I}_2(0.5\%)$	76	65	36	101	1.8
6.	$\text{Ga}(\text{C}_5\text{H}_5)_2$	61	70	36	106	1.9
7.	I_2	72	61	41	102	1.5
8.	$\text{In}(\text{C}_5\text{H}_5)_2$	59	31	68*	---	0.4
9.	$\text{Ir}(\text{CO})_3\text{Cl}$	77	65	34	99	1.9
10.	$\text{Mo}(\text{CO})_6$	75	68	32*	---	2.1
11.	$\text{Mo}(\text{CO})_6 \cdot \text{I}_2(0.5\%)$	80	71	32	103	2.2
12.	$\text{Ni}(\text{C}_6\text{H}_5)_2\text{O}_2$	64	73	29	102	2.5
13.	$\text{Pd}(\text{C}_6\text{H}_5)_2$	73	61	36	97	1.7
14.	$\text{Re}_2(\text{CO})_{10}$	73	64	36	100	1.8
15.	$\text{Rh}(\text{C}_5\text{H}_5)_2$	75	46	54*	---	0.9
16.	$\text{Ru}_3(\text{CO})_{12}$	75	61	37	98	1.6
17.	$\text{SnCl}_2 \cdot 2\text{H}_2\text{O}$	73	72	30	102	2.4

* values of percent yield oil were obtained as follows:
 $100 - \% \text{ yield asphaltene} = \% \text{ yield oil}$

TABLE 5 Effect of Time and Temperature on the Sum of the Percent Yield of Oil and Asphaltene in the Hydrogenation of York Canyon Mine Coal.

Temp., °C	PERCENT YIELD (OIL + ASPHALTENE)	
	None	$\text{Mo}(\text{CO})_6$
350-400 hr	580-600	580-600
400-450 hr	580-600	580-600
450-500 hr	580-600	580-600
500-550 hr	580-600	580-600
550-600 hr	580-600	580-600
Time hr		
1	- 100-110	- 95-97
6	102-91-89	100-91-85
24	92-86-78	90-78-59

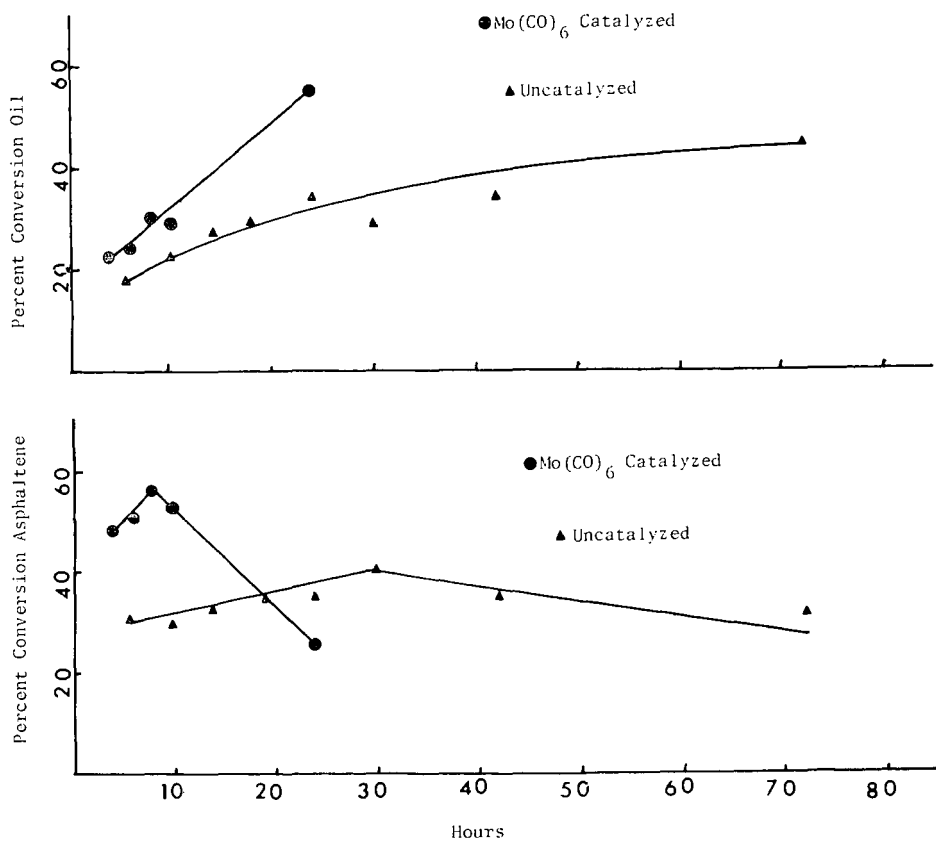


Fig. 1 Percent Conversion Asphaltene and Oil in the Hydrogenation of York Canyon Mine Coal.

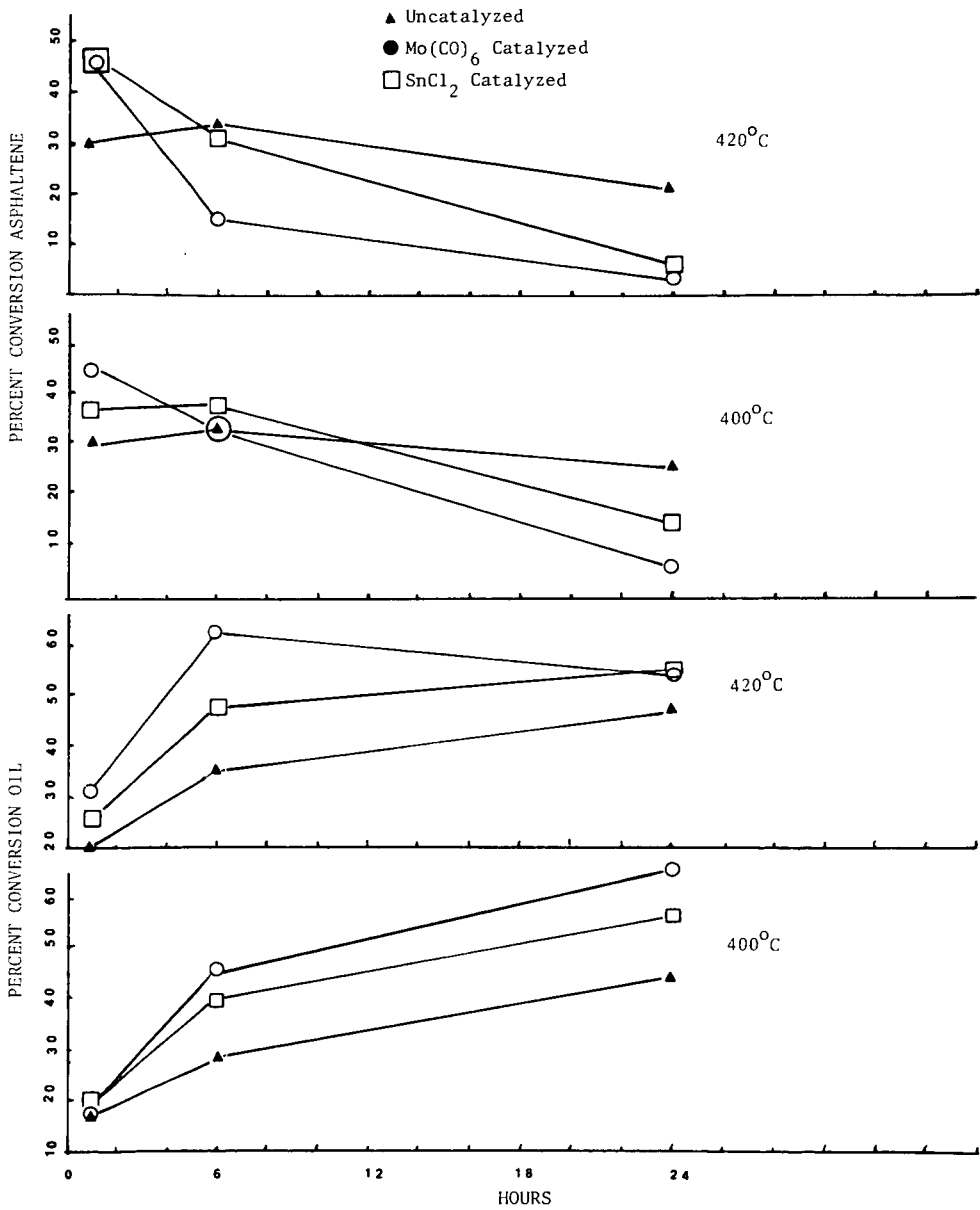


Fig. 2 Effect of Temperature and Reaction Time on the Percent Conversion Oil and Asphaltene.

SRC II PROCESSING OF WESTERN COALS WITH ADDED PYRITE

B. F. Alexander and R. P. Anderson

The Pittsburg & Midway Coal Mining Co.
P. O. Box 2970
Shawnee Mission, KS 66201

I. INTRODUCTION

A. History of the P&M Merriam Laboratory in Coal Liquefaction

The P&M Merriam Laboratory began a bench scale investigation of solvent refining of coal in 1962. Early work was to verify design concepts and operability for a one ton per day process development unit (PDU) in Kansas City which was built during 1963 and operated during much of 1964⁽¹⁾.

In 1967, bench scale studies resumed at Merriam, primarily to support the design effort for the 50 ton per day pilot plant at Ft. Lewis, Washington which operated from 1974 until 1981. Work has continued on a large variety of coal liquefaction problems since 1967 under sponsorship of the Office of Coal Research, Energy Research and Development Administration and the Department of Energy⁽²⁾.

B. Current Activities

The experiments described in this paper were conducted at the Merriam Laboratory during 1980 and 81. They were begun under DOE Contract 79ET14800 during a study on the relationship between coal properties and liquefaction behavior. Additional work was carried out during the current contract (81PC40005) to investigate SRC processing characteristics with disposable catalysts using alternate coals from different regions.

C. Previous Work

Earlier studies had shown subbituminous coals to be of low reactivity in SRC processes (3,4,5). The low reactivity of these coals was believed to be due primarily to a lack of iron to act as an in-situ catalyst. This was verified in the current work for a variety of coals from the Rocky Mountain and Great Plains Provinces where operation without added catalyst was not possible at normal SRC II conditions. Addition of moderate amounts of pyrite (4-5 wt % FeS₂, based on coal) resulted in trouble free operation, however, and attractive yields of high quality oils.

D. Factors Affecting the Results

The specific yields and product quality obtained in these experiments depended on the coal, source and level of pyrite added and on liquefaction conditions. Each of these factors will be discussed below.

II. EXPERIMENTAL

A. Bench Scale Unit

All of the experiments were conducted at Merriam using the bench scale unit depicted in Figure 1. This unit has been in operation since 1978 and allows for recycle of solid and liquid phases⁽⁶⁾. It has produced results which match closely those obtained in larger scale operations.

Coal was mixed with recycled solvent and recycled unfiltered coal solution and charged at 1800 or 2250 psig with a Hills-McCanna pump. Pure hydrogen was added at

the base of the preheater. The slurry passed through a 310 cm³ preheater, where the temperature was raised to 400°C, and 1 liter dissolver. The dissolver was housed in a 6-zone air furnace which allowed close temperature control and either an isothermal (at 450°C and 465°C) or simulated adiabatic (457°C average) profile. The dissolver effluent was separated into five streams by a system of four equilibrium flash vessels operated at reactor pressure as well as an atmospheric flash and distillation column.

B. Run Conditions

The conditions used in these runs are shown in Table I. This rather generous pressure of 2250 psig, used in all of the runs except one, was chosen initially to allow operation with a wide variety of coals. The runs with added pyrite were continued until steady state was achieved. The runs without added pyrite were conducted by lining out first with pyrite in the feed and then dropping pyrite out. Yields were determined at the point at which operation could no longer be sustained.

The coals used in this series of experiments are listed in Table II. Two were subbituminous, one high volatile C bituminous and two borderline between these two classifications. A low-iron Pittsburgh seam coal is included for comparison.

Four different pyrites were used with the properties shown in Table III. The Matheson, Coleman & Bell pyrites were mined in Georgia as a discrete mineral. They were ball milled and passed through a 140 mesh screen before use. The Robena pyrites were obtained from the coal cleaning operation of the U. S. Steel Robena Mine, Green County, Pennsylvania. They were finely ground by The Jet Pulverizer Company, Palmyra, New Jersey.

III. RESULTS

A. Effect of Coal Source

1. Sensitivity of Various Coals to Pyrite Addition

The primary difference in the SRC II processing of western coals with and without pyrite is that with pyrite they can be run, without pyrite they can not! Beyond that, there are dramatic changes in the yield patterns, as shown in Table IV. The changes shown are minimum values computed at the time when operation could no longer be sustained without additive. If the runs without additive could be lined out, the differences would be even greater.

With the western coals, total oil yield was 15 to 22 wt % (based on MAF coal) higher when pyrite was added and SRC yield from 9 to 12 wt % lower, with Belle Ayr Mine coal being the most responsive. For two of the coals, IOM yield decreased (total conversion increased) by 6 wt % and for Belle Ayr by 12 wt %. There were small variations in hydrocarbon gas yields, with two higher and two lower with additive. Hydrogen consumption increased by varied amounts.

The Blacksville No. 2 coal, a relatively low iron, low reactivity eastern bituminous coal, is included for comparison. The response in total oil, SRC and IOM yields to pyrite addition was about an order of magnitude less than with the western coals.

With Kaiparowits coal, a higher hydrogen level (8.6 vs 7.8 wt %) was achieved in the heavy distillate (>288°C) from the catalyzed run. With McKinley and Edna coals, however, the hydrogen levels actually decreased when catalyst was added, due to the large increase in conversion of material into the upper end of the heavy distillate boiling range. With all the western coals, the fusion point of the distillation residue was significantly lower with added pyrite and its solubilities in hexane and toluene considerably higher (lower preasphaltene content).

There were essentially no differences in elemental analyses for any of the products from the Blacksville No. 2 coal runs made with or without added pyrite.

2. Comparison of Coals with Added Pyrite

The yields and hydrogen consumptions resulting from the SRC II processing of five different coals at 450°C average dissolver temperature, 2250 psig and 1.0 hour residence time with added pyrite are compared in Table V.

The western coals yielded 49-57 wt % total oil (MAF coal basis) compared to approximately 44 wt % with Powhatan coals (at 457°C and 1800 psig) which are more typical of those used in development of the SRC II process. Kaiparowits and Edna Mine coals were at the high end of the range while Belle Ayr and McKinley were at the lower end.

SRC yields also varied widely, from 18-27 wt %, IOM yields from 2.8-4.6 wt %, hydrocarbon gas yields from 12-15 wt % and hydrogen consumption from 4 1/2 to 6 1/2 wt %. This compares to about 28 wt % SRC and 6 wt % IOM (MAF basis) in a conventional SRC II process with Powhatan coal. It is interesting to note that the hydrocarbon gas and hydrogen consumptions are quite low relative to oil yield compared to those for Powhatan coals. These typically yield 16 wt % hydrocarbon gas and consume a little over 5 wt % hydrogen (again, on a MAF basis).

B. Effect of Pyrite Source and Level in the Feed Slurry

1. Effect of Pyrite Source

The results of processing Belle Ayr coal with three different pyrite samples are compared in Table VI.

The Robena Pyrite II produced a much greater effect than the other two pyrite samples even though only about half as much was added and the total solids level in the feed slurry was about 5 wt % lower than in the other runs. Total oil yield was 11.3 wt % higher based on MF coal, than with Matheson, Coleman and Belle (MCB) pyrite while SRC, IOM and hydrocarbon gas yields were lower by 3.9, 5.0 and 1.3 wt %, respectively.

Addition of MCB pyrite results in a slightly higher total oil yield and slightly lower SRC yield than the Robena Pyrite III although total conversion to pyridine soluble material was less.

Hydrogen consumptions were nearly the same during these three runs.

There were no clear trends in the heavy distillate and distillation residue elemental analyses. The residue from the run with Robena Pyrite II had the lowest fusion point and highest solubilities in hexane and toluene (lowest preasphaltene content) while that from the run with MCB Pyrite II had the highest fusion point and lowest solubilities.

The conditions for these three experiments were identical except for the pyrite sample (and level) and feed slurry solids level. The Robena Pyrite II and III samples were obtained from a coal cleaning operation while the MCB pyrite was mined as a discrete mineral. The pyrite analyses differ somewhat, as shown in Table III.

As mentioned earlier, the MCB pyrite was ball milled, the Robena II was jet pulverized in air, and the Robena III was jet pulverized in a nitrogen atmosphere. The activity of the additive appears to correlate with surface area, perhaps as an indicator of differing surface structure. This conclusion is based on a small number of samples, however, and Sandia has reported that there is no correlation between surface area and pyrite activity(7).

2. Effect of Pyrite Level in the Feed Slurry

The effect of iron level in the feed slurry on yields was determined in run DOE 350R. The yields were calculated during steady-state operation with added pyrite and at 7 points after the additive was dropped from the formulation. It was found that yields plotted against total iron in the feed slurry on a logarithmic scale gave an essentially linear relationship, as shown in Figure 2.

The addition of 1 wt % pyrite to the feed in run DOE 350RA resulted in an iron level of about 2.5% in the equilibrated feed slurry. When pyrite addition was stopped in run DOE 350RC, the iron level in the slurry dropped to about 0.35 wt % before the run was terminated by a plug in the preheater. As iron concentration decreased over this range, total oil yield dropped from about 56 to 28 wt %, SRC yield increased from 14 to 28 wt % and IOM yield increased from 1.3 to 14 wt %. There was little effect on hydrocarbon gas yield.

The hydrogen level in the heavy distillate also dropped off significantly (from 8.5 to 7.7 wt %) as iron was worked out of the system. There was also a significant increase in distillation residue fusion point (from about 110 to 190°C).

C. Effect of Liquefaction Conditions

1. Temperature Effect

The effect of increasing the average dissolver temperature from 450 to 465°C with three different coals and added pyrite is shown in Table VII. In each case there was a significant increase in hydrocarbon gas yield and hydrogen consumption at the higher temperature, as expected. There were also decreases in oil and SRC yields and increases in IOM yields. From these results it is apparent that the optimum temperature for processing these coals with added pyrite is closer to 450°C than 465°C.

In each case, there were lower hydrogen levels in the heavy distillate and distillation residue at the higher temperature. Other product analyses were generally unaffected.

2. Combined Temperature/Pressure Effect

The results of processing Edna Mine coal at 450°C and 2250 psig or 457°C and 1800 psig are compared in Table VIII.

The results of run DOE 427RA are qualitative since the run was ended after three days due to increasing slurry viscosity. The higher reactivity in run DOE 427RB is still apparent, however.

The total oil yield was higher and the IOM yield lower at 450°C and 2250 psig. If run DOE 427RA could have been lined out, the differences would probably be more pronounced. The gas yield was higher at the higher temperature, as expected, and not much difference was observed in SRC yields and hydrogen consumptions.

Work is planned at Merriam to find the optimum conditions for processing western coals with added pyrite, and specifically to isolate the temperature and pressure effects. It is likely, however, that at least some of the improvement was due to the increased pressure.

3. Effect of Slurry Recycle

The scope of this paper has been limited to SRC II mode operation. It is interesting, however, to make at least one comparison to SRC I operation to determine the effect of recycling the added pyrite. This includes the effect of the higher

resulting iron concentration in the feed slurry as well as any changes that take place in the pyrite as it passes through the system.

Pyrite addition was highly beneficial in both modes of operation with Belle Ayr coal. Even with added pyrite, however, the SRC I studies with this coal indicated an unsatisfactory level of reactivity. Under the conditions used, 31 minutes residence time, 450°C, 1500 psig, 39 wt % coal concentration and 1 wt % pyrite addition, there was a 5 wt % deficiency of recycle solvent and overall conversion was poor as indicated by a 17 wt % insoluble organic matter yield. Thus, the SRC I studies would indicate that this coal was of low reactivity even with 1 wt % added pyrite.

As mentioned previously, dramatically different results were obtained in the SRC II mode (run DOE 350). With 1 wt % added pyrite (450°C, 2250 psig and 1 hr residence time), the Belle Ayr coal was one of the most reactive coals ever investigated at the Merriam Laboratory. Oil yield was 56 wt % (MF coal basis) and total organic residue yield (SRC + IOM) was only 15 wt %.

IV. CONCLUSIONS

1. Low iron, low rank coals can not be processed at normal SRC II conditions without added catalyst.
2. Addition of moderate amounts of pyrite (4-5 wt %, based on coal) results in attractive yields of high quality products and generally trouble-free operation.
3. Pyrites from different origins and those from the same origin obtained at different times may have varying activity. The factors influencing the catalytic activity of pyrite are not well understood, but in our studies activity generally increased with increasing surface area.
4. The yields from Belle Ayr coal at SRC II conditions vary with the logarithm of the iron concentration in the feed slurry over a wide range of the variables.
5. The optimum conditions for liquefaction probably vary with the coal and catalyst. The optimum temperature for the coals in this study was closer to 450°C than 465°C and yields can be expected to improve as hydrogen pressure is increased. Operating in the SRC II mode enhances the effect of added pyrite on coal reactivity.

REFERENCES

- (1) "Solvent Processing of Coal to Produce a Deashed Product," R&D Report No. 9, Kloepper, et al, Gulf Oil Corp., Merriam, Kansas; NTIS #PB167-809.
- (2) "Exploratory Research on Solvent Refined Coal Liquefaction," Quarterly Technical Progress Report for the Period April 1, 1979 through June 30, 1979; The Pittsburg & Midway Coal Mining Co., July 1980, FE/14800-10.
- (3) "Development of a Process for Producing an Ashless, Low-Sulfur Fuel from Coal," Interim Report #6 (Vol. II-Laboratory Studies; Part 1-Autoclave Experiments); The Pittsburg & Midway Coal Mining Co., 1975, GPO #163.10:53/INT 6, NTIS #PB236-305.
- (4) "Development of a Process for Producing an Ashless, Low-Sulfur Fuel from Coal," Interim Report #7 (Vol. II-Laboratory Studies; Part 2-Continuous Reactor Experiments Using Anthracene Oil Solvent); The Pittsburg & Midway Coal Mining Co., September 1977, FE-496-T4.

- (5) "Solvent Refined Coal (SRC) Process," Quarterly Technical Report for the Period April 1, 1977 through June 30, 1977; The Pittsburg & Midway Coal Mining Co., December 1977, FE-496-141.
- (6) "Solvent Refined Coal (SRC) Process," Quarterly Technical Report for the Period April 1, 1978 through June 30, 1978; The Pittsburg & Midway Coal Mining Co., May 1979, FE-496-157.
- (7) "The Relationship Between Properties of Iron Sulfides and Their Catalytic Activity," paper presented by F. V. Stohl and B. Granoff, Sandia National Laboratories, Albuquerque, NM, at the Disposable Catalysts for Synfuel Production Symposium at the 1981 AIChE Meeting at Houston, Texas, April 5-9, 1981.

TABLE I
RUN CONDITIONS

AVERAGE DISSOLVER	
TEMPERATURE:	450, 465°C (ISOTHERMAL) OR 457°C (SIMULATED ADIABATIC) 450°C INLET, 460°C OUTLET
PRESSURE:	1800 OR 2250 PSIG
RESIDENCE TIME:	1.0 HOUR
COAL CONCENTRATION:	30 WT % IN SLURRY
HYDROGEN FLOWRATE:	4 WT %, BASED ON SLURRY (52 MSCF/TON OF COAL)
MODE:	SRC II (RECYCLE OF UNFILTERED COAL SOLUTION)

TABLE II
COALS

MINE	STATE	SEAM	RANK
BELLE Ayr	WY	WYODAK- ANDERSON	SUBBITUMINOUS
(KAIPAROWITS PLATEAU)	UT	RED	HVC BITUMINOUS
ENERGY	CO	WADGE	SUB A/HVC BIT.
McKINLEY	NM	*	SUBBITUMINOUS
EDNA	CO	WADGE	SUB A/HVC BIT.
BLACKSVILLE	WV	PITTSBURGH	BITUMINOUS

* YELLOW, FUCHSIA, BLUE AND GREEN SEAMS ARE MINED.

TABLE III
PYRITES

	MCB* PYRITE	MCB* PYRITE	ROBENA PYRITE	ROBENA PYRITE
WT %				
Fe	43.61	41.65	30.20	38.75
S	53.01	50.11	34.38	41.36
C	0.09	0.10	5.81	5.42
H	0.04	0.09	0.69	0.40
MOLE RATIO S/Fe	2.12	2.10	1.99	1.86
PURITY, WT % BASED ON Fe	94	89	65	83
AVERAGE PARTICLE SIZE, μ M				
BY COULTER COUNTER	--	12	1.7	3.5
BET SURFACE AREA, M ² /G	2.0	1.1	5.9	2.6

* MATHESON, COLEMAN AND BELL

TABLE IV
SENSITIVITY OF VARIOUS COALS TO PYRITE ADDITION

CONDITIONS*	DOE 431RA/ 350RC-5	DOE 401R/ 353RC	DOE 422RA/ 422RB	DOE 424RA/ 424RB	DOE 402R/ 403R
COAL	BELLE AYR	Kaipar- OWITS	MC- KINLEY	EDNA	BLACKS- VILLE
CHANGE IN MAF YIELDS**					
C1-C4	+ 1.8	+ 0.2	- 0.9	- 2.3	- 0.1
TOTAL OIL	+22.0	+16.7	+20.3	+14.9	+ 2.6
SRC	-12.2	- 9.0	-10.5	- 9.1	- 0.7
IOM	-12.0	- 6.1	- 6.0	- 1.8	+ 0.3
CHANGE IN MAF HYDROGEN CONSUMPTION**	+ 0.1	+ 1.3	+ 2.2	+ 1.8	+ 0.7

* ALL AT 450°C, 2250 PSIG, 1.0 HOUR RESIDENCE TIME WITH 30 WT % COAL IN THE SLURRY AND 4 WT % HYDROGEN, BASED ON SLURRY.

** RUN WITH 1.86 WT % PYRITE III IN THE SLURRY COMPARED TO RUN WITHOUT ADDED PYRITE AT POINT WHERE OPERATION CEASED.

TABLE V
PROCESSING OF VARIOUS COALS WITH ADDED PYRITE

CONDITIONS*	DOE 431RA	DOE 401R	DOE 422RA	DOE 424RA	DOE 402R
COAL	BELLE AYR	KAIPAR- OWITS	Mc- KINLEY	EDNA	BLACKS- VILLE
<u>YIELDS, WT % MAF COAL</u>					
C ₁ -C ₄	12.7	11.8	12.4	14.8	13.0
TOTAL OIL	49.5	56.8	49.3	53.9	42.9
SRC	21.3	17.8	26.5	21.4	36.3
IOM	2.9	2.8	4.6	4.1	6.1
<u>HYDROGEN CONSUMPTION, WT % MAF COAL</u>	4.5	5.4	5.1	6.3	4.8

- * ALL AT 450°C, 2250 PSIG, 1.0 HR RESIDENCE TIME WITH 30 WT % COAL AND 1.86 WT % ROBENA PYRITE III IN THE SLURRY AND 4 WT % HYDROGEN, BASED ON SLURRY.

TABLE VI
EFFECT OF PYRITE CHARACTERISTICS

CONDITIONS*	DOE 350RA	DOE 380RA	DOE 380RB
PYRITE	ROBENA II	MCB II	ROBENA III
ADDITION LEVEL, WT % COAL**	2.15	4.18	4.26
TOTAL SOLIDS IN FEED SLURRY	44.6	50.7	49.8
<u>YIELDS, WT % MF COAL</u>			
C ₁ -C ₄	10.8	12.1	13.0
TOTAL OIL	55.9	44.6	41.6
SRC	13.5	17.4	19.0
IOM	1.3	6.3	5.2
<u>HYDROGEN CONSUMPTION, WT % MF COAL</u>	5.4	5.1	4.8

- * FOR ALL: 449-450°C, 2250 PSIG AND 1 HOUR RESIDENCE TIME WITH 30 WT % BELLE AYR COAL IN THE SLURRY AND 4 WT % HYDROGEN, BASED ON SLURRY.

- ** AS PURE FeS₂.

TABLE VII
EFFECT OF TEMPERATURE ON PROCESSING
WESTERN COALS WITH ADDED PYRITE

<u>CONDITIONS*</u>	<u>DOE</u> <u>350RA/B</u>	<u>DOE</u> <u>353RA/B</u>	<u>DOE</u> <u>355RA/B</u>
COAL	BELLE AYR	KAIPAR- OWITS	ENERGY
PYRITE	ROBENA II	MCB I	MCB I
<u>CHANGE IN MAF YIELDS**</u>			
C ₁ -C ₄	+3.5	+4.4	+3.3
TOTAL OIL	-4.3	-1.7	-2.5
SRC	-2.2	-4.6	-9.5
IOM	+2.0	+0.7	+6.2
<u>CHANGE IN MAF HYDROGEN</u> <u>CONSUMPTION**</u>	+0.9	+1.0	+0.2

* ALL AT 2250 PSIG AND 1 HOUR RESIDENCE TIME WITH 30 WT % COAL AND 1.0 WT % ADDED PYRITE IN THE SLURRY; 4 WT % HYDROGEN, BASED ON SLURRY.

** RUN AT 465°C COMPARED TO ONE AT 450°C.

TABLE VIII
COMBINED EFFECTS OF TEMPERATURE AND PRESSURE
ON THE SRC II PROCESSING OF EDNA COAL
WITH ADDED PYRITE

<u>CONDITIONS*</u>	<u>DOE 427RA</u>	<u>DOE 427RB</u>
AVERAGE DISSOLVER TEMP., °C	457	450
PRESSURE, PSIG	1800	2250
<u>YIELDS, WT % MF COAL</u>		
C ₁ -C ₄	14.4	12.2
TOTAL OIL	43.5	46.1
SRC	20.0	21.4
IOM	6.2	4.3
<u>HYDROGEN CONSUMPTION,</u> <u>WT % MF COAL</u>	4.9	5.1

* ALL AT 1.0 HOUR RESIDENCE TIME WITH 30 WT % EDNA MINE COAL AND 1.86 WT % PYRITE IN THE FEED SLURRY; 4 WT % HYDROGEN, BASED ON SLURRY.

FIGURE 1
MERRIAM LABORATORY
BENCH SCALE COAL LIQUEFACTION UNIT

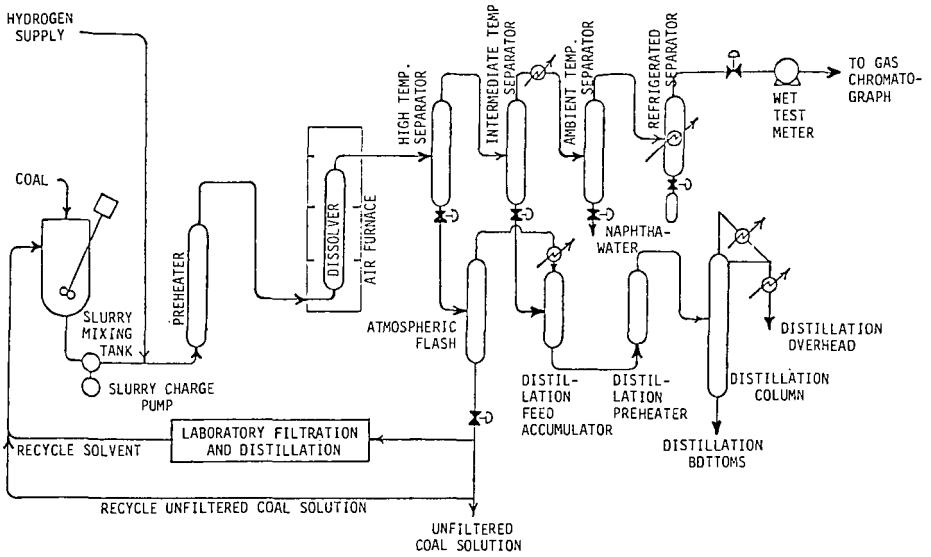
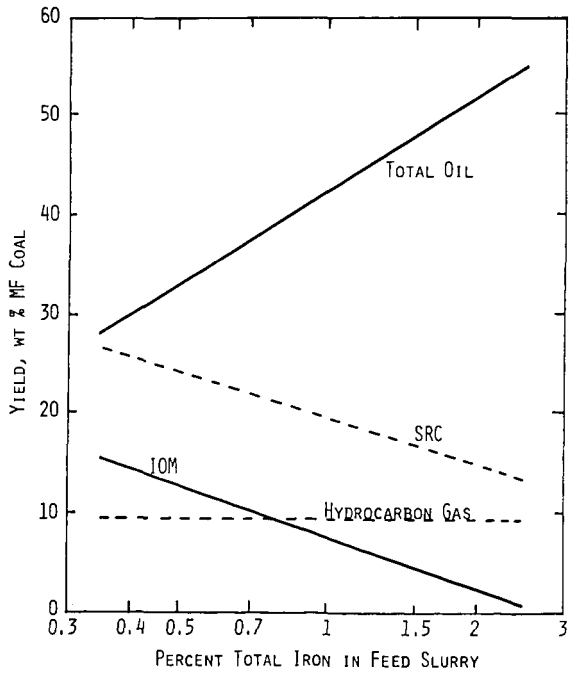


FIGURE 2
EFFECT OF IRON LEVEL ON YIELDS
RUN DOE 350RC



BATCH AUTOCLAVE TEMPERATURE-PRESSURE STUDIES ON THE
DIRECT CATALYTIC LIQUEFACTION OF VICTORIAN BROWN COAL

P.J. Cassidy, F.P. Larkins and W.R. Jackson

Department of Chemistry, Monash University
Clayton, 3168 Victoria, Australia

INTRODUCTION

Victorian brown coal is a low rank, low ash lignite with an elemental composition similar to North Dakota lignite (see Table 1).

Table 1: Comparison of Victorian Brown Coal and North Dakota Lignite

	<u>As Received</u>		<u>Daf basis</u>			
	<u>H₂O</u>	<u>C</u>	<u>H</u>	<u>O</u>	<u>N</u>	<u>S</u>
Victorian Morwell Coal (1)	62.5	69.3	5.0	24.5	0.6	0.6
North Dakota Lignite (2)	25.0	69.4	4.3	23.1	0.7	2.5

Previous batch autoclave studies^{3,4} using hydrogen gas with tetralin as the vehicle have confirmed that brown coal is suitable for direct catalytic hydrogenation giving high yields of liquid products. Furthermore, brown coal is an excellent ion-exchange medium primarily because a significant amount of the bound oxygen is present in carboxylic ($\sim 2.6 \text{ mol kg}^{-1}$) and phenolic ($\sim 3.2 \text{ mol kg}^{-1}$) functional groups.⁵ This property has been exploited to achieve high dispersion of metal catalysts throughout the coal.⁵

The work presented here is aimed at developing catalysts and reaction conditions which maximise the conversion to a low oxygen refinery feedstock. Product distribution dependences on reaction temperature (345-460°C : 6MPa H₂) and hydrogen pressure (1-10MPa : 385°C) using iron, tin and synergistic iron + tin (trace) catalysts are compared to those for untreated Morwell coal.

EXPERIMENTAL

Coal Preparation and Hydrogenation

The coal and catalysts were prepared for hydrogenation by the method of Jackson et al.³ The coal (3.0 g) was dried under nitrogen at 105°C to constant weight and slurried (1 : 1) with AR grade tetralin as the vehicle. The hydrogenations were performed in a 70 ml rocking autoclave heated to reaction temperature in 11 minutes. Reaction time was one hour at temperature after which the autoclave was quenched in an ice bath.

Catalyst concentrations used for the study were as follows:

<u>Coal</u>	<u>Catalyst Concentration (mmol/kg daf coal)</u>	
untreated	Fe	30
iron treated	Fe	300 ± 40
tin treated	Sn	200 ± 20
synergistic iron-tin treated:	Fe	300 ± 40
	Sn	20 ± 10

Product Analysis

Product gases (CO , CO_2 , CH_4 , C_2H_4 , C_2H_6 , C_3H_8 , C_3H_6 , $n\text{-C}_4\text{H}_{10}$, $i\text{-C}_4\text{H}_{10}$) were analysed by GLC using a standard gas mixture for calibration. Hydrogen was determined indirectly by difference. The liquid product was removed from the reaction using CH_2Cl_2 and the water produced was determined by azeotropic distillation. The insoluble material was Soxhlet extracted for 12-15 hours with CH_2Cl_2 and the residue dried at 105°C under nitrogen to determine the total conversion. The CH_2Cl_2 soluble material was further divided into asphaltene (insoluble in light petroleum) and oil (soluble in light petroleum). Elemental analyses for C, H, O, N, S were performed by the Australian Analytical Laboratories. The direct analysis for oxygen was cross checked by difference (Equation 1)

$$\text{wt}\% \text{ O} = 100 - \% \text{ C} - \% \text{ H} - \% \text{ S} - \% \text{ N} \quad (1)$$

Acidic oxygen was determined by non aqueous titration using the method of Brookes and Maher.⁶

TEMPERATURE DEPENDENCE

Total Conversion

The temperature dependences of the product distributions for untreated iron, tin and iron-tin treated coals at 6MPa initial hydrogen pressure are shown in FIGURES 1A-D. The total conversions are compared in FIGURE 2. The temperature range chosen for study was from $345\text{-}460^\circ\text{C}$. At temperatures below 345° conversion was too low for meaningful measurements and at temperatures above 460° decomposition of tetralin can become a significant problem.^{7,8}

The total conversion of untreated coal increases steadily from 37% to 63% between 345°C and 425°C then it levels out to 65% at 460°C . An iron based catalyst results in a rapid increase in total conversion from 37% at 345°C to 63% at 385°C after which it increases steadily to 72% at 460°C . The tin catalyst increases the conversion dramatically from 43% at 345°C to 73% at 385°C after which it increases regularly to 81% at 460°C . The iron-tin catalyst is not as efficient as the tin catalyst up to 385°C as the conversion is only 66% at 385°C . However, above 385°C the conversion rises sharply reaching 85% at 425°C after which it levels out with a maximum of 88% at 460°C . Above 400°C the products from the tin and iron-tin coals are increasingly unstable with increasing amounts of CH_2Cl_2 insoluble material being precipitated during product work up. The result is reduced total conversions at all temperatures compared with findings using a larger 1 litre autoclave.^{5,9,10} The results should therefore be viewed as internally consistent, but not directly comparable with work in larger autoclaves with different temperature profiles.

Conversion to Useful Liquid Products (Oil and Asphaltene)

Between 365 and 425°C the three catalysed coals offer significantly improved CH_2Cl_2 soluble liquid (oil + asphaltene) yields compared to untreated coal (FIGURE 3). At 345°C tin gives an 8% improvement while the iron-tin and iron catalysts offer no improvement over the untreated coal yield of 20% (daf coal) at that temperature. In the region $365\text{-}385^\circ\text{C}$ tin continues to be superior giving 4-5% more liquid product than the Fe-Sn, 10-14% better than Fe and 22% more than untreated coal. However, above 405°C the yield of liquid product from tin coal deteriorates significantly from 50% at 405°C to 42% at 460°C . This can be attributed to increased yields of hydrocarbon gases and significant repolymerisation of asphaltenes during product workup. (The total oil + asphaltene yield in these small scale experiments is only 0.5 to 1.5 g.) Above 385°C the Fe-Sn catalyst dramatically increases the yield of useful liquid products from 44% at 385°C to 57% at 425°C after which it decreases slightly to 55% at 460°C . This improvement in yield at higher temperatures is due

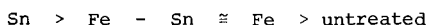
to the formation of a more stable product relative to the Sn catalyst system while the slight decrease at 460°C can be attributed to the increased production of hydrocarbon gases and some repolymerisation. The iron catalyst smoothly increases the liquid yield at 41% at 405°C and then levels out. The liquid yield from untreated coal increases steadily to 37% at 425°C after which there is little improvement.

The asphaltene temperature dependence (FIGURES 1A-D) is similar for the four coals with the yield increasing with temperature to a maximum of 405°C for untreated, iron and iron-tin coals and 385°C for tin treated coal after which it decreases regularly with increasing temperature. The iron-tin catalyst is clearly superior to the other three coals for producing oil (FIGURES 1A-D) at all temperatures except in the region of 400°C. The maximum oil production is 35-38% daf coal with the iron-tin catalyst between 425°-460°C. The oil production for the untreated, iron and tin coals is similar reaching a maximum of 30% daf coal at 460°C. The minor variations in the trend can be attributed to the formation and breakdown of the asphaltenes. The major effect of all the catalysts is to produce more asphaltenes at temperatures below 405°C which are degraded to oils at higher temperatures.

Oxygen Distribution in the Products as a Function of Reaction Temperatures

In developing useful catalysts for brown coal liquefaction one major objective is to achieve a high yield of low oxygen content liquid. It is important to know how the oxygen is distributed in the products and in what form (H₂O, CO₂, CO) it is removed from the coal system. The oxygen distributions for products from the four coals are shown in FIGURES 4A-D.

Generally raising the reaction temperature removes more oxygen, primarily as water. In all cases carbon monoxide production increases slightly with increased temperature while CO₂ formation appears to reach a maximum in the region of 385°C after which it decreases slightly for the three catalysed coals. There is no such maximum reached in the carbon dioxide produced from the untreated coal. As the majority of the carbon dioxide is formed at low temperatures (200-300°C) by decomposition of carboxyl groups, any variation on this level is probably a response to changes in the equilibrium of the water gas shift reaction. Tin is clearly the superior catalyst for removing oxygen from the coal products with the general order being



At 460°C tin has removed 98% of the oxygen, iron and iron-tin approximately 80% and untreated coal has lost only 67%. In fact little further oxygen is removed from untreated coal above 405°C. The distribution of acid oxygen in the CH₂Cl₂ insoluble residue is similar for all three catalysed reactions. The dramatic difference is that tin has removed significantly more non acidic oxygen from the residue at lower reaction temperatures. The oxygen content in the asphaltene is similar for the three catalysts, reaching a maximum in the region of 385°C and decreasing at higher temperatures. The oxygen level in the asphaltenes from untreated coal is almost invariant with reaction temperature. Tin is also the best catalyst for the removal of oxygen from the oil fractions at temperatures above 385°C while the iron and iron-tin catalysts have similar activity and are better than untreated coal. At temperatures below 385°C there is, in all cases, an increase in the oxygen level in the oil fraction as the reaction temperature decreases with the trend being most marked for the tin and iron-tin catalysts. This suggests that the catalysts are breaking carbon-oxygen bonds at low reaction temperature but do not have the ability to remove the oxygen completely from the system at low temperatures. It is a reasonable presumption that it is the trace of tin in the synergistic iron-tin catalyst which facilitates the improved bond breaking compared to the iron catalyst. Increasing the reaction temperature to 385°C is sufficient to remove this oxygen from the oil. The increase in total oxygen in the oil fraction

above 385°C for untreated, iron and iron-tin coals suggests that these catalysts have difficulty in removing oxygen from certain classes of oxygen containing functional groups. However, the ability of tin to catalyse the almost total removal of oxygen does lead to problems of product stability. Some of the derived products repolymerise even on standing in dichloromethane solution. It is possible that higher concentrations of reactive poly-enes are formed which are not hydrogenated in the absence of iron or other metals capable of catalysing liquefaction.

HYDROGEN PRESSURE DEPENDENCE

The hydrogen pressure dependence reactions were performed at 385°C for the four coals and at 425°C for the coals with iron-tin synergistic catalyst (see FIGURES 5 to 7). The most significant feature is that in all catalysed reactions the total conversion (FIGURE 5) increases with pressure until a critical pressure is reached above which increasing the hydrogen pressure has a reduced effect. For the iron and iron-tin catalysts at 385°C the critical pressure is 4MPa initial hydrogen while for the tin at 385°C and iron-tin at 425°C 6MPa is the critical hydrogen pressure. Furthermore increasing hydrogen pressure results in significantly more asphaltene being produced for the tin (385°C) and iron-tin (at 385°C and 425°C) catalysts (FIGURE 6) while it has little effect on oil production from both catalysed and non catalysed coals at 385°C (FIGURE 7). However, at 425°C the oil production from iron-tin coal shows a marked hydrogen pressure dependence (FIGURE 7) and these studies suggest that a suitable initial hydrogen pressure for obtaining high conversion in catalysed reactions is not very high e.g. an initial pressure of 6MPa for the iron-tin system for 425°C.

CATALYTIC EFFICIENCY - USEFUL CARBON/HYDROGEN VERSUS OXYGEN REMOVAL

While developing catalysts that remove oxygen from brown coal is a major objective it is also important to ensure that the maximum amount of carbon and hydrogen from the coal be carried through into the useful liquid products, i.e. oil and asphaltene. An additional view of conversion then is a measure of the percentage of carbon and hydrogen carried through to the useful products. Recognising that approximately 4% of the carbon is always lost from the system as carbon dioxide and carbon monoxide and that the coal contains ~25% oxygen, the maximum yield of carbon and hydrogen can only be 71% of the daf coal. Considered from this point of view the iron-tin catalyst converts 75% of the available carbon and hydrogen into liquid products at 425°C while the tin converts only 63%, iron 53% and untreated coal 46%.

FIGURE 8 compares the ability of the catalyst to remove oxygen and to convert the available carbon and hydrogen into useful products. The most efficient catalyst will be closest to the 45 degree line on the coordinate system. All of the coals lie to the left of the line which shows that all four of the reaction systems have a preference for the removal of oxygen relative to converting the carbon and hydrogen to useful products. This trend is particularly true for high temperature reactions where the shift to the left is associated with greater production of hydrocarbon gases and, in the case of tin catalysed reactions, significant repolymerisation of material which was initially soluble in methylene chloride. The exception is the iron-tin catalyst which lies very close to the line and at one point (corresponding to 425°C) actually shows a slight preference for converting the carbon and hydrogen into liquid products. In order of catalyst efficiency the four coals are ranked in order:

iron - tin > tin >> iron > untreated

CONCLUSION

The development of suitable catalysts and reaction conditions in the liquefaction of brown coal is a compromise of the ability of the catalyst to fulfill the following

requirements;

- Remove all of the organically bound oxygen
- Carry the maximum amount of carbon and hydrogen through to the liquid products
- Minimise production of hydrocarbon gases

Under the reaction conditions chosen for this study (6MPa initial hydrogen pressure and a low (1:1) hydrogen donor solvent to coal ratio) the synergistic iron-tin catalyst is superior to the other three coals. It achieves its objectives remarkably well at reasonably low reaction temperatures (425°C) and correspondingly low reaction pressure (14.6 MPa/2190 psi at 425°C). Under these conditions 75% of the available carbon and hydrogen is converted to liquid products and 5% to hydrocarbon gases. A large proportion (60%) of the liquid product is present as oil (X4 soluble) while 73% of all oxygen has been removed as CO₂, H₂O and CO. The tin catalyst is superior at removing oxygen (94% at 460°C) but produces more hydrocarbon gases and is less efficient at carrying the available carbon and hydrogen through to liquid products (63% at 425°C). It is possible that the tin requires higher hydrogen pressures to prevent repolymerisation of the unstable asphaltenes at these temperatures. At 425°C/6MPa hydrogen the iron catalyst is only 7% better than untreated coal for converting available carbon and hydrogen into useful liquids.

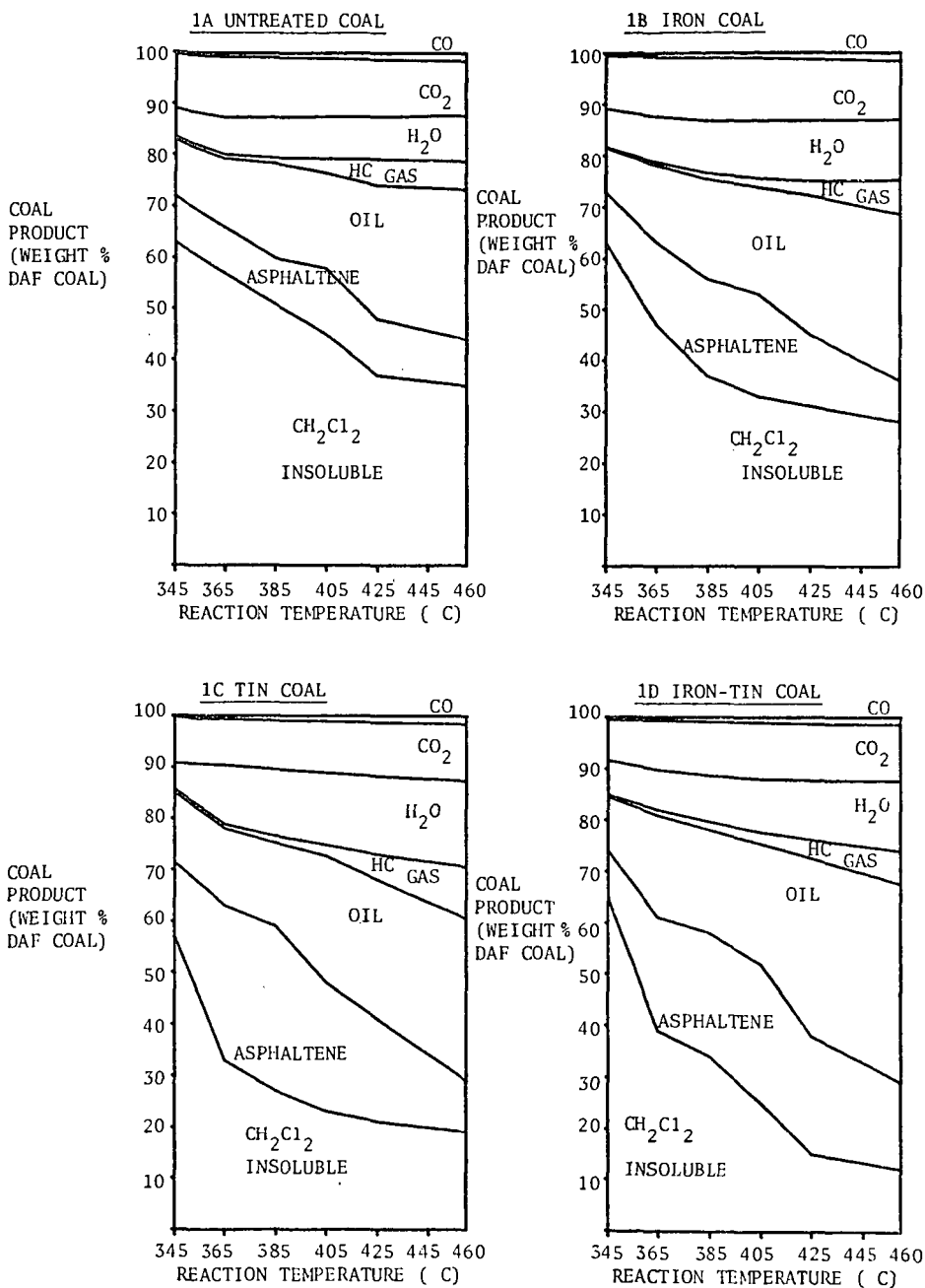
ACKNOWLEDGEMENTS

We gratefully acknowledge financial assistance for this work provided by the Victorian Brown Coal Council. The responsibility for the views expressed rest entirely with the authors. We also thank M. Marshall, D. Rash and P. Redlich for valuable discussions and assistance.

REFERENCES

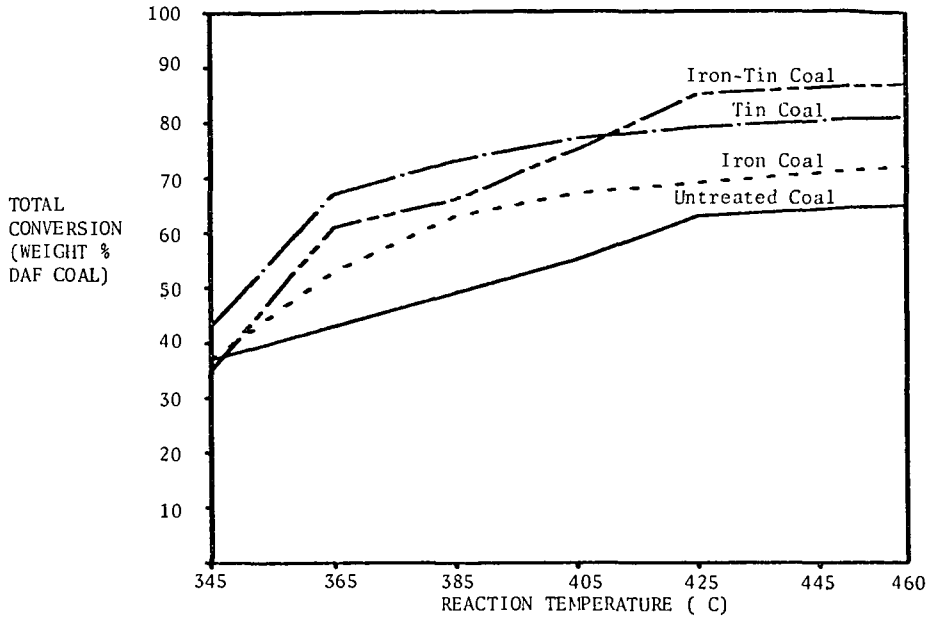
1. State Electricity Commission of Victoria - Scientific Division Test Report CS/79/31 1979 Sheet 2.
2. H.R. Appell, R.D. Miller, E.G. Illig, E.C. Moroni, E.W. Steffgen, PETC/TR-79/1 1979 52.
3. W.R. Jackson, F.P. Larkins, M. Marshall, D. Nicolson and D. Rash, Fuel, 58, (1979) 156.
4. W.R. Jackson, F.P. Larkins, D. Rash and N. White, Fuel 58 (1979) 281.
5. M.R. Hatswell, W.R. Jackson, F.P. Larkins, M. Marshall, D. Rash and D.E. Rogers, Fuel 59 (1980) 442.
6. J.D. Brooks and T.P. Maher, Fuel 36 (1957) 51.
7. B.M. Benjamin, E.W. Hagaman, V.F. Raaen, and C.J. Collins, Fuel 58 (1979) 386.
8. J.M. Charlesworth, Fuel, 59 (1980) 859.
9. M. Marshall, W.R. Jackson, F.P. Larkins, M.R. Hatswell and D. Rash submitted for publication in Fuel.
10. F.P. Larkins, W.R. Jackson, M.R. Hatswell, S.J. Cochran, P.J. Cassidy, M. Marshall, D. Rash and P. Redlich, Proceedings of the International Conference on Coal Science Düsseldorf 7-9/9/1981 C12, pp. 392-397.

PRODUCT DISTRIBUTION vs REACTION TEMPERATURE FIGURE 1.



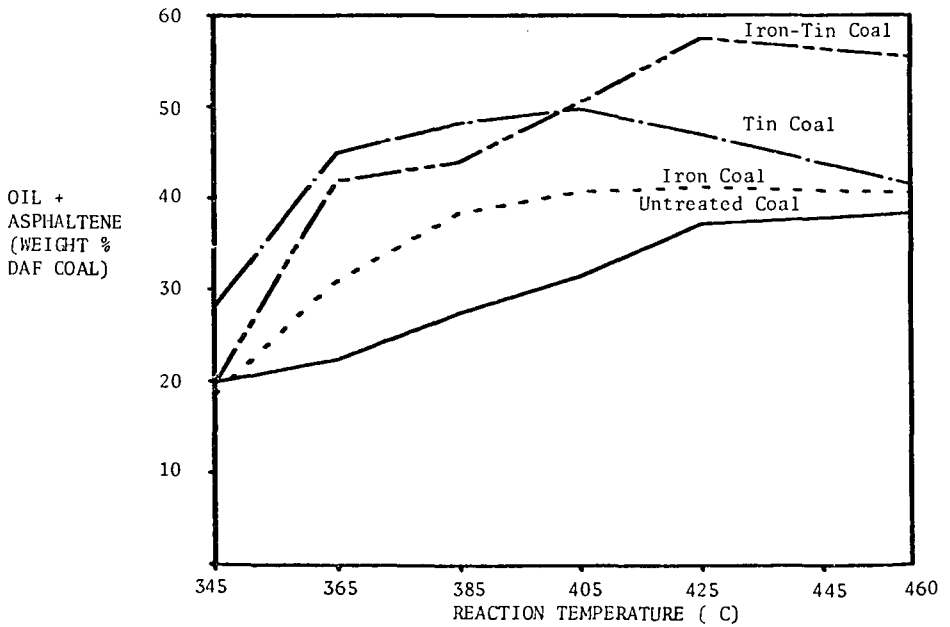
TOTAL CONVERSION vs REACTION TEMPERATURE

FIGURE 2.

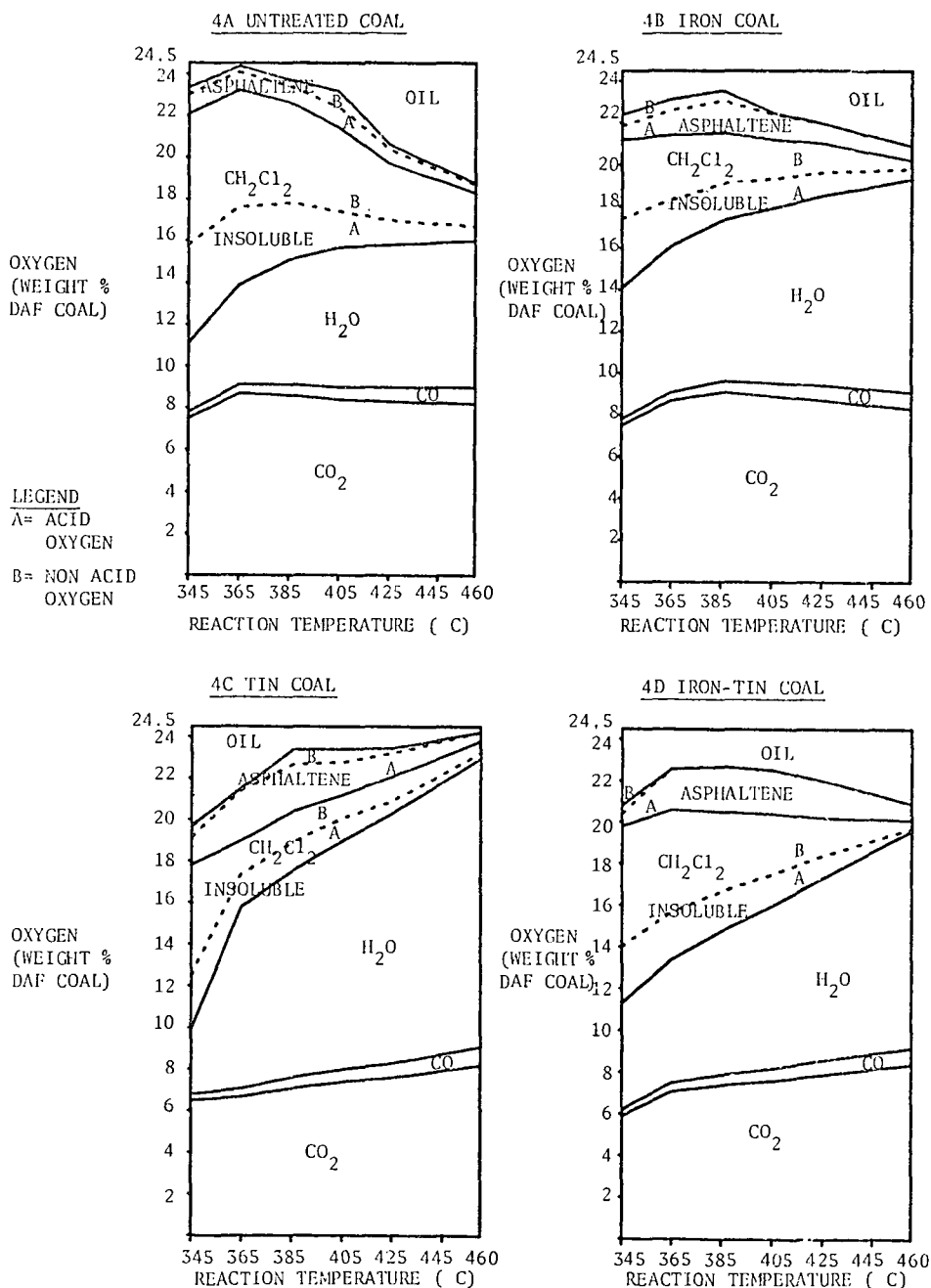


OIL + ASPHALTENE vs REACTION TEMPERATURE

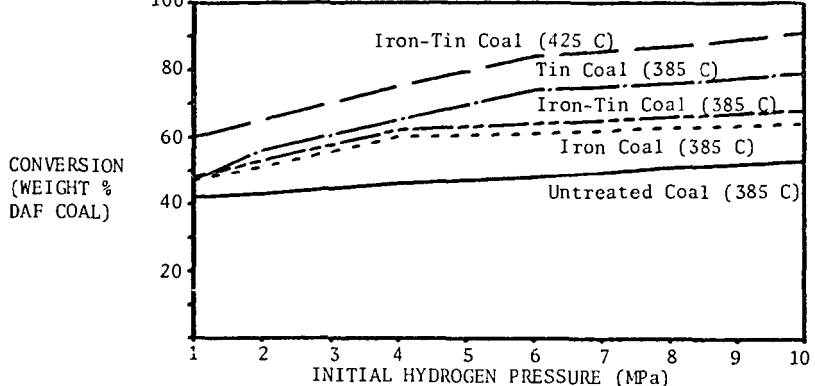
FIGURE 3.



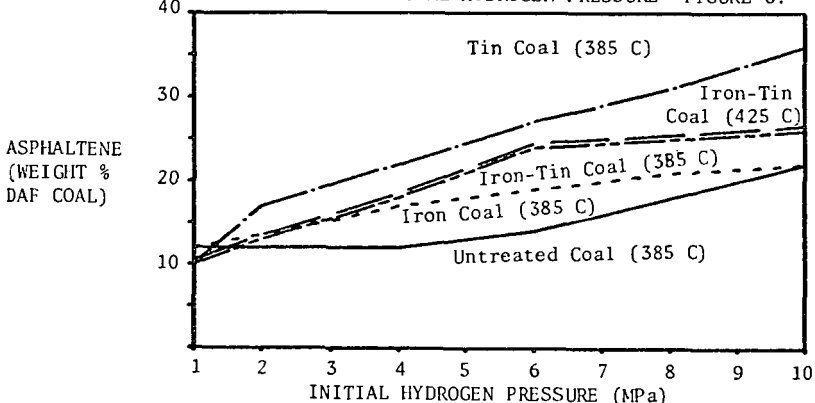
PRODUCT OXYGEN DISTRIBUTION vs REACTION TEMPERATURE FIGURE 4.



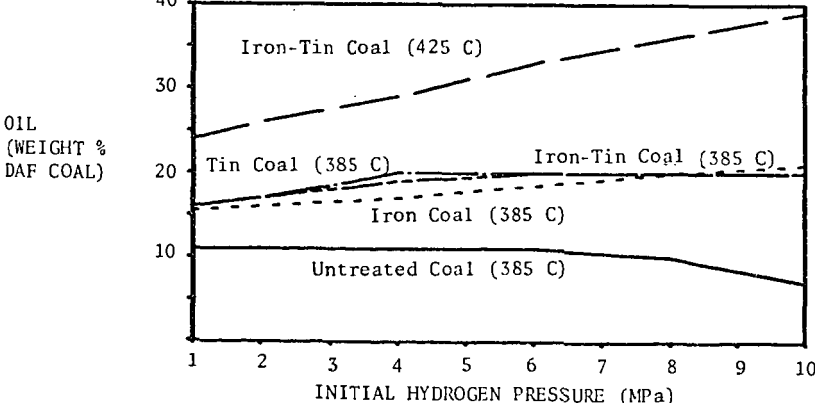
TOTAL CONVERSION vs INITIAL HYDROGEN PRESSURE FIGURE 5.



ASPHALTENES vs INITIAL HYDROGEN PRESSURE FIGURE 6.

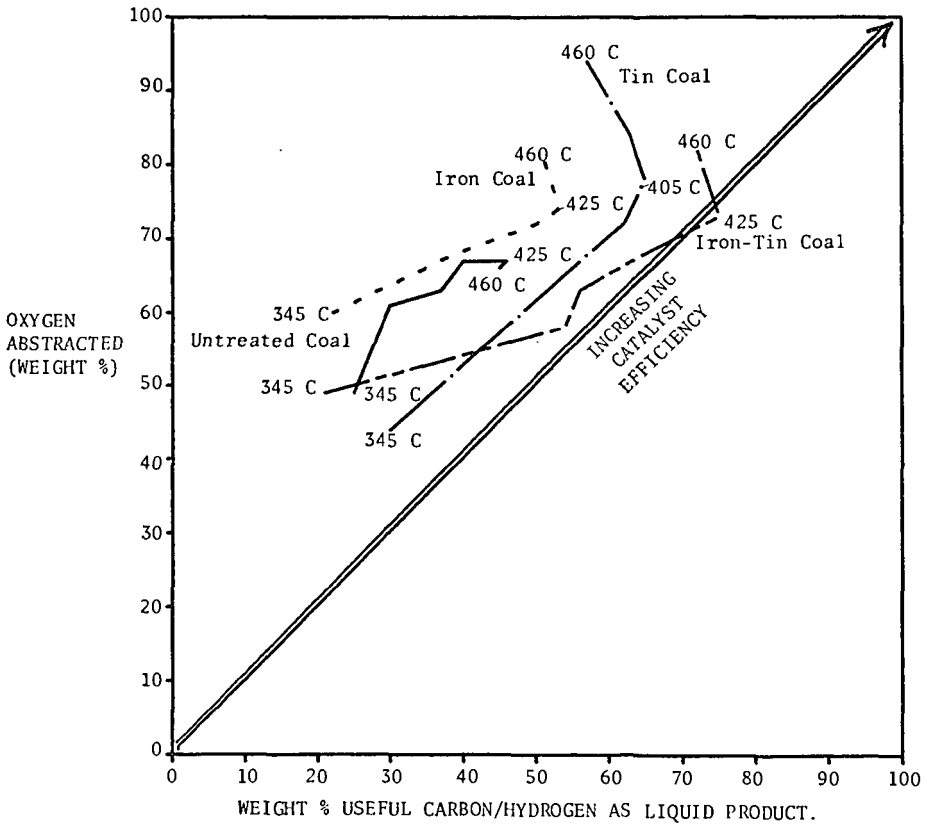


OIL vs INITIAL HYDROGEN PRESSURE FIGURE 7.



CATALYST EFFICIENCY

FIGURE 8.



Note: Temperatures quoted on the graph are the reaction temperatures for the areas of interest.

EFFECT OF CATALYST DISTRIBUTION IN COAL LIQUEFACTION

Diwakar Garg and Edwin N. Givens
Corporate Research and Development Department

Air Products and Chemicals, Inc.
P.O. Box 538, Allentown, PA 18105

Effect of the mode of catalyst addition was studied for the liquefaction of Eastern Kentucky Elkhorn #2 coal in a continuously stirred tank reactor. Particulate addition of iron as pyrite significantly catalyzed the coal liquefaction reaction. Both coal conversion and oil yield increased on addition of pyrite to the feed slurry; oil production increased by more than a factor of two both at 825° and 850°F. Pyrite Concentration had negligible effect on product distribution, but the mode of catalyst addition had a big impact on coal liquefaction. Impregnation of coal with one weight percent iron gave a similar product distribution as obtained with addition of 3.5 weight percent iron in the form of particulate pyrite. Significantly lower hydrocarbon gas make and hydrogen consumption were noted with impregnation over particulate addition. SRC sulfur content was marginally higher with impregnation. Solvent hydrogen content increased with particulate addition whereas it decreased with impregnation.

Introduction

The basic non-catalytic process for liquefaction of coal was developed by Bergius¹ in Germany circa 1912. In 1925 Brown-coal tar was catalytically hydrogenated for the first time with molybdenum oxide. This advance led to the development of the catalytic hydrogenation of coal.

A number of catalysts were studied and reported to give improved yield and product quality². Adding two percent molybdenum on coal as ammonium molybdate substantially increased the liquefaction performance. Subsequent experiments showed that 0.05 percent molybdenum gave a yield equal to that obtained with two percent when the alkalinity of coal was reduced. Because molybdenum was expensive and in short supply in Germany, it was replaced by iron catalyst. The Germans found that adding iron as iron sulfate to the feed slurry improved the liquefaction of coal². Bayermasse, an iron oxide-containing material obtained as by-product from aluminum manufacture was also shown to be active in coal liquefaction. In terms of iron content, twice as much Bayermasse as sulfate was needed to produce the same results in hydrogenation of coal. In certain cases the addition of sulfur to the system also improved the catalytic liquefaction effect of the iron². The iron to sulfur ratio in the liquefaction residue suggested that iron sulfide (FeS) was the ultimate form of the iron. With the advent of x-ray diffraction technique the FeS was found to be in the form of pyrrhotite³, $Fe_{1-x}S$.

Wright and Severson reported that the addition of iron as contained in the residues from coal liquefaction increased the hydrogen transfer capacity of anthracene oil.⁴ Seitzer⁵ magnetically separated the iron sulfur compound from coal liquefaction residues and used it as a catalyst in subsequent liquefaction reactions. He found that the magnetically separated material had, per

weight of iron, about the same catalytic effect as ferrous sulfate. Furthermore, he found that the magnetically separated material catalyzed the addition of hydrogen to the dissolved coal.

Moroni and Fischer⁶, who reviewed many papers in the area of coal mineral catalysis, concluded that pyrite was active in coal conversion. Neither the addition of the coal liquefaction residue nor the magnetically separated residue delineated whether pyrrhotite had better catalytic activity than pyrite. A significant amount of work has been done more recently to determine the true catalytic activity of pyrite and pyrrhotite. A detailed summary of literature on pyrite and pyrrhotite catalysis has been made by Garg and Givens.⁷

The distribution of catalyst in the coal appears to be a critical factor in coal conversion. The method of applying the catalyst to the coal affects the catalyst distribution. For example, iron sulfate was shown to be much more effective when impregnated than when mixed mechanically.^{2,8} Although prolonged mixing improved the effectiveness of the catalyst, the improvement was less than gained by impregnation. The method of impregnation is also quite important as was shown in one case in which an attempt to impregnate coal in-situ during hydrogenation gave poor results.⁸

A reduction in particle size of the pyrite, reported to play an important role in catalyzing the coal liquefaction reaction, improved the catalytic activity of the pyrite.⁹ Significantly more oil production was reported with the use of finely divided pyrite¹⁰ than with hand ground pyrite.¹¹

The contact between catalyst and coal can be increased either by adding finely divided catalyst (two to three micron size) or impregnating it on coal using a water soluble compound like iron sulfate or dispersing it at the molecular level in the reaction mixture by using thermally unstable organic compounds like iron naphthenate. In the present paper data are presented which show the catalytic activity of pyrite and impregnated iron sulfate in coal liquefaction. The effect of simple particulate addition of pyrite is compared to catalyst impregnation. The catalytic activity for the coal conversion reactions are related to the product distribution including hydrocarbon gas make, oil, asphaltene and preasphaltene yields, and degree of coal conversion. All of the data reported in this paper refer to results in a continuous 100 pounds per day coal process unit.

Experimental

Materials: Elkhorn #2 was a washed sample taken from a preparation plant in Floyd County, Kentucky. The coal sample was ground to 95% minus 200 mesh particles and dried in air. The coal was screened through a 150 mesh sieve prior to use. The detailed analysis of the screened coal is reported in Table 1.

A 550-850°F cut of SRC-II heavy distillate supplied by The Pittsburg and Midway Coal Mining Company was used as a process solvent. The chemical analysis of the process solvent is shown in Table 2. The solvent contained 93.8% pentane-soluble oils, 5.0% asphaltenes and 0.4% preasphaltenes.

The pyrite sample was received from an operating mine in southwestern Pennsylvania. The sample was dried at 110°C in nitrogen and then ground to 99.9% minus 325 U.S. mesh size in the presence of liquid nitrogen. The chemical analysis of the pyrite is given in Table 3. The sample was comprised of 75%

pyrite, 5% carbonaceous organic material and 20% magnetite, quartz, and other inorganic materials. The BET surface area of the pyrite was $1.0 \text{ m}^2/\text{g}$ and the material was relatively non-porous.

Iron sulfate ($\text{FeSO}_4 \cdot 7\text{H}_2\text{O}$) was received from Textile Chemical Company, Reading, Pennsylvania. The chemical analysis of the iron sulfate is given in Table 4. The sample contained approximately 97% iron sulfate crystals.

Equipment: Process studies were done in a continuous 100 pound/day coal liquefaction unit equipped with a continuous stirred autoclave. The use of a stirred tank reactor insured that solvent vaporization matched that of an actual SRC-I dissolver and that coal minerals did not accumulate. Since there was no slurry preheater, all of the sensible heat had to be provided by resistance heaters on the reactor. Because of this high heat flux, the reactor wall was about 27°F hotter than the bulk slurry. Multiple thermocouples revealed that the slurry temperature inside the reactor varied by only 9°F from top to bottom. A detailed description of the reactor is presented elsewhere.¹²

The products were quenched to 320°F before flowing to a gas/liquid separator that was operated at system pressure. The slurry was throttled into the product receiver while the product gases were cooled to recover the product water and organic condensate. The product gases were then analyzed by an on-line gas chromatograph.

Procedure: Coal liquefaction runs were performed at 825 and 850°F , 2000 psig hydrogen pressure, 1000 rpm stirrer speed, hydrogen feed rate equivalent to 5.5 wt.% of the coal and a superficial slurry space velocity of 1.5 inverse hours. The coal concentration in the feed was 30 wt.%. Iron sulfate was impregnated on the coal by dissolving it in water and mixing it with coal. Impregnated coal sample was dried in nitrogen and ground to minus 200 mesh prior to use. The concentration of impregnated iron was 1.0 wt.% on the basis of coal. The concentration of pyrite was varied from 2.5 to 10 wt.% of feed slurry.

At least 10 reactor volumes of the product were discarded prior to collecting a product sample. A complete sample consisted of one 8-oz. sample of product slurry, one 1-liter sample of product slurry as back-up sample, a light condensate sample and a product gas sample.

The product slurry from the continuous reactor was solvent separated into four fractions: (1) pentane-soluble material (oil), (2) pentane-insoluble and benzene-soluble material (asphaltenes), (3) benzene-insoluble and pyridine-soluble material (preasphaltenes), and (4) pyridine-insoluble material. The latter contains insoluble organic material (IOM) and mineral residue. A detailed procedure for performing this separation will be reported elsewhere. The overall coal conversion is calculated as the fraction of organic material (moisture-ash-free coal) soluble in pyridine.

Results and Discussions

Effect of Pyrite on Coal Liquefaction - At 825 and 850°F , addition of pyrite increased the coal conversion from ~ 85 to $\sim 92\%$ (Table 5). The production of hydrocarbon gases, $\text{CO} + \text{CO}_2$, and water, marginally increased with pyrite. Oil production increased by more than a factor of two; 12 to 28% and from 8 to 27%

on addition of pyrite at 825 and 850°F, respectively. Production of preasphaltenes decreased and asphaltenes remained apparently unchanged. The additional converted coal and preasphaltenes with pyrite ended up in the oil fraction. Hydrogen consumption increased from 0.64 to 1.68% and from 0.53 to 2.41% on addition of pyrite at 825 and 850°F, respectively. Also, an additional amount of 0.5% hydrogen was consumed in reducing the added pyrite. X-ray diffraction analysis of coal liquefaction residue showed a complete conversion of pyrite to pyrrhotite. SRC sulfur content remained the same. Oil hydrogen content unchanged in the absence of pyrite but increased in its presence.

In summary, the addition of pyrite to coal during liquefaction improved conversion of coal and preasphaltenes, increased production of oil and hydrocarbon gases, promoted rehydrogenation of the process solvent and increased consumption of hydrogen. Increasing reaction temperature in the presence of pyrite increased conversion of preasphaltenes and increased production of hydrocarbon gases and hydrogen consumption. The conversion of coal and production of oil and asphaltenes marginally decreased with increasing temperature.

Effect of Pyrite Concentration on Coal Liquefaction - Conversion of coal and production of hydrocarbon gases remained the same upon increasing the pyrite concentration from 2.5 to 10 wt. percent. (Table 6, Figures 1 and 2). The production of CO + CO₂, water and oil shown in Table 6 and Figures 2 and 3 increased slightly as pyrite concentration increased. Asphaltenes remained the same and preasphaltenes decreased with increasing concentration of pyrite (Figure 4). Hydrogen consumption increased significantly as the pyrite concentration increased as shown in Table 6 and Figure 5. SRC sulfur content plotted in Figure 6 also marginally increased. Finally, increasing the concentration of pyrite from 2.5 to 10 wt.% of feed slurry had no significant effect on liquefaction of Elkhorn #2 coal.

Effect of Iron Impregnation on Coal Liquefaction - Conversion of coal was not significantly affected by impregnation at both 825 and 850°F. The production of hydrocarbon gases decreased considerably with iron impregnation while oil production increased by over a factor of two at both temperatures (Table 7). Asphaltene yield was unchanged but preasphaltene yield decreased considerably with iron impregnation. X-ray diffraction analysis of coal liquefaction residue showed a complete conversion of iron sulfate to pyrrhotite. Hydrogen consumption and SRC sulfur content were not significantly affected by iron impregnation. Oil hydrogen content was maintained without any additive but decreased with iron impregnation at both 825 and 850°F. Finally, iron impregnation significantly reduced the hydrocarbon gases and preasphaltenes production and increased the oil production.

Comparison of Iron Impregnated Versus Particulate Addition - The liquefaction of coal impregnated with one wt.% iron based on coal is compared with addition of 3.5 wt% particulate iron in the form of pyrite to coal-oil slurry. Conversion of coal was slightly lower with iron impregnation compared to pyrite addition. Iron impregnation gave significantly lower hydrocarbon gases production and hydrogen consumption (Table 8, Figures 7 and 8). Oil, asphaltenes and preasphaltenes production with iron impregnation were comparable to that obtained by pyrite addition. SRC sulfur content was marginally higher with iron impregnation. Oil hydrogen content was improved with pyrite, whereas it decreased with iron impregnation.

The above data emphasize the importance of the method of catalyst distribution in coal liquefaction. The effectiveness of a metal catalyst can be enhanced significantly by increasing the intimate contact between catalyst and coal. The mode of catalyst distribution therefore determines the amount of catalyst required for the reaction.

Conclusion

Addition of pyrite significantly catalyzes the coal liquefaction reaction. It improves coal conversion, increases oil and gases production, increases hydrogen consumption and rehydrogenates the process solvent. Changing the concentration of pyrite does not significantly alter the coal liquefaction reaction. Mode of catalyst addition is very important in coal liquefaction. The activity of a catalyst depends on the level of intimate contact of catalyst with coal. Therefore, the concentration of the metal catalyst can be greatly reduced without affecting product distribution by insuring efficient contact between catalyst and coal. The reduction in catalyst loading will eventually increase the overall throughput of the plant, drastically reduce the load in the solid-liquid separation unit, and improve the overall process economics.

References

1. Bergius, F., and Billwiller, J., German Patent 301,231, August 1, 1913.
2. Wu, W. R. K., and Storch, H. H., "Hydrogenation of Coal and Tar", U.S. Department of the Interior, Bureau of Mines Bulletin 633, 1968.
3. Given, P. H., Spackman, W., Davis, A., Walker, P. L. Jr., and Lovell, H. L., "The Relation of Coal Characteristics to Coal Liquefaction Behavior", Report No. 1 Submitted to NSF (RANN Division) by the Pennsylvania State University, 15 March 1974.
4. Wright, C. H., and Severson, D. E., ACS Division of Fuel Chem., Preprints, 1972, 16, 68.
5. Seitzer, W. H., "Miscellaneous Autoclave Liquefaction Studies," Final Report Prepared for EPRI by Suntech, Inc., under the contract EPRI AF-612 (RP-779-7), February, 1978.
6. Moroni, E. C. and Fischer, R. H., "Disposable Catalysts for Coal Liquefaction," Paper Presented at the 179th National Meeting of American Chemical Society, Houston, March, 1980.
7. Garg, D. and Givens, E. N., "Pyrite Catalysis in Coal Liquefaction," Paper Accepted for Publication in I&EC Process Design and Development.
8. Weller, S. W. and Pelipetz, M. G., Ind. Eng. Chem., 1951, 43, 1243.
9. Guin, J. A., Tarrer, A. R., Lee, J. M., Lo, L. and Curits, C. W., Ind. Eng. Chem. Process Des. Dev., 1979, 18, 371.
10. Anderson, R. P., "Low Cost Additives in the SRC Processes," Paper Presented at the Dept. of Energy Project Review Meeting on Disposable Catalysts in Coal Liquefaction held in Albuquerque, New Mexico, June, 1979.
11. Solvent Refined Coal (SRC) Process, Quarterly Technical Progress Report FE/496-155 Prepared for U.S. Dept. of Energy by The Pittsburg and Midway Coal Mining Co., Shawnee Missio, Kansas, March, 1979.
12. Skinner, R. W., and Givens, E. N., "Effects of Solvent Hydrogen Content in the SRC Process," Paper Presented at the 179th National Meeting of American Chemical Society, Houston, March, 1980.

TABLE 1
CHEMICAL ANALYSIS OF COAL SAMPLE

	ELKHORN #2 WEIGHT %
ULTIMATE ANALYSIS (AS RECEIVED)	
CARBON	77.84
HYDROGEN	5.24
OXYGEN	7.20
SULFUR	1.08
NITROGEN	1.75
PROXIMATE ANALYSIS (AS RECEIVED)	
ASH	6.29
MOISTURE	1.55
DISTRIBUTION OF SULFUR	
TOTAL SULFUR	1.08
SULFATE SULFUR	0.04
PYRITE SULFUR	0.25
ORGANIC SULFUR	0.79

TABLE 3
ANALYSIS OF PYRITE

	WEIGHT %
CARBON	4.48
HYDROGEN	0.34
NITROGEN	0.61
SULFUR	41.34
OXYGEN	5.97
IRON	42.30
OTHER IMPURITIES (BY DIFFERENCE)	4.96
TOTAL	100.00

SURFACE AREA = 1.0 m²/g

TABLE 4
ANALYSIS OF IRON SULFATE

	WEIGHT %
FERROUS SULFATE, FeSO ₄	53.78
IRON, Fe ₂ O ₃	0.06
TITANIUM, TiO ₂	0.33
MAGNESIUM SULFATE, MgSO ₄	1.80
COPPER	0.0004
LEAD	0.0005
WATER OF CRYSTALLIZATION	42.28
TOTAL	99.25

TABLE 2
ANALYSIS OF HEAVY DISTILLATE

ELEMENT	WEIGHT %
CARBON	89.44
HYDROGEN	7.21
OXYGEN	1.70
NITROGEN	1.10
SULFUR	0.55
NUMBER AVERAGE MOLECULAR WEIGHT	222

TABLE 5
LIQUEFACTION OF COAL IN THE PRESENCE AND ABSENCE OF PYRITE

	70% SOLVENT + 30% COAL	60% SOLVENT + 30% COAL + 10% PYRITE	70% SOLVENT + 30% COAL + 10% PYRITE
FEED COMPOSITION			
Fe CONC., WT. % COAL	0.0	0.0	14.1
TEMP., °F	825	850	825
PRESSURE, PSIG	2000	2000	2000
RESIDENCE TIME, MIN.	35	37	39
HYDROGEN TREAT RATE, MSCF/T	18.9	23.0	19.9
PRODUCT DISTRIBUTION, WT. % MAF COAL			
HC	5.2	7.0	5.7
CO, CO ₂	0.7	0.6	0.9
H ₂ S	0.3	0.3	0.0
OIL	12.2	8.3	28.2
ASPHALTENES	21.2	21.6	24.3
PRESASPHALTENES	44.2	43.4	29.6
I.O.M.	14.7	15.7	8.1
WATER	1.5	3.1	3.2
CONVERSION, % MAF	85.3	84.3	91.9
HYDROGEN CONSUMPTION, * WT. % MAF	0.64	0.53	1.68
OIL HYDROGEN CONTENT, WT. %			
START	7.2	7.2	7.2
FINISH	7.2	7.2	7.5
SRC SULFUR, %	0.61	0.55	0.60

*HYDROGEN CONSUMPTION DOES NOT INCLUDE THE HYDROGEN REQUIRED FOR REDUCING FeS₂ TO FeS

TABLE 7
EFFECT OF IRON IMPREGNATION ON COAL LIQUEFACTION

	NO	NO	YES	YES
IRON IMPREGNATION	0.0	0.0	1.0	1.0
Fe CONC., WT. % COAL			70% SOLVENT + 30 COAL	
FEED COMPOSITION				
TEMPERATURE, °F	825	850	825	850
PRESSURE, PSIG	2000	2000	2000	2000
RESIDENCE TIME, MIN.	35	37	33	41
HYDROGEN TREAT RATE, MSCF/T	18.9	19.9	20.6	27.3
PRODUCT DISTRIBUTION, WT. % MAF COAL				
HC	5.2	7.0	3.5	4.4
CO, CO ₂	0.7	0.6	0.6	0.5
H ₂ S	0.3	0.3	0.2	0.2
OIL	12.2	8.3	25.0	30.3
ASPHALTENES	21.2	21.6	19.1	20.8
PRESASPHALTENES	44.2	43.4	35.8	27.5
I.O.M.	14.7	15.7	13.5	13.1
WATER	1.5	3.1	2.3	3.2
CONVERSION	85.3	84.3	86.5	86.9
HYDROGEN CONSUMPTION, * WT. % MAF	0.64	0.53	0.40	0.60
OIL HYDROGEN CONTENT, WT. %				
START	7.2	7.2	7.2	7.2
FINISH	7.2	7.2	7.1	7.0
SRC SULFUR, %	0.61	0.55	0.61	0.57

TABLE 8
IRON IMPREGNATION VERSUS PARTICULAR ADDITION

	PYRITE	IMPREGNATION
IRON ADDITION	3.5	1.0
Fe CONCENTRATION, WT. % COAL		
TEMPERATURE, °F	850	850
PRESSURE, PSIG	2000	2000
RESIDENCE TIME, MIN.	38	41
HYDROGEN TREAT RATE, MSCF/T	24.2	27.3
PRODUCT DISTRIBUTION, WT. % MAF COAL		
HC	10.2	4.4
CO, CO ₂	0.9	0.5
H ₂ S	0.3	0.2
OIL	25.6	30.3
ASPHALTENES	22.3	20.8
PRESASPHALTENES	28.2	27.5
I.O.M.	13.1	13.1
WATER	3.2	3.2
CONVERSION, % MAF	90.7	86.9
HYDROGEN CONSUMPTION, * WT. % MAF	1.75	0.80
OIL HYDROGEN CONTENT, WT. %		
START	7.2	7.2
FINISH	7.3	7.0
SRC SULFUR, %	0.49	0.57

*HYDROGEN CONSUMPTION DOES NOT INCLUDE THE HYDROGEN REQUIRED FOR REDUCING FeS₂ TO FeS

TABLE 6
EFFECT OF PYRITE CONCENTRATION ON COAL LIQUEFACTION

	850	850	850
TEMP., °F	2.5	5.0	10.0
PYRITE CONCENTRATION, WT. % FEED SLURRY	3.5	7.1	14.1
IRON CONCENTRATION, WT. % COAL	2000	2000	2000
RESIDENCE TIME, MIN.	38	38	39
HYDROGEN TREAT RATE, MSCF/T	24.2	22.2	22.5
PRODUCT DISTRIBUTION, WT. % MAF COAL			
HC	10.2	9.9	10.6
CO, CO ₂	0.9	1.0	1.2
OIL	25.6	24.3	27.0
ASPHALTENES	22.3	18.6	22.3
PRESASPHALTENES	28.2	32.3	29.5
I.O.M.	13.1	13.1	13.1
WATER	3.2	3.5	4.0
CONVERSION, % MAF	90.7	89.6	90.7
HYDROGEN CONSUMPTION, * WT. % MAF	1.75	1.81	2.41
OIL HYDROGEN CONTENT, WT. %			
START	7.2	7.2	7.2
FINISH	7.3	7.5	7.5
SRC SULFUR, %	0.49	0.51	0.57

*HYDROGEN CONSUMPTION DOES NOT INCLUDE THE HYDROGEN REQUIRED FOR REDUCING FeS₂ TO FeS

Figure 1
Variation in the Conversion of Coal
With the Concentration of Pyrite

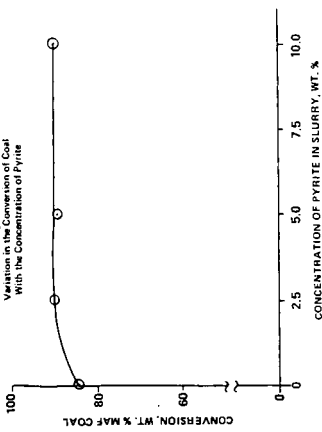


Figure 2
Variation in the Production of Gases and Water
With the Concentration of Pyrite

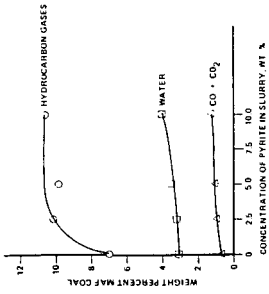


Figure 3
Variation in the Production of Oils
With the Concentration of Pyrite

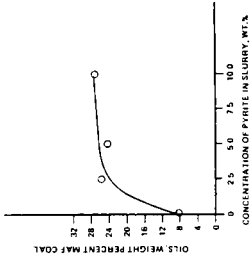


Figure 4
Variation in the Production of Asphaltenes and Preasphaltenes
With the Concentration of Pyrite

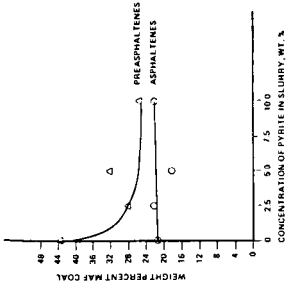


Figure 5
Variation of Hydrogen Consumption With the
Concentration of Pyrite

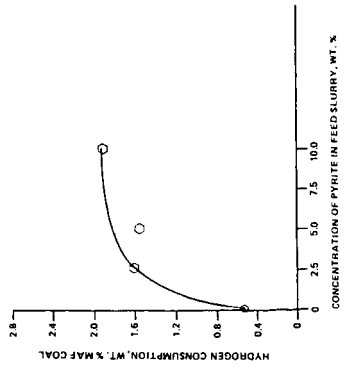


Figure 6
Variation of SRC Sulfur Content With the Concentration
of Pyrite

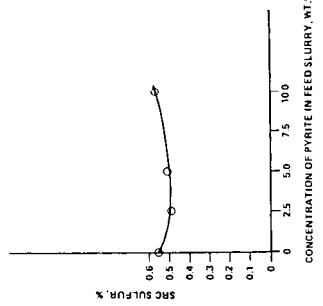


Figure 7
Iron Impregnation Versus
Particulate Addition

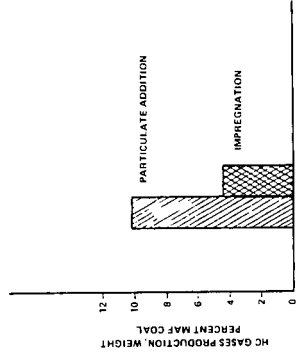
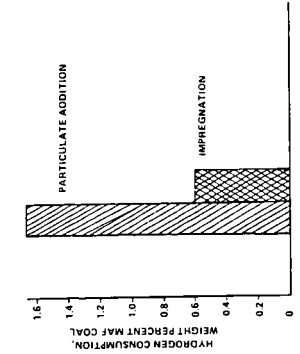


Figure 8
Iron Impregnation Versus
Particulate Addition



CATALYTIC HYDROPYROLYSIS OF COAL TO DISTILLATE OILS

Shaik A. Qader

Jet Propulsion Laboratory
California Institute of Technology
4800 Oak Grove Drive
Pasadena, California 91103

INTRODUCTION

Coal is predominantly aromatic in nature and deficient in hydrogen. It contains only about 4.5-5.0 percent hydrogen as compared to crude oils which contain 11-13 percent hydrogen. Coal therefore, can be converted to a crude oil type liquid either by removing carbon from it or by adding hydrogen to it. Pyrolysis processes come under the first category which produce large quantities of carbon rich char and small quantities of hydrogen rich tar. Under practical conditions of pyrolysis¹, tar yield varies between 20 and 25 percent with char yield of about 50 percent. Pyrolysis tars are poor in quality and require catalytic hydrotreatment for conversion to refined products.

The yield and quality of tar can be improved by carrying out coal pyrolysis under hydrogen pressure. In hydrolysis, hydrogen improves tar yield by stabilizing reactive fragments formed from coal during pyrolysis. In the absence of hydrogen, some of the reactive fragments undergo polymerization and condensation reactions forming char. Hydrogen also improves tar quality by promoting hydrocracking and hydrorefining of₂₋₈ tar during the pyrolysis process. In most of the hydrolysis work,²⁻⁸ light oils containing mostly BTX are produced in low yields of 10-20 percent. The hydrolysis processes operate at very high temperatures of 700-1000°C where the primary tar undergoes extensive hydrocracking forming BTX and gas.

The yield and quality of tar can be further improved by carrying out hydrolysis at medium temperatures of 500-600°C in the presence of a catalyst that promotes hydrogenation and hydrocracking reactions. Though work on pyrolysis and hydrolysis¹⁰ of coal was done¹ extensively, very little is known about catalytic hydrolysis. Schroeder¹¹ patented a catalytic hydrogenation process where he claimed that a bituminous coal impregnated with ammonium molybdate yielded 30-60 percent light oil at 800°C and 2000 psi pressure. Friedman et al¹² hydrogenated a New Mexico coal impregnated with one percent molybdenum in the form of ammonium molybdate in fixed and fluid beds. Most of the experimental work was done at 600-900°C under a pressure of 6000 psi. Most of the coal was converted to gas with a liquid yield of less than 20 percent. But high yield of coal liquid of up to 57 percent was obtained when the hydrogenation was carried out at 480°C under a pressure of 6000 psi. Steinberg and Fallon¹³ hydrolyzed a lignite impregnated with ammonium molybdate at 700°C and 1500 psi pressure in a free fall tubular reactor. The yield of liquid product was reported to be about 18-25 percent but the catalyst did not affect the conversion. Franklin et al¹⁴ studied the effect of mineral matter on rapid pyrolysis and hydrolysis of a bituminous coal and found no significant effect by iron-sulfur minerals at a hydrogen pressure of about 1000 psi. In this paper, the results of catalytic hydrolysis of coal in a hanging basket reactor and a fluid bed reactor are described. Refined distillate oils are obtained from coal at medium temperatures and pressures in the presence of a hydrocracking catalyst.

EXPERIMENTAL

The experimental work was done in a Hanging Basket Reactor (HBR) system shown in Figure 1 and a Fluidized Bed Reactor system shown in Figure 2. The Hanging Basket Reactor consists of a high pressure vessel of 2" i.d. and 4' long provided with a heater at the bottom and a basket at the top. The basket hangs from a shaft connected to a valve and carries a crucible. The HBR was designed for a pressure of 7000 psi at a temperature of 500°C. Physical mixtures containing one gram of coal and three grams of catalyst were taken in the crucible and the system was pressurized and heated to the desired conditions. After the system conditions were stabilized, the crucible was lowered to the hot zone and kept there for different periods of time and then raised to the original position. The lowering and raising operations take 2-3 seconds. After this operation, the system was cooled, depressurized and the crucible was taken out of the system. The weight lost by coal during the reaction was taken as the conversion. Some experiments were also done with 50 and 100 grams of coal in a 1-litre Magne-drive Autoclave under simulated conditions of the HBR work to prepare bulk quantity of liquid product for analysis.

The Fluid Bed Reactor System was designed for a working pressure of 4000 psi at a maximum temperature of 700°C. It consists of a fluid bed reactor of 1.5" i.d. and 4' height, two hydrogen heaters, three coolers, two liquid collection bottles, a steam injection system, a flow control valve, a dry gas meter and a pump to circulate chilled water through the coolers. The fluid bed reactor has a liner of 1.25" i.d. and 3.5' height which is provided with a perforated disc at the bottom to support the coal-catalyst mixture. The system is fully instrumented with controllers, indicators and recorders for temperature, pressure, Δp and gas flow. The reactor system was housed in a high pressure cell and operated from outside at the control panel.

The fluid bed reactor was operated in a batch mode with hydrogen flowing through it continuously. A physical mixture of coal and catalyst was placed in the liner which was then introduced into the reactor. The size of coal and catalyst and fluidization velocity were predetermined using a glass fluid bed reactor at ambient temperature. Fluidization studies with coal-catalyst mixtures showed that coal and catalyst particles of 35-150 mesh fluidize well with good mixing at velocities of 0.25 to 0.5 ft./sec. which give gas phase residence times of 6-12 seconds for a coal-catalyst fluid bed height of 3'. After the introduction of the liner into the reactor, the system was flushed with nitrogen, pressurized and closed to the atmosphere. The hydrogen heaters were heated to the desired temperature and the nitrogen in the system was replaced by hydrogen through a bypass line. Flow of hydrogen through the bypass was continued until the desired gas flow and temperature were attained. At that stage, the hot hydrogen flow was diverted through the reactor where it came into contact with the coal and catalyst and fluidized the mixture. The reaction was carried out for 10 to 30 minutes. At the end of the reaction period, the hydrogen flow was diverted back through the bypass and was replaced by nitrogen. During the operation, chilled water was circulated through the coolers. The liquid product was condensed in the coolers and was collected in the collection bottles. The gas was let out into the atmosphere through the gas meter where its volume was recorded. The solid char remained in the liner with the catalyst.

A bituminous coal from Utah was used in the HBR work. The analysis of the coal is given in Table 1. A Wyoming subbituminous and a Kentucky bituminous coal

were used in the FBR work. The analysis of the coals is given in Table 2.

Prereduced tungsten disulfide (WS_2) of -200 mesh size was used in the HBR experiments. A commercial catalyst containing sulfides of cobalt and molybdenum supported on silica-alumina was used in the FBR experiments. The catalyst was ground to 60-140 mesh size before use. The analyses of coals, coal liquids and gases were done by standard methods.

RESULTS AND DISCUSSION

The Hanging Basket Reactor experiments were done with and without the catalyst at 450-550°C under a pressure of 2000-4000 psi. The effect of reaction time and temperature on coal conversion is shown in Figure 3. The conversion increased with temperature and time. In the case of non-catalytic experiments, a maximum conversion of 43 percent was obtained at 550°C and 4000 psi pressure. The addition of catalyst increased the conversion significantly. Coal conversion of over 90 percent was obtained at 550°C and 4000 psi pressure. The data show that adequate catalytic effect can be obtained in coal conversion when coal and catalyst are present in a physical mixture at high temperatures, high pressures and high catalyst-coal ratios. The data also show that high coal conversions can be obtained in catalytic hydropyrolysis at short reaction times of less than 10 minutes.

The effect of hydrogen pressure and reaction time on coal conversion at 550°C is shown in Figure 4. Hydrogen pressure did not affect the non-catalytic conversion but increased the catalytic conversion significantly. It was reported in the earlier publications¹⁵ that hydrogen pressure increased conversion in the non-catalytic hydropyrolysis of coal. But most of the published work was carried out at lower pressures and thus can not be compared with the data obtained in the present work. It is therefore concluded from the data of Figure 4 that hydrogen pressure increases coal conversion in non-catalytic hydropyrolysis only at pressures lower than 2000 psi but it does not affect the conversion at pressures of 2000 psi or higher unless a catalyst is present. The pressure effect in catalytic hydropyrolysis appears to be similar to the effect observed in catalytic hydrogenation of coal.^{16,17}

Significant differences were observed in the nature of liquid and gaseous products obtained in the HBR work. Table 3 contains the analysis of liquid and gaseous products. The product obtained in the non-catalytic work was a very high boiling liquid and contained large quantities of preasphaltene, asphaltene, sulfur and nitrogen. On the other hand, the catalytic product was lighter and contained substantial amounts of light and middle oils. The preasphaltene, asphaltene, sulfur and nitrogen content of the product was very low. The properties of the catalytic liquid product indicate that the primary liquid formed from coal underwent hydrorefining and hydrocracking in the presence of the catalyst yielding a refined distillable oil. The data suggest that in catalytic hydropyrolysis the conversion of coal to liquid product takes place by a two step reaction mechanism shown in Figure 5. In pyrolysis, the organic matter of coal undergoes thermal breakdown forming an intermediate product consisting of reactive fragments. Some of the fragmented coal molecules undergo stabilization forming tar and some of the fragments undergo polymerization and condensation reactions forming coke or char. In hydropyrolysis, hydrogen reacts with the fragmented coal molecules and stabilize them before they undergo polymerization and condensation reactions which lead to coke or char formation. Tar yield

therefore increases in hydropyrolysis when compared to just pyrolysis of coal. In catalytic hydropyrolysis, the primary coal liquid appears to be forming due to pyrolysis and catalytic hydrogenation of coal. The primary coal liquid in turn undergoes catalytic hydrocracking forming a lighter liquid product.

It is concluded from the foregoing discussion on catalytic hydropyrolysis that physical contact between coal and a solid catalyst provides adequate catalytic effect to get high coal conversion of up to 90 percent. The coal undergoes liquefaction and the liquefied coal undergoes refinement in a single step, thus producing good quality light and middle oils. Though not discussed in this paper, catalyst to coal ratios of 3 to 1 were found to provide adequate catalytic effect and to reduce agglomeration of caking coals when the size of coal was >200 mesh. It is therefore feasible to produce refined distillate oils in high yields from caking bituminous coals in a single step by catalytic hydropyrolysis under the conditions used in the HBR work. The HBR system does not have any potential for use as a practical system to liquefy coal on a large scale in a continuous manner. An evaluation of several practical reactor systems led to the conclusion that a fluidized bed reactor is the most suitable for this application.

The results of the Fluidized Bed Reactor System are given in Tables 4-6. Table 4 contains the test conditions used in the FBR work. The size of coal and catalyst and fluidization velocity were determined from fluidization studies made in a glass fluid bed reactor at ambient temperature and atmospheric pressure with nitrogen as the fluidizing gas. The temperature and pressure were selected from the HBR work. Table 5 contains the material balance of FBR work. The yield of liquid product from the subbituminous coal was about 33 percent as compared to about 43 percent from the bituminous coal. The hydrogen consumption was 2.5 and 3.8 percent respectively. It is conceivable that the liquid product yield can be improved under optimal processing conditions. Table 6 contains the properties of liquid products. The coal liquids contain small amounts of sulfur and benzene insolubles and large quantities of light and middle oils. The liquid from the subbituminous coal contains 75 percent distillate and the liquid from the bituminous coal contains 86 percent distillate boiling up to a temperature of 450°C. The data indicate that coal liquefaction and refining of liquefied coal took place in a single step in the FBR which is in conformity with the HBR data. The data also support the two step reaction mechanism shown in Figure 5.

ACKNOWLEDGMENT

This work was supported by the Energy Systems Division of the National Aeronautics and Space Administration and the JPL Director's Discretionary Fund.

REFERENCES

1. Jones, J.F., Schmid, M.R., and Eddinger, R.T., "Fluid Bed Pyrolysis of Coal", Chem. Eng. Prog., 60, No.6, 69 (1964).
2. Squires, A.M., Graff, R.A., and Dobner, S., "Flash Hydrogenation of a Bituminous Coal", Science, 189, 793 (1975).
3. Pelofsky, A.H., Greene, M.I., and LaDelfa, C.J., "Short Residence Time (SRT) Coal Hydropyrolysis", American Chemical Society National Meeting, Fuel Chemistry Division Preprints, 21, No.5, 154 (1976).
4. Coles, E.T., "CoalCon's Hydrocarbonization Technology", paper presented at the 82nd National Meeting of the American Institute of Chemical Engineers, Atlantic City, New Jersey, August 29 - September 1, (1976).
5. Beeson, J.L., Duncan, D.A., and Oberle, R.D., "Flash Hydrogenation of Lignite and Bituminous Coal in an Entrained Flow Reactor", American Chemical Society National Meeting, Fuel Chemistry Division Preprints, 24, No.3, 72 (1979).
6. Finn, M.J., Fynes, G., Ladner, W.R., and Newman, J.O.H., "The Formation of BTX by the Hydropyrolysis of Coal", American Chemical Society National Meeting, Fuel Chemistry Division Preprints, 24, No.3, 99 (1979).
7. Ranieri, F.D., Combs, L.P., and Falk, A.Y., "Experimental Investigation of Peat Hydrogasification", American Chemical Society National Meeting, Fuel Chemistry Division Preprints, 24, No.3, 64 (1979).
8. Cypres, R., "Hydrogenopyrolysis of Coal and Coal Derivatives", American Chemical Society National Meeting, Fuel Chemistry Division Preprints, 26, No.3, 44 (1981).
9. Anthony, D.B., and Howard, J.B., "Coal Devolatilization and Hydrogasification", AIChE Journal, 22, 625 (1976).
10. Belt, R.J., and Bissett, L.A., "Assessment of Flash Pyrolysis and Hydro-pyrolysis", METC/R1-79/2, U.S. Department of Energy, Morgantown Energy Technology Center, Morgantown, West Virginia, (1978).
11. Schroeder, W.C., U.S. Patent 3, 030, 298 (1962).
12. Friedman, S., Hiteshue, R.W., and Schlesinger, M.D., "Hydrogenation of New Mexico Coal at Short Residence Time and High Temperature", Bureau of Mines Report of Investigations 6470, United States Department of the Interior, (1964).
13. Steinberg, M., and Fallon, P., "Coal Liquefaction by Rapid Gas Phase Hydrogenation", American Chemical Society National Meeting, Petroleum Chemistry Division Preprints, 20, No.2, 321 (1975).
14. Franklin, H.W., Peters, W.A., and Howard, J.B., "Mineral Matter Effects on the Rapid Pyrolysis and Hydropyrolysis of a Bituminous Coal", American Chemical Society National Meeting, Fuel Chemistry Division Preprints, 26, No.3, 35 (1981).
15. Fallon, P.T., Bhatt, B., and Steinberg, M., "The Flash Hydropyrolysis of Lignite and Subbituminous Coals to both Liquid and Gaseous Hydrocarbon products", American Chemical Society National Meeting, Fuel Chemistry Division Preprints, 24, No.3, 52 (1979).
16. Qader, S.A., Haddadin, R.A., Anderson, L.L., and Hill, G.R., "Coal Can Also Yield Liquid Fuels", Hydrocarbon Processing, 48, No.9, 800 (1969).
17. Qader, S.A., "Catalytic Hydrosolvation Process Converts Coal to Low Sulfur Liquid Fuel", Energy Sources, 3, No.3/4, 323 (1978).

Table 1. Analysis of Utah Coal

<u>Proximate Analysis, Wt. %</u> (Dry basis)		
Volatiles	:	46.8
Fixed Carbon	:	46.5
Ash	:	6.7
<u>Ultimate Analysis, Wt. %</u> (Dry basis)		
Carbon	:	81.22
Hydrogen	:	5.99
Nitrogen	:	1.61
Sulfur	:	2.41
Oxygen (By difference)	:	9.18

Table 2. Analysis of Coals

<u>Proximate Analysis, Wt. %</u> (Dry basis)	Subbituminous Coal (Wyoming)	Bituminous Coal (Kentucky #6 and #11)
Volatiles	: 43.22	46.43
Fixed Carbon	: 50.55	44.17
Ash	: 6.23	9.40
<u>Ultimate Analysis, Wt. %</u> (Dry basis)		
Carbon	: 70.21	73.44
Hydrogen	: 4.94	5.30
Nitrogen	: 1.05	1.21
Sulfur	: 0.71	3.35
Oxygen (By difference)	: 16.86	7.30

Table 3. Analysis of HBR Products

<u>Reaction Conditions</u>		
Temperature	:	550°C
Pressure	:	400 psi
Reaction time	:	10 minutes
<u>Liquid product</u>	<u>Catalytic</u>	<u>Non-Catalytic</u>
Sp. gr. at 25°C	: 0.9915	-
Sulfur, Wt. %	: 0.42	1.24
Nitrogen, Wt. %	: 0.68	1.34
Light oil, Wt. % (-200°C)	: 18.0	3.0
Middle distillate, Wt. % (200-450°C)	: 72.0	28.0
Heavy liquid, Wt. % (+450°C)	: 10.0	69.0
<u>Gaseous product</u>		
Methane, Vol. %	: 11.0	28.0
Ethane, Vol. %	: 24.0	40.0
Propane, Vol. %	: 36.0	17.0
Butanes, Vol. %	: 29.0	15.0

Table 4. FBR Test Conditions

Wt. of coal in each test, g	:	130
Wt. of catalyst in each test, g	:	145
Size of coal, Tyler mesh	:	35-60
Size of catalyst, Tyler mesh	:	60-140
Fluidization velocity, ft./sec.	:	0.45
Temperature, °C	:	550
Pressure, PSI	:	2000
Reaction time, min.	:	20

Table 5. FBR Material Balance
(daf Coal)

		Subbituminous Coal	Bituminous Coal
<u>Input, g.</u>			
Coal	:	100.0	100.0
Hydrogen	:	<u>2.5</u>	<u>3.8</u>
TOTAL		102.5	103.8
<u>Output, g.</u>			
Liquid	:	32.6	42.7
Gas (Includes H ₂ S and NH ₃)	:	12.3	17.0
Water	:	3.5	5.3
Solid	:	54.1	38.8

Table 6. Analysis of FBR Liquid Product

		Subbituminous Coal	Bituminous Coal
Sp. gr., 25°C	:	1.02	1.04
Sulfur, wt.%	:	0.38	0.41
Nitrogen, wt.%	:	1.04	1.11
Light oil, wt.% (-200°C)	:	15.0	17.0
Middle distillate, wt.% (200-450°C)	:	60.0	69.0
Benzene insolubles, wt.%	:	9.1	6.1

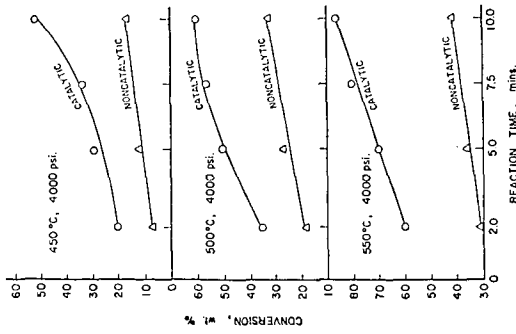


FIGURE 3. EFFECT OF TEMPERATURE AND REACTION TIME ON CONVERSION

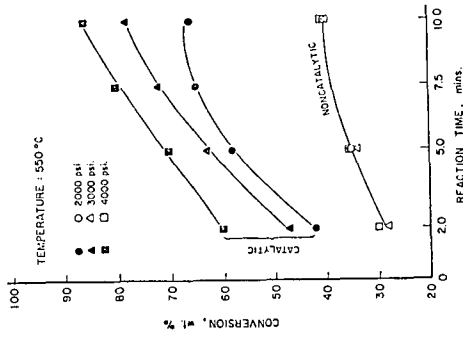


FIGURE 4. EFFECT OF PRESSURE AND REACTION TIME ON CONVERSION

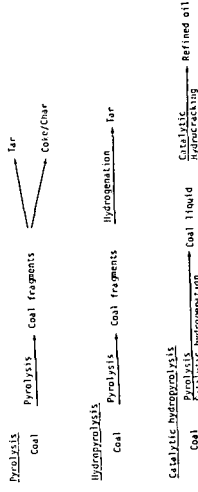


FIGURE 5. MECHANISM OF CATALYTIC HYDROLYSIS

THE APPLICATION OF FT-IR AND SOLID STATE ^{13}C NMR
TO THE CHARACTERIZATION OF A SET OF VITRINITE CONCENTRATES

D.W. Kuehn, A.Davis, R.W. Snyder, M. Starsinic and P.C. Painter

The Pennsylvania State University, University Park, PA 16802

J. Havens and J.L. Koenig

Case Western Reserve University, Cleveland, Ohio 44106

INTRODUCTION

In a recent review of coal structure Neavel (1) remarked that coal is analogous to fruitcake in that it is an aggregate of different and distinguishable components. Consequently, the characterization of coal structure (or for that matter, fruitcake) demands a recognition and investigation of the separate components, macerals. For most U.S. coals the major maceral type present is vitrinite, so that an understanding of many structure/property relations will ultimately depend on a knowledge of the structure of this maceral. As part of a systematic study of the variability of coal properties within a single seam, a set of vitrinite concentrates has been obtained from samples taken from the Lower Kittanning seam (2). This seam is particularly interesting because of its broad extent and the range of environments by which it is thought to have been affected. However, even though the far from trivial task of obtaining and storing these maceral concentrates under optimum conditions has been accomplished (2), there remains the formidable task of structural characterization.

Because of the heterogeneous, non-crystalline, largely insoluble nature of coal, it is practically impossible to apply the traditional methods of organic and physical chemistry to structural characterization work. Such methods essentially rely on the separation and identification of the constituent simple molecules of a complex system. In fact, for coal it is a notoriously difficult task to obtain reliable data on even the most fundamental property, the average molecular weight and the molecular weight distribution of the macromolecular constituents. Consequently, the most useful information concerning coal structure that we can reasonably expect to obtain is a quantitative identification of the molecular types of hydrocarbons present (eg aromatic and aliphatic carbon) and the type and distribution of specific functional groups (aliphatic CH , CH_2 and CH_3 ; phenolic OH , alkyl OH , carbonyl etc). It is precisely this information that spectroscopic methods are uniquely capable of elucidating.

Spectroscopic techniques have been widely applied to the study of coal, but have met with only limited success (3-6). Advances in spectroscopic instrumentation however, should allow us to obtain new insights into coal structure. Of particular significance is the recent application of Fourier transform infrared (FT-IR) spectroscopy (7-17) and solid state ^{13}C NMR spectroscopy, using magic-angle spinning in conjunction with cross-polarization and high power decoupling (18-21). In this communication we will consider the initial results of applying these two techniques to the set of vitrinite concentrates mentioned above.

SAMPLE CHARACTERISTICS

A set of 24 vitrinite concentrates were selected for initial study. These samples have been characterized by a number of methods and an extensive body of basic data has been reported (reference 2 and subsequent reports) Space does not permit reproduction of all of this data here. However, Neavel (1) has pointed out the critical importance of reporting reflectance values and the petrographic analysis of coals on which structural studies are performed. Accordingly, a plot

of reflectance as a function of carbon content of the concentrates used in this study is shown in Figure 1. Petrographic analysis of the concentrates demonstrated that most were 95-96% vitrinite with one or two higher (up to 98%) and one odd sample that was significantly lower (88% vitrinite).

TYPE OF INFORMATION THAT CAN BE OBTAINED FROM FT-IR AND ^{13}C NMR

Both FT-IR and ^{13}C NMR have already been used to obtain valuable information concerning coal structure. However, in many ways these techniques are still being developed and it should be possible to obtain new information as instruments and methodology are improved. In this section we will briefly describe the type of complementary information that can be obtained from each method and anticipate areas where we believe advances can be made.

Typically, infrared spectroscopy is sensitive to specific functional groups. The spectra of three of the vitrinite concentrates, chosen so as to represent samples of different rank, are presented in Figure 2. Four regions of the spectrum have been used to obtain quantitative information; the O-H stretching region near 3400 cm^{-1} , the aromatic C-H stretching modes between 3100 and 3000 cm^{-1} , the aliphatic C-H stretching modes between 3000 and 2800 cm^{-1} , and the aromatic C-H out-of-plane bending modes between 900 and 700 cm^{-1} .

The central problem with infrared spectroscopic studies of coal is the absence of reliable extinction coefficients (relating band intensities to the concentration of the corresponding functional group). Usually, the integrated intensity in an entire region of the spectrum (for example the aliphatic C-H stretching modes) is used and the extinction coefficients of individual bands are thus averaged. Calibration has in the past most often been based on model compound work or on proton magnetic resonance studies of coal extracts. More recently, Solomon (16,17) has equated the concentration of hydrogen containing functional groups to the total hydrogen determined by elemental analysis in order to obtain extinction coefficients. We have previously discussed the problems associated with infrared analysis (22,23), the most critical of which would appear to be the use of entire regions of the spectrum rather than individual bands. It may be that there is no viable alternative to this approach, but one possibility is to use well-defined curve resolving methods. We have previously reported (22,23) the use of such procedures in distinguishing the products of acetylation. This has allowed us to separately determine phenolic OH, alkyl OH and NH groups. We have recently applied these methods to the aromatic C-H out-of-plane bending modes between 900 and 700 cm^{-1} . These results will be considered below in the context of the analysis of vitrinite concentrates.

In most of the solid state ^{13}C NMR results reported to date, including those utilizing magic angle spinning and cross-polarization (18-21), only two broad bands are usually discerned, one for aromatic carbon and one for aliphatic. A careful examination of these spectra reveals the presence of shoulders, but the signal to noise ratio is such that they are not well defined. Nevertheless, the spectra allow useful estimates of the degree of aromaticity, f_a , to be obtained. We have recently applied to coal studies a spectrometer with a static field of 3.5T , approximately 2.5 times the field strength for which most ^{13}C spectra of solid coals have been reported. The resulting increase in sensitivity and potential resolution are considerable, as demonstrated by the spectrum of a vitrinite concentrate shown in Figure 3. Shoulders are clearly visible on both the aromatic and aliphatic peaks and can be readily assigned using appropriate polymer model compounds. We have previously reported the surprising but satisfying similarities between the infrared spectra of certain phenolic resins and coal (22). These materials should also be an important aid in assigning shoulders in the aromatic and aliphatic resonances of coals. The spectrum of a simple phenol-formaldehyde resin and a phenol/dihydroxynaphthalene-formaldehyde copolymer are also presented in Figure 3. Based on the known structure of these polymers a

number of assignments can be made. For example, in the model compounds aromatic carbons directly attached to hydroxyl groups resonate near 153 ppm and this agrees well with a low field shoulder on the aromatic resonance of vitrinite concentrates. This assignment can also be confirmed by acetylation studies. The ^{13}C NMR spectrum of a coal before and after acetylation is presented in Figure 4, together with a difference spectrum. A negative peak centered near 155 ppm indicates the loss of carbon attached to phenolic OH groups. Furthermore, the carbonyl resonance near 170 ppm and the methyl resonance near 22.2 ppm characteristic of the acetyl groups introduced into the coal can be clearly distinguished and used in conjunction with FT-IR studies of the same samples to obtain quantitative data.

The potential of suitable polymeric materials as models for coal is clearly outstanding. However, before proceeding to a discussion of some of the results of the analysis of vitrinite concentrates we wish to draw attention to another procedure that should be extremely useful in resolving shoulders on the broad aromatic and aliphatic resonances of coal macerals. We are presently only just starting to apply this method to coal studies, but preliminary results are sufficiently interesting to report here. It is possible to use pulse sequences to differentiate among carbons contributing to the broad aromatic and aliphatic resonances (21). Figure 5 shows the application of a sequence which incorporates a delay before the beginning of acquisition during which the proton pulse is switched off (24). The protonated carbons dephase preferentially during this period, leaving only the nonprotonated carbons to contribute to the accumulated free induction decay. It can be seen from the difference spectrum shown in Figure 5 that both the aliphatic and the high field side of the aromatic resonance consist of protonated carbons. This type of information should prove extremely valuable in conjunction with FTIR studies, where bands due to various aliphatic groups (CH , CH_2 and CH_3) and aromatic hydrogen arrangements (lone C-H, two adjacent C-H etc.) can be observed. It should be noted that weak spinning sidebands are observed in this spectrum. These arise when the magic-angle rotation rate is less than the chemical shift anisotropy, as is almost always the case for the aromatic resonances of coal. The contribution of these sidebands can be accounted for by various methods, but recently a pulse sequence has been introduced which allows elimination of first order sidebands (25). Both this pulse method and a correction based on the observed intensity of the high field aromatic sideband have been applied to coal studies. The aromatic carbon fraction f_a was determined to be the same.

ANALYSIS OF VITRINITE CONCENTRATES

Our initial aim in these studies is to correlate the concentration of various functional groups to rank parameters. In preliminary work we plotted the area of bands assigned to specific functional groups against %C (dmmf). A typical result is shown in Figure 6, where the area of the 1770 cm^{-1} band in the acetylated vitrinite concentrates has been used. This band area is a measure of the concentration of phenolic OH groups (22, 23). We found much less scatter when our spectroscopic data was plotted against reflectance, as illustrated in Figure 7. It can be seen that the concentration of phenolic hydroxyl groups drops off in an almost linear fashion with increasing rank of the coal. A band at 1740 cm^{-1} representing alkyl OH concentration (22, 23) displays precisely the same behavior, but its intensity is almost exactly half of the 1770 cm^{-1} band. (In fact, a plot of the 1770 cm^{-1} band against the 1740 cm^{-1} band is linear). Conversion factors relating the intensities of these bands have been determined (26) and total OH concentration, (measured as % O as OH) for the lowest rank coal shown in Figure 7 is about 6%.

In order to determine the concentration of aliphatic and aromatic CH groups as a function of rank equivalent extinction coefficients need to be determined. Values are available in the literature and we have applied similar calibration procedures. We have little faith in the results, however. There are a number of reasons for

this, the most important of which is that entire areas of the spectrum are used for measuring aliphatic and aromatic areas, as we noted in the introduction to this work. As the bands in these regions may each be independently related to rank parameters considerable scatter in the results can be anticipated. This is precisely what we observe, as shown in Figure 8. The aliphatic C-H stretching and aromatic out-of-plane bending modes ($900-700\text{ cm}^{-1}$) form almost a "scatter-shot" pattern. Of course this behavior could represent incompetent sample preparation and errors in methodology on our part, but the evidence indicates otherwise. The aromatic C-H stretching mode shows a nice consistent trend to increasing values with increasing rank. (Unfortunately, because this band is weak it is not the most useful for quantitative work). Furthermore, if we consider individual bands, carefully curve resolved using precisely defined criteria (22,23), then a relationship to rank of aliphatic and aromatic C-H groups to rank emerges. For example, Figure 9 shows the intensity of the 2853 cm^{-1} mode, representing aliphatic CH_2 groups, as a function of reflectance. The concentration of these groups clearly decreases with increasing rank. Similarly, certain bands in the aromatic C-H out-of-plane bending region increase in intensity as a function of the rank of vitrinite rank, as shown in Figure 10 using the 753 cm^{-1} band (4 adjacent aromatic C-H groups) as an example. Consequently, we can conclude that the scatter in the results observed using integrated intensities of entire spectral regions makes a major contribution to poorly defined behavior as a function of rank. However, if we consider individual bands assigned to specific functional groups, a pattern of behavior emerges.

One other reason for the scatter in the results obtained by plotting the integrated intensity of the aromatic C-H out-of-plane bending modes became apparent from our curve-resolving work. Also shown in Figure 10 is a plot of the intensity of a band near 830 cm^{-1} as a function of reflectance. Clearly, this band behaves differently to the 753 cm^{-1} band. The curve resolved $900-700\text{ cm}^{-1}$ region of the spectrum of a typical vitrinite concentrate is shown in Figure 11. (The initial positions and half widths of the bands were initially well defined using derivative techniques, as discussed previously (22,23), so that we can be reasonably confident that the bands shown in Figure 11 actually exist and are not artifacts of the curve resolving procedure). Bands at 801, 815 and 864 (assigned to 3 adjacent, 2 adjacent and lone aromatic C-H groups, respectively) display the same trend with rank as the 753 cm^{-1} band shown in Figure 10. However, the 785 cm^{-1} band displayed behavior similar to the 830 cm^{-1} band. We suggest that these bands have at least a partial contribution from CH_2 rocking modes that are expected to appear in this region of the spectrum. We are presently synthesizing phenolic resins that will allow us to assign these modes with more certainty. However, if we plot the total intensity of the aromatic out-of-plane bending modes, less the contribution of the 830, 785 cm^{-1} bands, against reflectance, a good correlation to rank emerges, as shown in Figure 12.

One result of these studies is that there is clearly an increase in aromatic C-H and loss of phenolic OH as a function of increase in rank. In fact, these two trends are related, as shown in Figure 13, where the area of the acetylated phenolic OH band (1770 cm^{-1}) is plotted against the total area of the $900-700\text{ cm}^{-1}$ out-of-plane modes (less the contribution of the 830, 785 cm^{-1} bands). Of course, there is not simply a straight replacement of phenolic OH by aromatic C-H with increasing rank, as the ^{13}C NMR results show an increasing degree of aromaticity with reflectance, as shown in Figure 14. (At the time of writing not all of the samples had been characterized by NMR).

Although these results demonstrate the trends in the concentration of specific functional groups in vitrinite concentrates as a function of rank, there is obviously additional work required to convert infrared band intensities to a quantitative measure of specific functional groups. In this respect we are pursuing the use of polymer model compounds and ^{13}C NMR pulse methods, which should provide the necessary data. It was shown above that the contribution of protonated carbons to

the NMR spectrum can be determined by such methods, allowing a quantitative determination of aromatic C-H. This can then be used to calibrate the intensities of the aromatic C-H out-of-plane bending modes.

ACKNOWLEDGEMENTS

The authors gratefully acknowledge the financial support of the Department of Energy under contract No. DE-AC22-OP30013 and the Penn State Cooperative Program in Coal Research.

REFERENCES

1. Neavel, R.C. Coal Structure and Coal Science: Overview and Recommendations, Chapter 1 in Coal Structure, Advances in Chemistry Series No. 192. (M.L. Gorbaty and K. Ouchi, editors).
2. Davis, A. "A data base for the analysis of compositional characteristics of coal seams and macerals", Quarterly Technical Progress Report, May-July 1980, D.O.E. contract DOE - 30013-2.
3. Friedel, R.A. in Applied Infrared Spectroscopy, p. 312, Edited by Kendall, D. N., Reinhold, New York (1966).
4. Dryden, I.G.C. in 'The chemistry of coal utilization' (H.H. Lowry, Ed.) Suppl. Vol. John Wiley and Sons, New York, p. 232 (1963).
5. Speight, J.P. Applied Spectroscopy Reviews (ed. E.G. Brame, Jr.) 5, 211 (1971).
6. Speight, J.G. in 'Analytical Methods for Coal and Coal Products', (C. Karr, Jr. ed.), volume II, 75 (1978) Academic Press.
7. Painter, P.C., Coleman, M.M., Jenkins, R.G., Whang, P.W. and Walker, P.L., Jr., Fuel, 57, 337 (1978).
8. Painter, P.C., Coleman, M.M., Jenkins, R.G., and Walker, P.L., Jr. Fuel, 57, 125 (1978).
9. Painter, P.C., Snyder, R.W., Youtcheff, J., Given, P.H., Gong, H. and Suhr, N., Fuel 59, (1980).
10. Painter, P.C., Stepusin, S., Snyder, R.W. and Davis, A. Applied Spectroscopy (In Press).
11. Painter, P.C., Youtcheff, J. and Given, P.H., Fuel, 59, 523 (1980).
12. Painter, P.C. and Coleman, M.M., Fuel, Vol. 58, 301 (1979).
13. Painter, P.C., Yamada, Y., Jenkins, R.G., Coleman, M.M. and Walker, P.L., Jr., Fuel, Vol. 58, 293 (1979).
14. Painter, P.C., Snyder, R.W., Pearson, D.E. and Kwong, J., Fuel 59, 282 (1980).
15. Painter, P.C., Coleman, M.M., Snyder, R.W., Mahajan, O., Kamatsu, M. and Walker, P.L., Jr., Applied Spectroscopy (In Press).
16. Solomon, P.R. ACS Division of Fuel Chemistry Preprints 24 #3, 184 (1979) and Advances in Chemistry series #192, 95 (1981).
17. Solomon, P.R. Paper presented at meeting, Chemistry and Physics of Coal Utilization, Morgantown, WV, June 2-4 (1980), to be published.
18. G.E. Maciel, V.J. Bartuska, and F.P. Miknis, Fuel 58, 391 (1979).
19. H.A. Resing, A.N. Garroway, and R.N. Hazlett, Fuel 57, 450 (1978).
20. E.P. Miknis, G.E. Maciel, and V.J. Bartuska, Org. Geochem. 1, 169 (1979).
21. F.P. Miknis, M. Sullivan, and G.E. Maciel, Org. Geochem., in press.
22. Painter, P.C., Snyder, R.W., Starsinic, M., Coleman, M.M., Kuehn, D. and Davis, A., Applied Spectroscopy, 35, 475 (1981).
23. Painter, P.C., Snyder, R.W., Starsinic, M., Coleman, M.M., Kuehn, D. and Davis, A., Adv. Chem. Ser. (to be published).
24. Frey, M.H. and Opella, S.J., J.C.S. Chem. Comm. 474 (1980).
25. Dixon, W.T. at the 22nd Experimental NMR Conference, Asilomar, CA (1981).
26. Snyder, R.W. and Painter, P.C. (to be published).

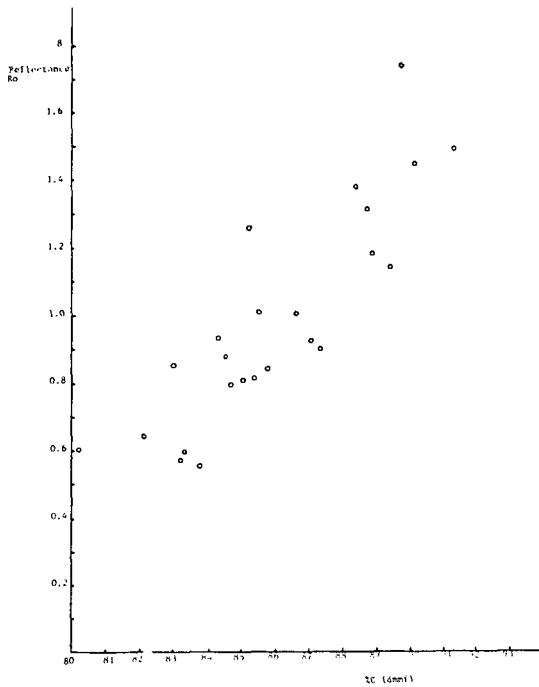


Figure 1. Plot of reflectance (Ro) values vs % C (dmmf) for a set of vitrinite concentrates.

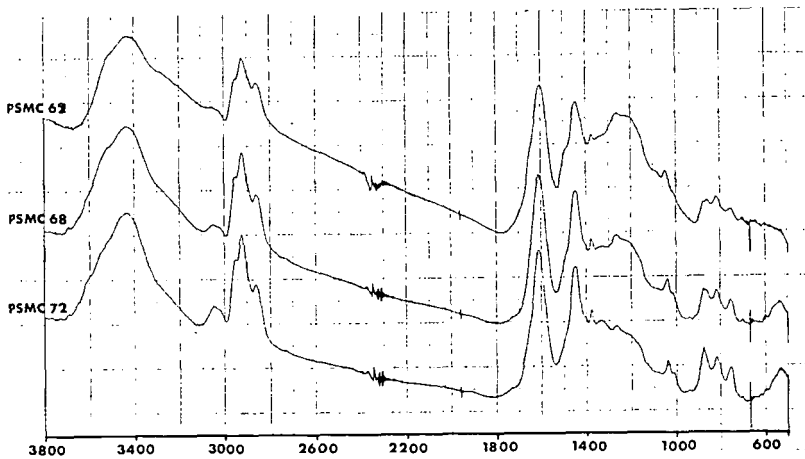


Figure 2. FT-IR spectra of three vitrinite concentrates obtained on a Digilab FTS 15B instrument (400 scans at 2 cm^{-1} resolution). Top to bottom, PSMC 67 (83.22% C dmmf), PSMC 68 (87.04% C dmmf), PSMC 72 (88.74% C dmmf).

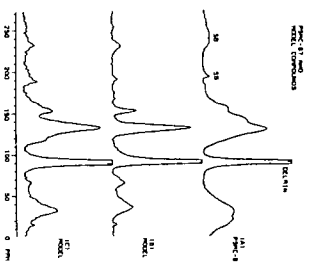


Figure 3. ^{13}C spectra of PSIG 67 (A) and model compounds.
 B: phenol-formaldehyde resin; C: phenol/dihydroxybiphenylene-formaldehyde copolymer (Spectra recorded on a Nicolet ND 150 instrument).

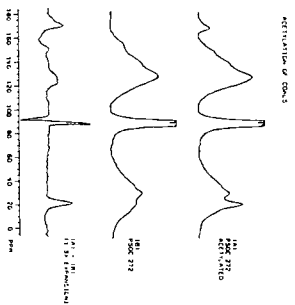


Figure 4. Spectra illustrating changes occurring in ^{13}C NMR spectra of acetylated coals.

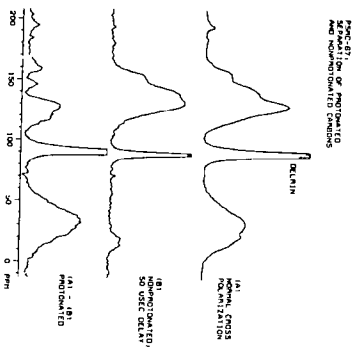


Figure 5. Spectra showing the isolation of protonated and nonprotonated carbons for a maceral, PSIG-67. Spectrum (B) is obtained by allowing the carbon spins to dephase for 50 msec by coupling to nearby protons before the beginning of acquisition. Digital subtraction is then performed to isolate the protonated carbons.

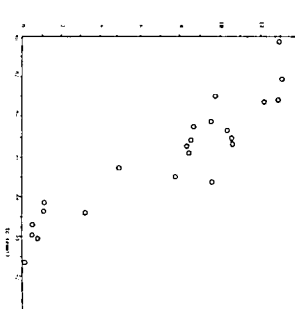


Figure 6. Plot of area of 1770 cm^{-1} band in acetylated vitrinites (proportional to phenolic OH content) vs % C (dmm).

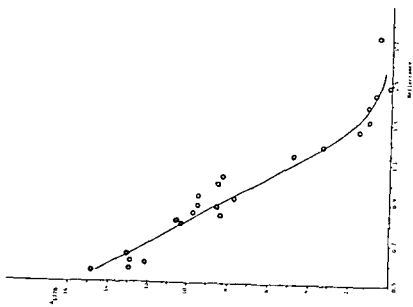


Figure 7. Plot of area of 1770 cm^{-1} band in acetylated vitrinites vs. reflectance (R_0).

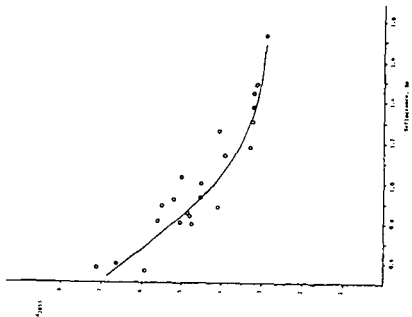


Figure 9. Plot of area of 2853 cm^{-1} band (aliphatic CH_2 mode) vs reflectance (R_0).

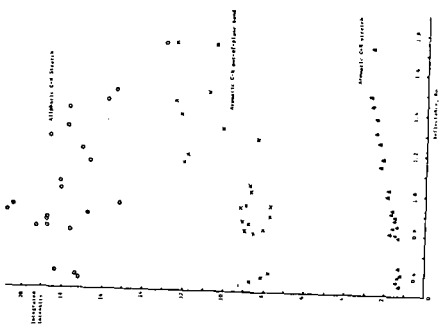


Figure 8. Plots of (top to bottom) integrated area of aliphatic C-H stretching modes; integrated area of aromatic C-H out-of-plane bending modes; integrated area aromatic C-H stretching modes vs reflectance (R_0).

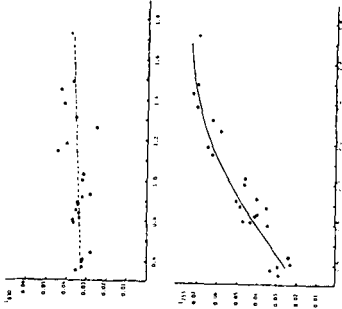


Figure 10. Top: Plot of peak height of 830 cm^{-1} band vs reflectance, (R_0) Bottom: Plot of peak height of 753 cm^{-1} band vs reflectance, (R_0)

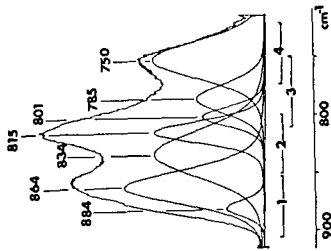


Figure 11. Curve resolved bands in the 900 to 700 cm^{-1} region of the FT-IR spectrum of a vitrinite concentrate.

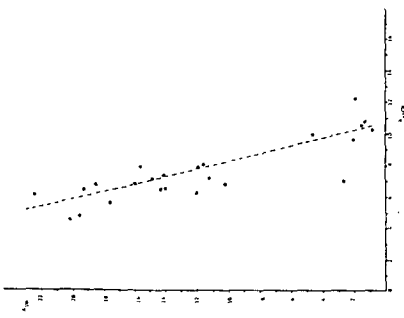


Figure 13. Plot of area 1770 cm^{-1} band in acetylated vitrinites (a measure of phenolic OH content) vs area of aromatic C-H out-of-plane bending modes (excluding 830, 785 cm^{-1} bands)

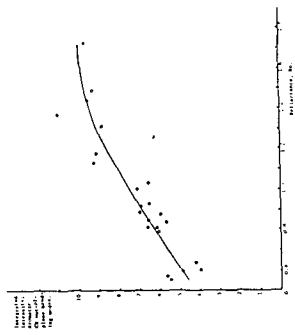


Figure 12. Plot of integrated intensity of aromatic C-H out-of-plane bending modes (excluding the 830, 785 cm^{-1} bands) vs reflectance (80).

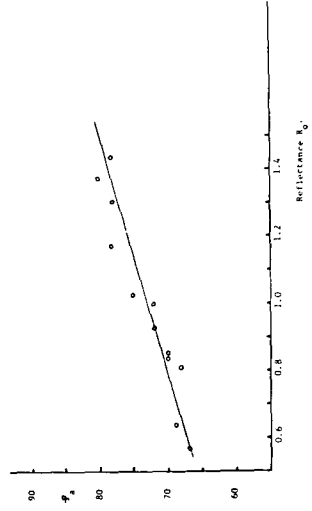


Figure 14. Plot of aromaticity f_a vs reflectance for vitrinite concentrates.

CHARACTERIZATION OF FRACTIONATED COAL
LIQUIDS BY ^{13}C NMR AND FTIR SPECTROSCOPY

K. S. Seshadri and D. C. Cronauer

Gulf Research & Development Company
P. O. Box 2038
Pittsburgh, Pennsylvania 15230

INTRODUCTION

Coal liquids derived from solvent refined processes are complex mixtures of widely differing compounds with a high proportion of nonpolar aromatic compounds. The remainder is made up of polar compounds. A knowledge of these compounds is of importance for upgrading coal liquids and producing useful chemicals.

Computer-assisted Nuclear Magnetic Resonance and Infrared Spectroscopy have opened up new possibilities for a fairly detailed characterization of coal liquids. The present trend has been to depend more on ^{13}C NMR spectrum which is often congested with multiple signals. Direct observation of ^{14}N and ^{15}N nuclei and derivitization of coal liquids to silicon and fluorine derivatives followed by the observation on ^{29}Si and ^{19}F nuclei are on the horizon. The results of spectroscopic techniques, despite their sophistication, is of little value unless assisted by chromatographic methods capable of separating coal liquids into fractions that differ according to their chemical functionality.

Several chromatographic separation schemes are described in literature including SARA⁽¹⁾ and SESC.⁽²⁾ In the latter technique the coal liquid is eluted from silica gel as the stationary phase with a sequence of solvents. We have expanded upon the analysis of combining SESC and spectroscopic techniques. Painter and Coleman⁽³⁾ have examined the IR spectra of fractions of whole coal liquid obtained by SESC. However, more detailed structural information can be obtained when the whole coal liquid is first separated into light, middle and heavy distillate and bottoms followed by SESC separation and spectroscopic analysis. We have taken this approach, and the results on middle and heavy distillate cuts are reported here.

EXPERIMENTAL

The coal liquid used in this work was from the Ft. Lewis SRC-II facility (Tacoma, WA). The nominal run conditions with Powhatan No. 5 coal were 455°C, a space time of 60 min, and a hydrogen pressure of 1250 psi. The distillate yield (C_5 -900°F) was about 40%, and the conversion of organic matter to pyridine solubles about 95%. The liquid was distilled into light distillate (C_5 -380°F), middle distillate (380-550°F), heavy distillate (550-900°F), and residue (>900°F). Further separation of these fractions was by SESC⁽²⁾ using Fisher S-662 silica gel of 60-200 mesh.

The ^{13}C NMR spectra of the fractions were recorded on a Varian FT-80A spectrometer. The solvent, CDCl_3 , was used as a field-frequency lock, and chemical shifts are in ppm downfield from internal TMS. Spectra of some of the fractions were obtained with Cr(III) acetylacetonate and by suppressing nuclear Overhauser enhancement. Infrared spectra were recorded on a Nicolet Model 7199 Fourier transform spectrometer. Each spectrum was obtained by the co-addition of 100 interferograms at 2 cm^{-1} resolution and as thin films between KBr windows.

RESULTS AND DISCUSSION

The relative quantities of the middle and heavy distillate (MD, HD) fractions are given in Table I along with the elemental analysis of the first four HD fractions. The ^{13}C NMR and FTIR spectra of individual fractions are examined in the

following sections to demonstrate the effectiveness of combining these two spectroscopic techniques with chromatographic separation.

Fraction 1MD (50.5% of Middle Distillate)

The ^{13}C NMR and FTIR spectra of this fraction are shown in Figures 1 and 2, respectively. Aromatic ring C-C vibrations result in IR absorptions near 1600 cm^{-1} and 1500 cm^{-1} . The relative intensity of the former depends on the nature of substitution on the ring. Here, the 1600 cm^{-1} band is of low intensity (vide infra) and the 3300 cm^{-1} region is flat, indicating that this fraction is composed of nonpolar aromatic compounds.

Certain features of the carbon spectrum, in particular multiple signals between $124.0\text{--}127.0\text{ ppm}$, among which the signal at 125.7 ppm being most intense, suggest that naphthalene and alkyl naphthalenes are the dominant nonpolar compounds. The signals due to quaternary carbons are in the $132.0\text{--}137.0$ region with a prominent signal at 135.1 ppm . The shielding of bridgehead or methyl-bearing carbon atoms in 1,8-dimethyl, 2,3-dimethyl, and 2-methyl naphthalenes is 135.2 or 135.4 ppm .⁽⁴⁾ Therefore, a substitution pattern is established by the signal at 135.1 ppm and the IR spectrum is in agreement with this pattern. Out-of-plane hydrogen vibrational frequencies in alkylbenzenes in the $900\text{--}670\text{ cm}^{-1}$ region correlates well with the number of adjacent hydrogen atoms in the ring, and this correlation is also applicable to naphthalene.⁽⁵⁾ Bands at 735 cm^{-1} , 780 cm^{-1} , and 805 cm^{-1} can be assigned to 4, 3, and 2-adjacent hydrogen wagging vibrations. The signals at 25.6 ppm , 21.5 ppm , and 19.2 ppm in the carbon spectrum are due to methyl carbons in 1,8-DIMeN, 2-MeN, and 1-MeN, respectively.⁽⁴⁾

The signals at 14.0 , 22.0 , 29.0 , and 32.0 ppm are due to short-chain alkanes. The signal at 14.2 ppm is definitely a doublet, and the less intense of the doublet along with the signal at 20.9 ppm could be assigned to methyl carbons in 1,2-dimethylnaphthalene. Tetralin and homologs of tetralin are also possible, accounting for signals near 29.0 ppm and 23.0 ppm .⁽⁶⁾

Fraction 2MD (3.0% of Middle Distillate)

The carbon and the IR spectra of this fraction are shown in Figures 3 and 4, respectively. This fraction, has a very low population of sp^3 carbons. In addition, the carbon spectrum has a signal at 118.9 ppm , suggesting a structure with carbon atoms in the vicinity of an oxygen nuclei. Since the IR spectrum has no evidence for phenolic compounds, aromatic ether is a possibility. The signals at 118.9 , 123.1 , 129.7 , and 157.3 ppm and their relative intensities favor diphenyl ether. The other signals at 141.2 , 128.7 , 127.2 , and 127.1 ppm have been assigned to biphenyl. About 62% of this fraction is diphenyl ether and the balance is biphenyl.

The signals in the IR spectrum also support the presence of diphenyl ether and a high aromaticity of the fraction. The intense signal at 1238 cm^{-1} is due to asymmetric C-O-C stretch. In aromatic ethers, the C-O bond has double bond character due to resonance and, therefore, higher force constant than aliphatic C-O bond.⁽⁵⁾ The signal due to the ether linkage, therefore, appears about 200 cm^{-1} higher than in aliphatic ethers. Other features of the IR spectrum are in agreement with the low population of sp^3 carbons.

Fraction 3MD (8.7% of Middle Distillate)

The carbon and the IR spectra of this fraction are shown in Figures 5 and 6, respectively. The IR spectrum has a broad absorption due to hydroxyl stretching near 3300 cm^{-1} with a narrower band at 3409 cm^{-1} . They are due to free and hydrogen-bonded NH groups and hydrogen-bonded phenolic hydroxyl groups. Therefore this fraction has phenolic and pyrrole-type compounds.

To understand the spectra of this and the subsequent fraction, reference is made to a library of carbon and IR spectra of alkyl phenols and indoles available in literature. (7,8,9)

The shielding of carbon nuclei in phenols bearing the -OH group extends from 155.0-152.0 ppm, and the exact location depends on the position of the methyl substitution. The carbon spectrum of this fraction has signals in the 153.5-151.0 ppm range, suggesting the presence of 2-, 2,5-, and 4-methylphenols. Signals around 15.5 and 15.2 ppm support this conclusion. A strong band at 752 cm^{-1} in the IR spectrum can be correlated with the vibrations of four adjacent unsubstituted aromatic H atoms. The band at 805 cm^{-1} correlates with two adjacent hydrogen wag or 4-methylphenol.

Other types of compounds that can be expected in this fraction are indoles and benzofurans. (2) The shielding of quaternary carbons in benzofuran and methylbenzofurans are in the 155.0-154.0 ppm range. Here this region has no absorptions. Moreover, furans and arylethers in our experiments are eluted along with nonpolar aromatics. Several features of the carbon spectrum agree well with indole and methylindoles. Part of the aromatic region of the carbon spectrum can be divided into five regions: (1) 130.0-126.9 ppm, (2) 124.2-119.6 ppm, (3) 116.6-113.5 ppm, (4) 111.1-108.7 ppm, and (5) 103.0-100.3 ppm. Many of the signals in these five regions are due to indoles. The signals in the fourth and the fifth regions are particularly diagnostic of indoles. They are due to carbons with an intervening carbon to nitrogen. The signals in the second region are due to carbons in the six-membered ring of the indoles and, since the shielding of three of them can be expected in this region, this region is congested. Indoles, at least those for which shielding data are available, (8) do not contribute to the third region, and signals in this region are due to phenolic compounds. The shielding of one of the quaternary carbons in indoles falls in the first region and that of the other quaternary carbon is near 136.0 ppm. The spectrum shown in Figure 5 was obtained with a short pulse delay. Therefore, the contribution to the intensity in the first region as well as the region around 136.0 ppm is marginal. Nevertheless, the first region has numerous signals, and they are indeed from protonated carbon atoms of phenolic compounds. Judging from the intensity distribution in the carbon spectrum, phenolic and the pyrrolic compounds are approximately in equal amounts.

In the saturated region of the spectrum, a strong signal is observed at 14.0 ppm. This signal is due to CH_3 carbons, and part of its intensity could be due to the CH_3 carbon in 2-methylindole. This is a reasonable structure since in the corresponding fraction of HD, carbazole has been recognized, and opening up of an aromatic ring could result in alkylindoles and possibly 2-methylindole.

Fraction 4MD (23.7% of Middle Distillate)

The carbon and the IR spectra of this fraction are shown in Figures 7 and 8, respectively. The broad absorption in the 3300 cm^{-1} region of the IR spectrum is due to hydroxyl stretching vibration. The band maximum is at 3320 cm^{-1} and it drops to the base line at almost 3600 cm^{-1} . The broad absorption is primarily due to hydrogen-bonded phenolic-hydroxyl groups. Bands due to N-H stretching vibrations also appear in this region of the spectrum. However, the carbon spectrum of this fraction has no absorption around 110.0 or 102.0 ppm, ruling out appreciable amounts pyrrolic nitrogen. Therefore, phenolic compounds are the major constituents of this fraction.

The aromatic region is again divided into appropriate regions to understand the types of phenolic compounds, namely: (1) 156.0-151.0 ppm; (2) 140.0-139.0 ppm; (3) 130.0-127.0 ppm; (4) 123.0-120.0 ppm; (5) 117.2-115.9 ppm; and (6) 114.0-111.0 ppm. The shielding of C-2 (C-6) in phenol is 115.4 ppm. However, in m-cresol relative to phenol, the shielding of C-2 is shifted downfield by about 0.8 ppm; whereas, due to the para shielding effect of the CH_3 group, C-6 is shifted upfield to

112.5 ppm. m-Cresol, 3,5-dimethylphenol (3,5-DMP), and similar structures are responsible for the sixth region. The signal at 116.4 ppm can also be associated with these structures. In the two model compounds mentioned above, the shielding of carbon bearing the CH_3 group is at 139.3 and 139.0 ppm, respectively, and indeed two signals at 139.8 and 139.5 ppm are observed in the second region. The shielding of CH_3 carbons in m-cresol, 3,5-DMP, and p-cresol are not perturbed by the $-\text{OH}$ group relative to the corresponding CH_3 carbons in methylbenzenes. The signals at 21.2 and 20.4 ppm suggest phenols with $-\text{CH}_3$ groups, one or two carbons away from the carbon bearing the $-\text{OH}$ group. The first region can be subdivided into a singlet at 155.3 and a group of signals from 154-153 ppm. The shielding of C-OH carbon in phenol, m-cresol, 3,5-DMP is 155.0, 155.0 and 155.4 ppm, respectively. In ortho- and para-cresols, in 2,6-DMP, in 2-isopropylphenol, and in 2-tert-butylphenol, the shielding is shifted upfield by about -2.8 ppm. Therefore, part of the signals in the first group suggest the presence of these compounds. The shielding of other quaternary carbon atoms in o-cresol and 2,6-DMP is at 124.0 and 123.8 ppm, and signals with reduced intensity are observed near 124.0 ppm. Most of the intensities in the fifth region are due to two signals at 115.4 and 115.5 ppm. These signals are due to C-2 and C-6 protonated carbons and are arising from ortho- and para-cresols. Other diagnostic signals in the carbon spectrum are those near 15.5 ppm. The shielding of CH_3 carbon in the immediate vicinity of the OH group is shifted upfield relative to that of CH_3 carbons in toluene or m-xylene. Therefore, these signals are in agreement with the presence of 2,6-DMP and o-cresol. Shielding of other carbons in the structures mentioned above are around 120.0 and 129.0 ppm, and resonances have been observed in these regions.

Most of the prominent signals have been assigned to specific carbons in phenolic compounds. However, the unassigned signals around 146.3, 136.4, and 28.7 ppm are conspicuous. The signal at 28.7 ppm is intense and could be due to CH_3 carbons in 2-t-butylphenol. The signal at 136.4 ppm could also be associated with this structure. The signals around 146.3 ppm are assigned to quaternary carbons in diphenols. These assignments are tentative.

The carbon spectrum has assisted in deciding the location of methyl groups relative to the OH group. Additional proof and other pertinent information can be derived from the IR spectrum. The C-C vibration of an aromatic ring can be divided into 1600 cm^{-1} and 1500 cm^{-1} vibrations. The 1500 cm^{-1} region has several components, depending on the number of alkyl substitutions. More importantly, the 1600 cm^{-1} vibration is less intense than the 1500 cm^{-1} vibrations. However, with electron donor or acceptor groups, the intensity of the former vibration is enhanced due to the dipole moment change provided by different groups. The 1600 cm^{-1} band of this fraction is more intense compared to the same band in the spectrum of fraction 1, due to the OH group on the aromatic ring.

The OH deformation and C-O stretch frequencies in the case of phenols are close to each other and, therefore, they are strongly coupled.⁽⁵⁾ They fall above 1100 cm^{-1} and extend up to 1330 cm^{-1} . A broad absorption is observed in this region due to the presence of numerous phenols. However, a well resolved signal is observed at 1156 cm^{-1} which is probably due to C-O stretch in a 3-substituted phenol.

The signals in the $650\text{--}850\text{ cm}^{-1}$ region are due to out-of-plane H vibrations and ring bending vibrations. The band at 696 cm^{-1} has been assigned to ring puckering mode and the other three bands to out-of-plane C-H vibrations. The signal at 776 cm^{-1} can be assigned to a phenol with three adjacent H atoms. In the structures that have already been considered, two adjacent H atoms and an isolated H atom are possible. The wagging vibrations of these hydrogen atoms are responsible for the bands at 856, 836, and 816 cm^{-1} .

In this fraction we have identified cresols and xylenols as major components. A small percentage of phenol cannot be ruled out. This fraction has 14% of phenolic oxygen estimated from the carbon spectrum. Among phenols, cresols and

xyleneols are in equal amounts--40% and 48%, respectively--and about 10% of phenol itself.

Fraction SMD (2.4% of Middle Distillate)

The carbon spectrum of this fraction is shown in Figure 9. An unusual feature of the carbon spectrum, is the signals at 156.0-159.0 ppm. These signals along with signals in the 152.0-146.0 ppm, an isolated signal at 136.7 ppm with satellites is a strong indication that pyridine and methylpyridines are present in this fraction. The carbon spectrum also suggests the presence of carbon nuclei in the vicinity of the OH group. The signals at 115.8 and 112.3 ppm are diagnostic of phenolic compounds. Further upfield there are prominent signals at 107.2, 107.0, 103.1, 102.7 ppm. These are probably due to carbon nuclei in the complexes of phenolic and basic nitrogen compounds.

Fraction 1HD (50.7% of Heavy Distillate)

This fraction, which is yellow in color, turns cloudy on refrigeration, suggesting the presence of waxy materials. The carbon spectrum has appropriate signals to substantiate the presence of alkanes. No attempt was made to assign the other signals to specific carbon nuclei. However, the spectrum has two signals around 111.5 ppm and a group around 156.0 ppm which are diagnostic of dibenzofuran (DBF).⁽¹⁰⁾ Since more than one signal has been observed in these regions, DBF and alkyl derivatives of DBF are possible. Subject to this assignment, the weight percent of oxygen in this fraction was obtained from the carbon spectrum (0.32%) agreeing fairly well with the results of elemental analysis (0.54%). This fraction has an equal amount of sulfur, that could be present as dibenzothiophene.

Fraction 2HD (24.5% of Heavy Distillate)

The carbon spectrum of this fraction is shown in Figure 10. Unlike the carbon spectrum of the previous fraction, only a limited number of signals are observed, partly due to the high aromaticity (92.5%) of the fraction. Signals at 131.9, 130.1, and 130.9 ppm are due to quaternary carbons. The former two have been assigned to phenanthrene and the latter to pyrene. The other signals in the spectrum support these structures. Weak signals in the spectrum are due to hydroaromatic hydrocarbons derived from phenanthrene and pyrene.

The signal at 131.9 and 130.9 ppm are of equal intensity. However, four carbons of pyrene contribute to the intensity of the latter signal; whereas, two carbons of phenanthrene are at 131.9 ppm. Therefore, phenanthrene is twice as abundant as pyrene in this fraction.

The low frequency region (900-700 cm^{-1}) of the IR spectrum is in agreement with the carbon spectrum. Bands in this region arise from C-H wagging vibration. The vibrational frequencies of C-H bonds approximately parallel to the long axis of the molecule are near 740 cm^{-1} , and those of C-H bonds approximately perpendicular to the long axis are near 850 cm^{-1} .⁽¹¹⁾ Also due to angular condensation, a characteristic band is observed between these two regions. The bands at 744 cm^{-1} and 736 cm^{-1} are assigned to C-H bonds parallel to the long axis in phenanthrene and pyrene, and those at 860 cm^{-1} and 840 cm^{-1} are assigned to CH bonds perpendicular to the long axis. The band at 810 cm^{-1} which is characteristic of C-H bending vibration in angular polynuclear aromatic hydrocarbons supports the two structures that we have selected to assign signals in the carbon spectrum.

Fraction 3HD (13.2% of Heavy Distillate)

The carbon and the IR spectra of this fraction are shown in Figures 11 and 12, respectively. The IR spectrum has a broad absorption at 3300 cm^{-1} and a narrower band at 3410 cm^{-1} , suggesting that this is analogous in composition to

fraction 2MD; that is, it has a structure with N-H linkage and phenolic compounds. The carbon spectrum has signals at 110.6, 119.20, 120.22, 123.2, 125.7, and 139.6 ppm. These match exactly with the resonances observed for carbazole.⁽¹⁰⁾ This fraction is very aromatic (93.1%) and, therefore, it is not surprising that one of the major components of this fraction is carbazole. The signals at 139.6 and 123.2 ppm appear with reduced intensity because they arise from quaternary carbons.

From the intensity of the signal at 110.6 ppm, the percentage of nitrogen is 2.3% compared to 3.27% from the elemental analysis. Therefore, most of the nitrogen in this fraction is accounted for by carbazole. Signals near 115.8 ppm and weak shoulders to signals at 110.6 ppm and 120.2 ppm suggest the presence of hydroxy aromatic compounds. However, in the absence of shielding data for hydroxy aromatic compounds with three or more rings, assignment of these signals to specific carbon nuclei has not been possible.

Fraction 4HD (7.8% of Heavy Distillate)

The carbon and the IR spectra of this fraction are shown in Figures 13 and 14, respectively. The aromaticity of this fraction is much less (61.5%) than that of the previous fractions.

The aromatic region of the spectrum is divided into four regions: (1) 157.0-150.0 ppm; (2) 147.0-132.0 ppm; (3) 132.0-125.0 ppm; and (4) 120.0-109.0 ppm. The first region has three well defined signals at 156.9, 156.2, and 154.7 ppm. The broad absorption near 3300 cm^{-1} and the enhanced intensity of 1600 cm^{-1} relative to the 1450 cm^{-1} band in the IR spectrum indicate the presence of hydroxy aromatic compounds. The shielding of carbon-bearing OH groups in phenols are in the 155-152 ppm region, whereas in naphthols and 9-hydroxyphenanthrol, the shielding of the corresponding carbon is shifted upfield to 153.0-151.0 ppm in CDCl_3 . If this trend should continue, the carbon spectrum, for example, of hydroxy-benzanthracene, should have a signal near 151.0 ppm. Therefore, signals around 156.0 ppm are somewhat surprising. This fraction has 1.3% nitrogen, and if this nitrogen is present as basic nitrogen, hydroxy basic nitrogen heterocyclics, like hydroxypyridines, have carbons with shieldings near 156.0 ppm. This possibility is unlikely since hydroxypyridines and 8-hydroxyquinoline do not have carbons with chemical shifts near 114.3 ppm. Therefore, the nitrogen is present as pyrrolic nitrogen, although there are no pronounced evidences both in the carbon and the IR spectrum for the N-H linkage.

The IR spectrum has two well defined signals at 730 cm^{-1} and 905 cm^{-1} which are characteristic of C-H wagging vibration in polynuclear aromatic hydrocarbons with four or more condensed rings. The 730 cm^{-1} is a singlet, except for a weak shoulder suggesting that PNAs are sparsely substituted. Therefore, the major portion of the sp^3 carbons are in the hydroaromatic rings, and the hydroaromatic structures account for the group of signals in the second region. The signals in the third and the fourth region arise from carbons well removed from the OH group and those in the immediate vicinity of the OH group, respectively.

These observations suggest that the hydroxyaromatic compounds in this fraction have partially hydrogenated three or more condensed rings. It is likely that in such structures the shielding of aromatic carbon bearing the OH group is near 156.0 ppm and not at 151.0 ppm as in 9-phenanthrol.

SUMMARY

The results presented here amply demonstrate that the combined results of ^{13}C NMR and FTIR spectroscopy can provide a wealth of information not only about the functional groups in coal liquids, but also details regarding the structure of molecules carrying these groups.

The first two fractions of SESC are homogeneous; they contain nonpolar aromatic compounds. Included in this category are the diaryl ethers, benzofurans, and benzothiophenes. The rest of the fractions are heterogeneous. All of them to a greater or lesser extent contain hydroxyaromatic compounds. However, fraction 3 is highly homogeneous, containing mainly phenolic compounds. The presence of phenolic compounds does not interfere with the identification of other functional groups in fractions 3 and 5 due to: (1) their low concentration and (2) high resolution of absorptions in the ^{13}C NMR spectrum. The type of functional groups in each fraction, according to the carbon and IR spectroscopic results are summarized in Table 2.

REFERENCES

1. Ruberto, R. G., Jewell, D. M., Jensen, R. K., and Cronauer, D. C., Advances in Chemistry Series, No. 151, Chapter 3, American Chemical Society, Washington, DC, 1976.
2. Farcasiu, M., Fuel 1977, 56, 9.
3. Painter, P. C., and Coleman, M. M., Fuel 1979, 58, 301.
4. Wilson, N. K., and Stothers, J. B., J. Mag. Resonance 1974, 15, 31.
5. Colthup, N. B., Daly, L. H., and Weberley, S. E., Introduction to Infrared and Raman Spectroscopy, Academic Press, New York and London, 1964.
6. Seshadri, K. S., Ruberto, R. G., Jewell, D. M., and Malone, H. P., Fuel, 1978, 57, 111.
7. Johnson, L. F., and Jankowski, W. C., Carbon-13 NMR Spectra, Wiley-Interscience, New York, 1972.
8. Breitmaier, E., Haas, G., and Voelter, W., Atlas of Carbon-13 NMR Data, Heyden, Long-Philadelphia-Rheine, 1979.
9. Shrewsbury, D. D., Spectrochimica Acta 1960, 16, 1294.
10. Seshadri, K. S., Unpublished results.
11. Jones, R. N., and Sandorfy, C., The Application of Infrared and Raman Spectroscopy to the Elucidation of Molecular Structure, Chapter IV, Volume IX, in A. Weissburger, Technique of Organic Chemistry, Interscience, New York, 1956.

Table 1

FRACTIONS OF MIDDLE AND HEAVY DISTILLATE OF
COAL LIQUID AND ELEMENTAL ANALYSIS OF HD

<u>Fraction</u>	<u>Eluent</u>	<u>Wt% of MD</u>					
1	Hexane	50.5					
2	Hexane + Benzene(15%)	3.0					
3	Chloroform	8.7					
4	Chloroform + Ether(4%)	23.7					
5	Ether + EtOH(3%)	2.4					
Losses (Volatiles)		11.7					
		<u>100.0</u>					
		<u>Wt% of HD</u>	<u>C</u>	<u>H</u>	<u>O</u>	<u>N</u>	<u>S</u>
1		50.7	90.60	8.11	0.54	0.00	0.54
2		24.5	92.18	5.91	0.31	0.10	0.47
3		13.2	81.92	7.16	3.69	3.27	0.23
4		7.8	82.25	7.40	5.54	2.03	0.12
5		2.9					
Losses		0.9					
		<u>100.0</u>					

Table 2

TYPES OF COMPOUNDS IN THE FRACTIONS OF MD AND HD

<u>Fraction</u>	<u>Type of Compounds</u>
1 and 2	Nonpolar aromatics, diaryl ethers, benzofurans, and benzothiophenes.
3	Mainly nonbasic N compounds; hydroxy aromatic compounds.
4	Hydroxy aromatic compounds.
5	Basic N compounds; hydroxy aromatic compounds.

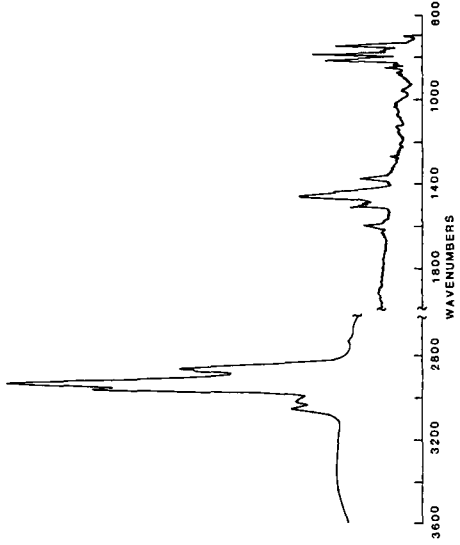


Figure 2 FTIR Spectrum of Fraction 1MD

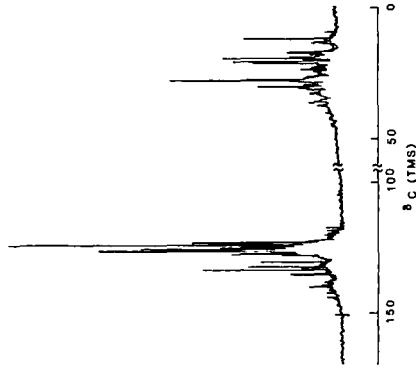


Figure 1 ¹³C NMR Spectrum of Fraction 1MD

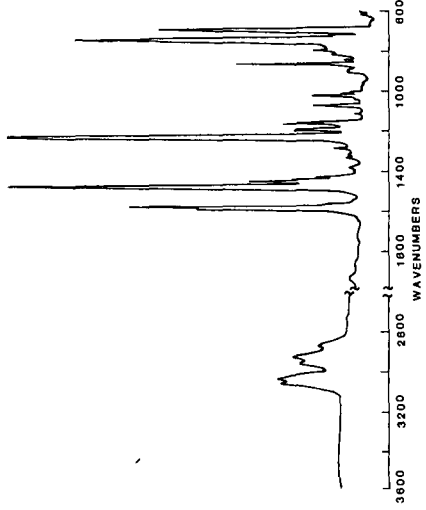


Figure 4 FTIR Spectrum of Fraction 2MD

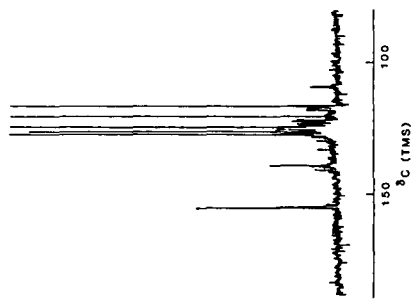


Figure 3 ¹³C NMR Spectrum of Fraction 2MD

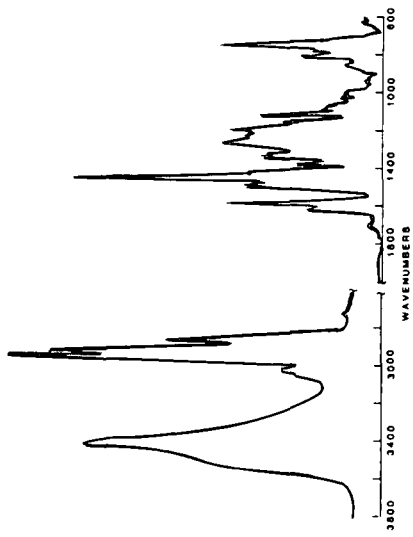


Figure 6 FTIR Spectrum of Fraction 3MD

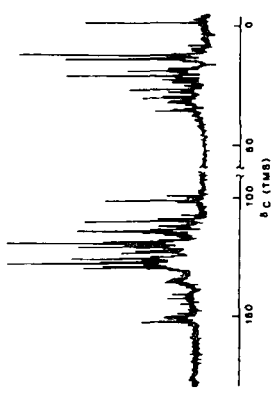


Figure 5 ¹³C NMR Spectrum of Fraction 3MD

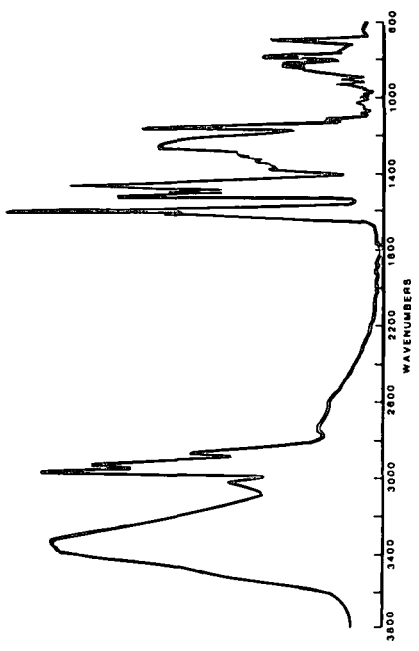


Figure 8 FTIR Spectrum of Fraction 4MD

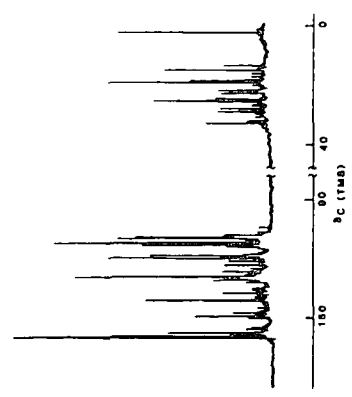


Figure 7 ¹³C NMR Spectrum of Fraction 4MD

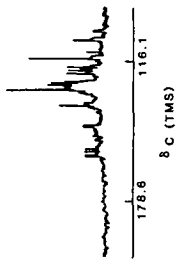


Figure 9 ¹³C NMR Spectrum of Fraction 5MD

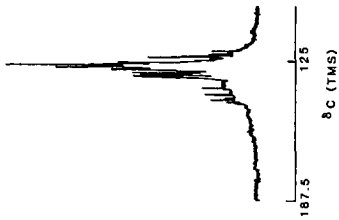


Figure 10 ¹³C NMR Spectrum of Fraction 2HD

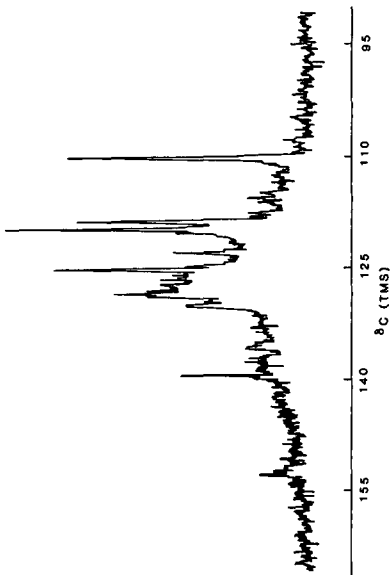


Figure 11 ¹³C NMR Spectrum of Fraction 3HD

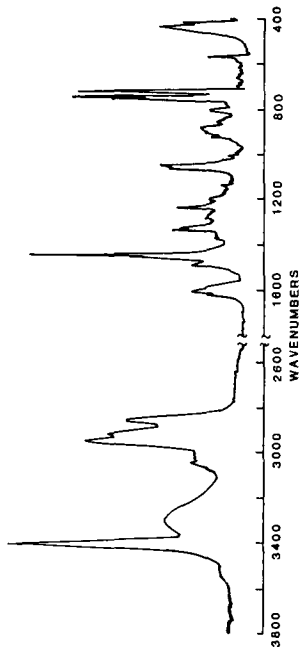


Figure 12 FTIR Spectrum of Fraction 3HD

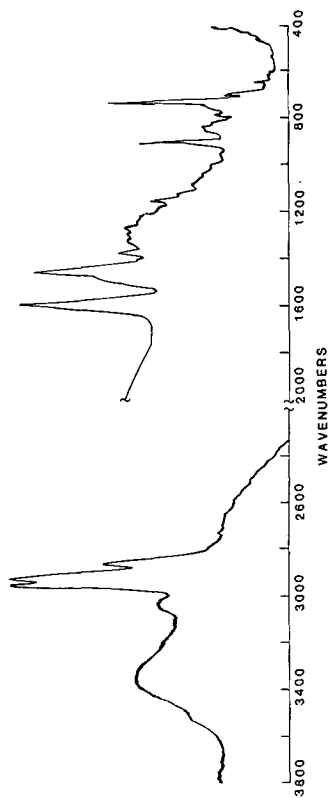


Figure 14 FTIR Spectrum of Fraction 4HD

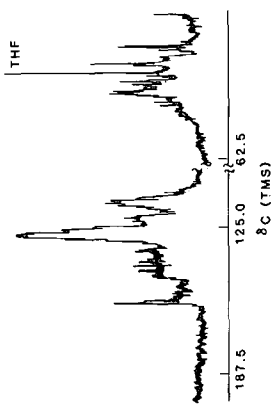


Figure 13 ¹³C NMR Spectrum of Fraction 4HD

OXIDATION AND FORMATION OF DEPOSIT PRECURSORS IN HYDROCARBON FUELS

Frank R. Mayo, S.E. Buttrill, Jr., Bosco Lan, G.A. St. John, and David Dulin

SRI International, Menlo Park, California 94025

The object of this research is to determine the mechanism of deposit formation in hydrocarbon fuels, and thus to predict and to prevent deposit formation (1). The deposits cause clogging of filters and hot fuel lines. Our premise is that such deposits, insoluble in hydrocarbons, arise from further condensation of soluble deposit precursors (2). The precursors are the oxidation products of the fuels and condensation products of these, formed in stepwise reactions. When their molecular weights and oxygen contents become high enough, they precipitate from solution (3) either on long storage or quick heating. The problems are: what oxidation products are most likely to condense; is the condensation a radical or nonradical reaction, or both; what fuels or fuel components are most likely to form precursors; and how can the reactions be prevented?

This paper describes our progress in applying field ionization mass spectrometry (FIMS) to these problems. We started with a No. 2 home heating oil (Fuel C) to represent an unstable jet turbine fuel, then used n-dodecane as a simple and common fuel component.

EXPERIMENTAL

As received, Fuel C was brown and contained so much material of high molecular weight and low solubility that it could not be used to follow the development of additional fuel precursors. It was therefore distilled at 2.3 kPa (17 torr) in a Claisen flask with a Vigreux neck. Aliquots of the distillate (10 mL) were oxidized by shaking them with air in 100-mL flasks in a bath at 130°C. Gas samples of 70 μ L were withdrawn through a septum and analyzed for O₂/N₂ by gas chromatography on a 183 x 0.32-cm stainless steel column at 0°C and 30 mL/min He flow rate. The column was packed with 13X molecular sieve.

Pure 99% n-dodecane was obtained from Phillips Chemical Company and distilled at 2.3 kPa. The first and last tenths were rejected.

Two mass spectrometers were used. In one, the whole 5- μ L fuel sample was injected through a septum into an evacuated 0.5-L glass expansion bulb of the batch inlet system. The sample vaporizes immediately and enters the field ionization source through a glass leak. Field ionization of this mixture produces molecular ions from each fuel component and gives a molecular profile of the fuel sample. A second FIMS system was used to analyze deposit precursors. A 0.5-mL sample of Fuel C was spiked with an internal standard, 10 μ g of decacyclene (molecular weight 450), then vacuum-evaporated to <100 μ L. A 5- μ L sample of the concentrate was placed in a standard mass spectrometer sample holder in the solids probe of the mass spectrometer. The probe was cooled to -50°C, introduced into the mass spectrometer vacuum system, and then warmed to 30° with continuous pumping to remove most of the remaining volatile components. The probe was then mated to the ion source. The field ionization spectrum of the residue, including deposit precursors and decacyclene internal standard, was collected with the PDP 11/10 computer system. The resulting FIMS spectra represent the composition of the least volatile components of the fuel sample including impurities. The concentrations of individual deposit precursors are calculated by comparing their intensities in the FI spectrum with that of the decacyclene standard.

Samples of oxidized dodecane were analyzed similarly, except that the internal standard was perylene (molecular weight 252). In general, the oxidation products con-

tained unoxidized fuel, which could not be entirely removed without loss of some oxidation products.

RESULTS

Fuel C. The molecular weight profile of Fuel C shows that the major components are alkanes with 10 to 14 C atoms, with a preponderance of alkylbenzenes with 3 to 5 side-chain C atoms at the low molecular weight end, alicyclics up to C₁₆ at the high end, and small proportions of a wide variety of hydrocarbons over the whole range.

Table 1 summarizes the results of one oxidation of distilled Fuel C; they show steady increases in rate of oxygen absorption (autocatalysis) and in concentration of less volatile materials.

TABLE 1. OXIDATION OF VACUUM-DISTILLED FUEL C AT 130°C

Time at 130°C (min.)	0	255	430	701
O ₂ consumed (mmol/liter)	0	6.55	13.1	32.2
Per minute ^a x 10 ²		2.6	3.7	7.0
Deposit Precursor Properties				
Concentration (ppm) ^b	74	132	2450	2600
Number Av. Mol. Wt., \bar{M}_n	435	388	355	318
Weight Av. Mol. Wt., \bar{M}_n	496	440	419	381

^aDuring preceding interval.

^bBased on total materials found by FIMS.

Figures 1 and 2 summarize FIMS data after the first two oxidation periods in Table 1. The ordinate and the numbers in the upper left corners of the figures are the percentage of the summed ion intensities. Most of the material of molecular weight ~ 250 corresponds to incorporation of one to four atoms of oxygen into fuel molecules (precursor monomers), retained because they are much less volatile than the fuel. Most of the material with molecular weights between 300 and 450 represents combinations of monomer precursors (dimers). Material of intermediate molecular weight presumably represents condensation of monomer precursors and their fragments formed by cleavage of alkoxy radicals. The figures show that the development of monomer precursors and dimer precursors, like the rate of oxygen absorption, is autocatalytic. Development of trimers can also be seen.

During the last oxidation period, the solution became lighter and a dark brown precipitate formed on the reactor walls. During this period, the concentration of precursor monomers increased sharply (these may be the oxidation products that don't condense easily), and the concentrations of dimers and trimers appear to decrease perceptibly (compared with the decacyclene standard), perhaps because they have grown and separated from the fuel mixture.

The precipitate that formed, after washing with hexane and drying, weighed about 3 mg/g of initial fuel. Acetone extraction of this residue gave 0.137 mg of extract/g initial fuel; its \bar{M}_n in N-dimethylformamide was ~ 600. It therefore appears that the deposits precipitated more because of their oxygen and heteroatom contents than because of their high molecular weights.

Although the research described above provides excellent evidence for the deposit formation by stepwise condensation of deposit precursors, the data give us little

indication of the chemical structures or mechanisms involved. However, there is an indication in Figure 2 of a problem that becomes much more obvious with n-dodecane. All the principal components should have even mass numbers, as will all compounds of C, H, and O (but not N). However, 1.1% of natural C is ^{13}C , and so for any C_{12} compound, about 13% of the molecules will contain one ^{13}C . Therefore, all the major peaks will have an obvious satellite with mass number one unit greater. Figure 2 shows that the oxidized products have more than the expected 12 to 20% of materials with odd mass numbers (in the spaces between the peaks with even mass numbers). Odd mass numbers in C, H, and O compounds, except that due to ^{13}C , mean that fragmentation of parent molecules has occurred in the FIMS.

n-Dodecane. To eliminate the multicomponent problem with Fuel C, we investigated the oxidation of n-dodecane. Because the extents of evaporation varied before taking FIMS data, the absolute concentrations of products vary considerably in the three spectra. Dodecane (mass number 170 and its satellite at 171) predominated in the FIMS concentrates but are irrelevant and neglected in this discussion. Table 2 therefore lists the 12 strongest other peaks for each spectrum in order of their relative intensities.

Table 2-A shows that with the untreated oxidation product, the three strongest peaks, and 7 of the 12 strongest, have odd mass numbers. These must represent molecule fragments, uncommon from hydrocarbons, and so we examined the FIMS of known 3-dodecanol and 2-dodecanone. The dodecanol shows little of the parent ion (186), but it decomposes in the FIMS to give six principal significant products: 50 mol % is dodecyl (169 by loss of OH); 20% is decyloxy (157 by loss of ethyl); 18% is dodecene (168 by loss of water); 13% is dodecanone (184 by loss of H_2); 5% is dodecyloxy (185 by loss of H); and 4% is undecyloxy (171 by loss of methyl). The second and last products are probably specific for 3-dodecanol, leaving dodecyl as the principal product from mixed dodecanols. 2-Dodecanone is relatively stable. The parent peak (184) and its ^{13}C satellite (185) comprise >90% of the observed ions. An effort was made to avoid fragmentation by acetylating, methylating, or benzoylating pure higher alcohols but only 6-tridecyl benzoate gave mostly the parent peak.

In the first oxidation of dodecane in Table 2, 120.6 mmol of dodecane absorbed 1.35 mmole oxygen, 1.12 mol %, in 22.3 h at 130° . Part of the product was subjected to FIMS directly, part was heated for one hour at 180°C in the absence of oxygen to destroy peroxides. A major portion was treated with aqueous KI and acetic acid to decompose peroxides; the liberated iodine corresponded to 34% yield of hydroperoxide on the oxygen absorbed. Part of the KI-treated products was then heated for one hour at 180° in the absence of air, and another was benzoylated with 20% excess benzoyl chloride in pyridine. Even after purification, benzoic acid, benzoic anhydride and benzoyl ions gave major FIMS peaks, which are neglected.

In the oxidation products, the 182 and 183 peaks are probably fragments from dodecyl hydroperoxides because their proportions decrease upon heating and are succeeded by alcohol-derived peaks at 169 and 185. The 184 parent peak for dodecanone is little changed on heating. The 169 peak is associated with both alcohol and hydroperoxide but must come only from alcohol in the heated product. The new 203 peak in the heated sample arises from peroxides with >2 oxygen atoms. Mass numbers 194 to 203 and 213 to 217 are closely related products corresponding to gain or loss of H atoms by alcohols and ketones; the borderline between the parent compounds is fuzzy. Volatility considerations must favor the higher oxygen compounds in the data observed for C_{12} products.

Table 2-A shows other effects of heating; the appearance of butyl, pentyl and hexyl radicals (57, 71, 85) in the FIMS of the heated sample and the displacement of the 196, 197, and 217 peaks from the 12 most prominent products after heating. The small radicals can come from cleavage in the FIMS of alcohols or hydroperoxides in the unheated oxidation products,

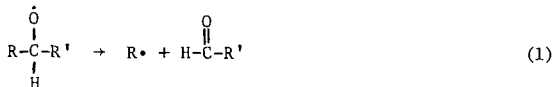


TABLE 2

PRINCIPAL IONS FROM 3-DCDECANOL, 2-DODECANONE, AND OXIDATION PRODUCTS OF n-DODECANE

Ranking	No oxidation		First oxidation				benzoylated	Second oxidn. ^e Ph ₃ P
	3-Do-decanol	2-Do-decanone	Un-treated	Heated to 180°C	KI + AcOH	KI + heating		
A. Ranking for all mass numbers								
1	169	184	183	169	182	182 _c	290 ^d	169
2	157 ^a	185	169	183	183	264 _c	98 ^d	184
3	168	182	199	184	169 _b	296 _c	184	168
4	131	122	184	185	311 _b	183 _c	182	182
5	184	183	182	203	370 _b	328 _c	198 ^d	185
6	185	150	185	198	256 _b	256 _b	194 ^d	157
7	171 ^a	155	197	57	184	184	370 _d	143
8	373	170	198	182	185	169 _c	189 ^d	129
9	186	186	217	199	198 _b	256 _c	203 ^d	
10	183	136	370	85	297 _b	266 _c	302 ^d	
11	182	156	196	71	283 _b	213 _c	185	
12	198	108	99	58	371 _b	196	183	
B. Ranking for mass numbers ≥ 337 only.								
1			370	337 ^f	370	450 ^g		
2			385	385	371	466		
3			399	399	385	436		
4			371	353	399	366		
5			337	367	337	385		
6			367	371	469	337		
7			369	355	355	340		
8			353	366	353	338		
9			355	370	339	365		
10			450	338	367	399		
11			436	351	338	451		
12			366	369	366	367		

Suggested identifications of ions above:

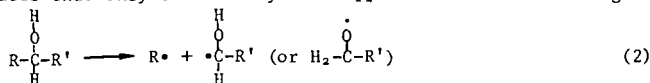
171 and below, C ₁₁ H ₂₃ O and smaller fragments	185 Dodecyl-O 186 Dodecanol	338 Dimer, C ₂₄ H ₅₀
168 Dodecene	194 to 232, mostly C ₁₂ compounds containing	350 to 466, dimer + 0 + fragments
169 Dodecyl	2 to 4 O atoms	
182 Dodecenone		
184 Dodecanone		506 Trimer, C ₃₆ H ₇₄

^a Specific products from 3-dodecanol. ^b Specific for KI.^c Appear or persist after heating KI product. ^d Peculiar to benzoilation product.

^e In 20 hours at 130°C, 7.25 g, 42.6 mmol, of n-dodecane absorbed 0.903 mmol O₂, 2.12 mol %. Hydroperoxide corresponding to 24.8% of the O₂ absorbed was found. The remainder of the product was then treated with 20% excess Ph₃P for 6 hours at 25° and then distilled at 1.7 kPa (13 torr) to remove Ph₃P and its oxide. Therefore, this sample should not contain high-boiling products.

^f Would rank 13 in Part A. ^g Peak height was 2/3 of that of the 196 peak.

but Table 2-A indicates that they come mostly from C₁₂ alcohols formed during heating:



Thus, 3-dodecanol apparently gave methyl and ethyl radicals. The short radicals probably do not come from short alcohols, which would be lost during concentration.

The KI treatment of the oxidation products was expected to decompose hydroperoxides to alcohols without forming free radicals or byproducts. However, the results indicate many byproducts, perhaps traces exaggerated by FIMS.

In comparison with the KI reduction, the triphenylphosphine reduction of the second oxidation products gives more products that are more typical of dodecanols (168, 169, 185) and thus may be a cleaner reduction. However, the absence of peaks above 190 in the triphenylphosphine products is probably due to distillation before FIMS.

The 370-371 peaks appear in several mixtures in Table 2-A and are prominent in all the mixtures in Table 2-B, except in the KI + heat group. They do not survive heating after KI treatment, but they survive benzylation and so are not associated with hydroxyl groups, even though mass number 370 corresponds to a dimer glycol.

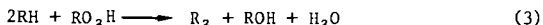
The heated products are similar to the KI products, containing considerable material of mass numbers 169, 182-185, and 198-199. However, the heated products contain more low mass number fragments and the KI products give more ions with mass number >256. Heating the KI products results in appearance or disappearance in Table 2-A of all products of mass number >256. Thus, substantial changes occur upon heating the KI product, even though there are no peroxides left, and hence nonradical reactions as well as radical reactions may lead to polymeric precursors.

Interposing the KI treatment before heating makes the dodecanone peak (182) most important, weakens or eliminates several peaks (57, 58, 71, 85, 185, 199, and 203) and forms several new ones, mostly >250.

The benzyolated KI-treated product contains more dodecyl benzoate (290) than anything else, and establishes hydroperoxide and alcohol as the major primary products. The absence of the 168 and 169 peaks shows that benzyolation of alcohol was essentially complete. The 182, 184, and 185 peaks that persist probably come from dodecanones, but in the KI-treated product, they and the 183 peak may also come from dodecanols.

Table 2-B show the relative ions concentrations from dimeric products. The most prominent also appear in Table 2-A. These products appear in groups corresponding to the dimer (338) and products containing 1, 2, and 3 additional oxygen atoms (near 354, 370, 386, and maybe 402) minus a few hydrogen atoms for formation of ketones or alkoxy radicals instead of alcohols. Starting at about mass number 399, most of the higher mass numbers must represent two dodecane residues plus oxygen plus additional carbon-containing fragments. No trimeric fragments (506 or above) have been observed, probably because of precipitation or volatility limitations. However, their absence may also be caused by low yields with dodecane, because trimers were observed with Fuel C.

We now consider the mechanism by which monomers are converted into dimeric products. The simplest condensation of dodecane by heating with a hydroperoxide would be:



The molecular weight of the C₂₄ dimer is 338, but none of this was found in an oxidation containing sufficient air. Instead, the C₂₄ products found had 2 to 4 oxygen atoms and mass numbers close to 370, 385, and 399. Thus, the dodecane oxidation products have

condensed during oxidation (whatever the mechanism) even though the parent dodecane concentration is 50 times greater than that of the oxidation products. However, the 337 ion, formed by loss of a hydrogen atom from the dimer, becomes a minor product when this oxidation product is heated and a major product in the heated portion of the oxidation in Table 2-B.

In the untreated oxidation products, the four most prominent peaks in Table 2-B correspond to a dimer plus two or three oxygen atoms and either a fourth oxygen atom or an additional carbon atom. The oxidation in Table 2, which absorbed less oxygen in more time, may have been depleted in oxygen, and tends to contain dimer units with fewer oxygen atoms and more fragments containing additional carbon atoms (436, 450).

Comparing the last two columns of Table 2-B shows that heating peroxide-free mixtures to 180° formed more compounds of molecular weight >400. Thus, there is a condensation or coupling reaction that does not depend on hydroperoxides, but probably involves other functional groups.

SUMMARY AND CONCLUSIONS

Our experimental results will now be used to formulate a general picture of deposit formation. Oxygen is required to produce deposits from hydrocarbon fuels, except at pyrolysis temperatures. For a given hydrocarbon, the process goes mainly through monomer oxidation, and coupling of these oxidation products to dimeric products. All of these are at first soluble in fuel, but as oxidation and condensation continue, the products become insoluble at molecular weights around 600. The insoluble products formed in storage probably remain soluble in good solvents (e.g., acetone), but when fuel containing soluble deposit precursors is heated, especially with a little oxygen, oxidation and condensation become rapid and precipitates form on the walls. These precipitates may at first be soluble in acetone but eventually become intractable. The oxidations are almost certainly conventional free radical chain reactions; the coupling of monomer units probably involves both a free radical coupling mechanism like Reaction 3, and a nonradical condensation (e.g., aldol (4)), in unknown proportions. Nitrogen and sulfur compounds concentrate in the precursors and deposits because they are more reactive in oxidation and condensation, and probably less soluble in fuel (5). Whether the effects of some very reactive fuel components are stoichiometric or catalytic remains to be determined.

Products and fragments between 190 and 338 (dimer) mass number must contain at least two oxygen atoms. Because peroxide links are not expected to survive FIMS, most products in this range contain two or more oxygen-functional groups. Their proportion is difficult to estimate with FIMS because of volatility differences, but the work of Jensen et al. (6) on the liquid-phase oxidation of hexadecane at 120 to 180°C shows that at least a quarter of the hydrocarbon molecules attacked contains two or more oxygen functions. Such products are more reactive than monofunctional compounds in radical-coupling and condensation reactions.

At 130°C in air, dodecane oxidizes much faster than Fuel C; it absorbs about 13.2 mmol of oxygen/mol fuel in 10 hours, compared with about 3.82 mmol for Fuel C in 20 hours. Fuel C oxidizes at a constant rate while the rate for dodecane is autocatalytic. However, by FIMS and observed deposit formation, dodecane produces fewer precursors and no visible deposits. Experiments with several Diesel fuels (to be described elsewhere) show little correlation between oxidation rate and gum formation, as measured by ASTM-D2274 before distillation. Paraffins usually predominate in fuels, but the gum formation apparently depends on the nature and amounts of other hydrocarbons, N and S compounds, and fuel history.

FIMS has been very useful for comparing fuel compositions, and for seeing the development of Fuel C deposit precursors at 130°C. Results with dodecane have been discouraging. The principal C₁₂ oxidation products, alcohols and hydroperoxides, fragment in the mass spectrometer and give similar peaks that overlap ketone peaks, probably in

different proportions, so that the primary products and their subsequent changes have been hard to identify. Yields of dimeric and trimeric precursors have been surprisingly low. Further, the relative concentrations of different compounds in the same mixture and of the same compound in different mixtures depend somewhat on the evaporation before the FIMS is taken.

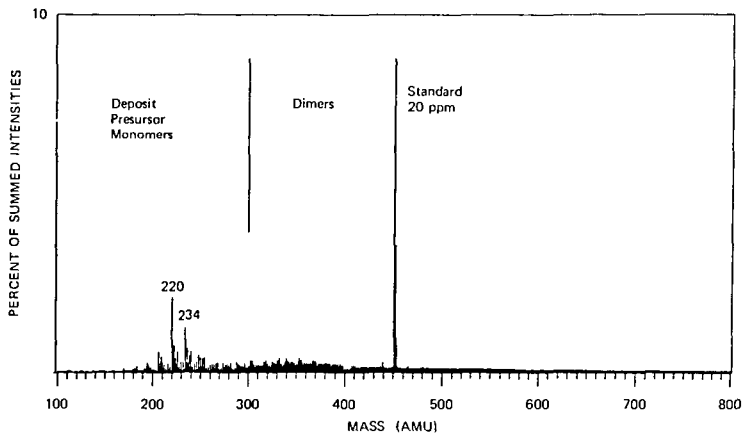
With enough oxygen, the C-C coupling reaction would be inhibited and the product would be unstable R_2O_2 . Hence gum and deposit formation may proceed best near the minimum oxygen concentration that permits oxidation. Some such measurements deserve a high priority.

ACKNOWLEDGMENT

This research was supported by Contracts NAS3-22510 with NASA-Lewis Research Center and DAAG29-80-C-0122 with the Army Research Office.

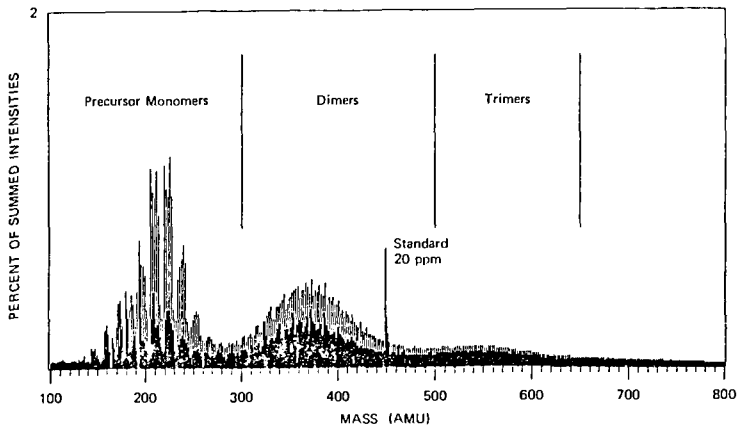
REFERENCES

1. A. C. Nixon, Chapter 17 in Autooxidation and Antioxidants, edited by W. O. Lundberg, Interscience Publishers, New York, London, 1962. An old but thorough review.
2. F. R. Mayo, H. Richardson, and G. D. Mayorga, Preprints, Division of Petroleum Chemistry, 20(1), 33 (1975). This paper is based on a final report, "The Chemistry of Fuel Deposits and their Precursors," prepared under Contract N00019-73-C-0318 for the Naval Air Systems Command (December 1973). This report briefly reviews the gas turbine fuel deposit problem.
3. R. M. Schirmer, "Morphology of Deposits in Aircraft and Engine Fuel Systems," Report No. 1, Naval Air Systems Command, Contract N00019-68-C-0252 (1968); SAE Preprint 700258 (April 1970).
4. G. E. Zaikov, E. A. Blyumberg, and N. M. Emanuel, Neftekhimiya, 5, 53 (1965); Chem. Abstr., 62, 1447 (1965), state that resins obtained by the liquid-phase oxidations of butane, methyl ethyl ketone, and ethanol are condensation products of acetaldehyde.
5. M. V. Shukkina, Ya. B. Chertkov, and T. I. Kirsanova, Neftekhimiya, 17 (2), 297 (1977); Chem. Abstr., 87, 87511 (1977).
6. R. K. Jensen, S. Korcek, L. R. Mahoney, and N. Zimbo, J. Amer. Chem. Soc., 101, 7574 (1979); 103, 1742 (1981).



JA-2115-2A

FIGURE 1 FI MASS SPECTRUM OF THE DEPOSIT PRECURSORS FORMED IN FUEL C AFTER OXIDATION FOR 255 MINUTES AT 130°C



JA-2115-4A

FIGURE 2 FI MASS SPECTRUM OF THE DEPOSIT PRECURSORS FORMED IN FUEL C AFTER OXIDATION FOR 430 MINUTES AT 130°C

SUPERCRITICAL CARBON DIOXIDE EXTRACTION OF RETAINED PYRIDINE FROM
PYRIDINE EXTRACTS

Barbara F. Smith, Clifford G. Venier, Thomas G. Squires,
Juliana C. Shei, and Jacqueline D. Hunt

Ames Laboratory*, Iowa State University, Ames, Iowa 50011

INTRODUCTION

Solvent extraction of coal is quite attractive to the organic chemist as a means of obtaining a coal model which (a) is directly related to coal, (b) is devoid of complicating mineral matter, and (c) is soluble in at least one solvent. Pyridine is one of the best common solvents for coals with a carbon content of less than 90% (1,2). It has been used extensively for bituminous coals, typically affording extraction yields of 15-30%.

Unfortunately, the use of pyridine as an extractant suffers the major disadvantage that significant amounts of pyridine are retained in coal extracts. Collins, et. al.(3) show that while only 0.24% of the extract weight is irreversibly bound pyridine, fully 11.8% by weight of pyridine cannot be removed under high vacuum (0.133 Pa) in 48 hours, and repeated benzene washing only lowers the pyridine content to 8.85% in an Illinois No. 6 coal extract.

Having qualitatively observed that at least some of the retained pyridine was removed from coal extracts by supercritical carbon dioxide (SC-CO₂), we proceeded to test the feasibility of SC-CO₂ extraction as a means of preparing pyridine free coal extracts.

EXPERIMENTAL

Supercritical CO₂ extraction: Pyridine extract (vlg) was placed in a 15x0.4 cm. stainless steel column containing 5 μ m frits on either end and 300 μ l. of water was added to the extract. The column was maintained at 40°C (the critical temperature of CO₂ is 31.3°C); the precolumn CO₂ pressure was 112 atm (11.4 MPa); a pressure drop of 12 atm (1.2 MPa) was measured across the column; and an exit flow rate of approximately one ml/sec. (atmospheric pressure) was maintained for 4 hours. A spiral glass tube connected to the exit valve collected any non-volatile material that was removed by CO₂ from the coal extract.

*Operated for the U.S. Department of Energy by Iowa State University under Contract No. W-7405-Eng-82. This research was supported by the Assistant Secretary for Fossil Energy, Office of Coal Mining.

Extraction of coal with pyridine: Extracts were obtained by ultrasonically mixing coal with five times its weight of pyridine for 30 minutes at room temperature with a Branson Sonifier 350 (20 kHz with an output power of 350 electrical watts to the converter) (4); filtering the mixture through a 0.5 μ m Teflon millipore pad; concentrating the filtrate on a rotary evaporator and freeze drying the concentrate with three times its volume of benzene overnight at a pressure of 1.33 Pa (5). Oxygen was excluded at all times.

RESULTS AND DISCUSSION

Figure 1 shows the difference spectrum generated by subtracting the infrared spectrum of the CO₂-washed extract from that of the unwashed pyridine extract of Western Kentucky #9 coal from the Ames Coal Library. The sharp spectrum standing out above the background is unambiguously that of pyridine (see Table 1), confirming that the major difference before and after the CO₂ washing is the amount of pyridine in the sample. A small amount of an oil which is primarily aliphatic in nature was also recovered in the eluent from the washing (see Table 3 for weights).

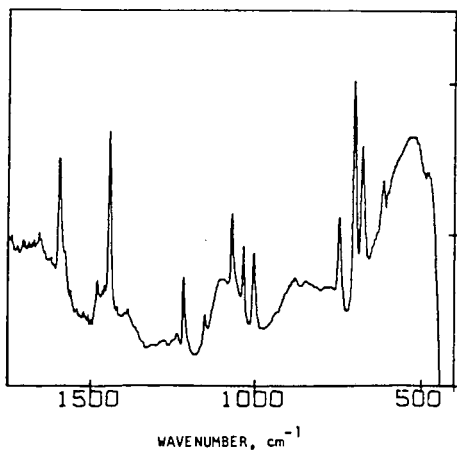


Figure 1. Difference Infrared Spectrum of the Pyridine Extract of a Western Kentucky No. 9 Coal Before and After Washing with Supercritical Carbon Dioxide.

Table 1. Infrared Absorption Maxima (cm⁻¹)

Difference Spectrum (Fig. 1)	Pyridine ^a
1593	1583, 1572
1479	1482
1442	1439
1213	1218
1148	1148
1067	1068
1034	1030
1003	992
748	749
703	700
679	---
616	605

^aA. R. Katritzky and P. J. Taylor, "Infrared Spectroscopy of Heterocycles," in Physical Methods in Heterocyclic Chemistry, vol. 4, Academic Press, New York, NY, 1971, pp. 266-434.

The chemical analyses of coals, extracts and CO₂-washed extracts are in Table 2. Note that the amount of nitrogen in the sample is an important indication of excess pyridine. Assuming that pyridine is the only nitrogen containing compound which would be lost in the carbon dioxide washing, the retained pyridine can be expressed as equation 1.

$$\% \text{pyridine} = \frac{\%N_{\text{obs}} - \%N_{\text{ext}}}{\%N_{\text{pyr}} - \%N_{\text{ext}}} \times 100 \quad 1)$$

where %N_{obs} is the nitrogen found, %N_{pyr} is the nitrogen content of pyridine (17.72%) and %N_{ext} is the nitrogen content of the pyridine free extract

However, the value of the numerator in equation 1 is very sensitive to the exact choice of %N_{ext} and this means that the % pyridine cannot be accurately calculated or used as a reliable basis for comparing samples. By expressing the difference in pyridine levels between the extract before and after CO₂ washing as Δ% pyridine, we obtain equation 2, which is relatively independent of the %N_{ext}.

$$\Delta\% \text{ pyridine} = \frac{\begin{matrix} \text{before} & \text{after} \\ \%N_{\text{obs}} & - \%N_{\text{obs}} \end{matrix}}{\%N_{\text{pyr}} - \%N_{\text{ext}}} \times 100 \quad 2)$$

Table 3 shows the values for Δ% pyridine, the weight percent of a small amount of a highly aliphatic oil which was co-extracted, and the gravimetrically measured weight losses due to the extraction with CO₂. The amount of pyridine removed by the carbon dioxide extraction (8.5 to 10.2%) is in good agreement with Collins' finding that 8.8 to 11.6% pyridine is retained by the extract but not irreversibly bound to it.

The removal of pyridine from the solid extract is analogous to the selective extraction of alkaloids from plant materials with supercritical CO₂(6). In many cases water is as essential for the extraction of nitrogenous bases (e.g. caffeine from coffee beans(7), nicotine from tobacco leaves(8)), as it is for the extraction of pyridine from coal extracts. When dry coal extracts are washed with supercritical CO₂, even for extended periods of time, infrared spectra show that pyridine has been only partially removed.

One intriguing possibility is the pyridine removed under dry conditions is that pyridine which can be removed by benzene washing and that wet carbon dioxide removes the more tightly bound non-extractable pyridine.

TABLE 2. Chemical Analyses of Samples^a

	ILLINOIS #6				WESTERN KENTUCKY #9			
	Coal ^b	Extract	CO ₂ -Washed Extracts		Coal ^b	Extract	CO ₂ -Washed Extracts	
			Exp. 1	Exp. 2			Exp. 1	Exp. 2
C	78.82	80.93	79.02	79.30	82.39	81.86	80.97	80.99
H	5.50	6.45	6.19	6.08	5.83	6.48	6.33	6.27
N	1.59	2.91	1.52	1.53	1.91	3.67	2.22	2.09
S _{org}	2.29	2.08	2.07	1.98	2.37	1.58	1.89	1.80

^aAnalyses by Galbraith Laboratory, Knoxville, TN.

^bDmmf^c; % mineral matter = 1.13 (%Ash) + 0.47 (%S_{pyr}) + 0.5(%Cl), and

%C_{org} = %C_{dry} - 0.014(%Ash) - 0.0055(%S_{pyr}), and

%H_{org} = %H_{dry} - 0.013(%Ash) + 0.02(%S_{pyr}).

^cGiven, P. H. and Yarzab, R. F., in Karr, C., Jr., ed., Analytical Methods for Coal and Coal Products, Volume II, Academic Press, New York, NY, 1978, Chapter 20.

TABLE 3. Results of Carbon Dioxide Extraction of Pyridine Extract

Source Coal	Δ% Pyridine ^a	% Oil Extracted	% Weight Loss ^b
Ill. No. 6 (1)	8.6	2.3	11.2
Ill. No. 6 (2)	8.5	2.3	12.2
W. Kent. No. 9 (1)	9.3	0.2	13.3
W. Kent. No. 9 (2)	10.2	0.6	13.9

^aCalculated according to equation 2, assuming %N_{ext} = 1.5 for Ill. No. 6 and 2.0 for W. Kent. No. 9.

^bBased on weight of sample before and after CO₂ extraction.

The effectiveness of supercritical carbon dioxide for removing pyridine may be due to one or all of the following explanations:

- (1) Supercritical carbon dioxide can penetrate the interior of the solid extract more effectively than liquid benzene;
- (2) Carbon dioxide has the ability to displace pyridine whereas benzene cannot;
- (3) The extracting agent is actually carbonic acid, not carbon dioxide, and the process is an acid-base extraction.

Our results suggest that the carbonic acid extraction of the basic pyridine is the most satisfying explanation.

REFERENCES

1. Van Krevelen, D. W., Coal, Elsevier Publishing Co., N.Y. 1961, Ch. X, p. 177-200.
2. Wender, I.; Heredy, J. A.; Neuworth, M. B.; Dryden, I.G.C., "Chemical Reactions and the Constitution of Coal" in Chemistry of Coal Utilization, Second Supplementary Volume, M. A. Elliot, ed., Wiley, New York, N. Y., 1981, Ch. 8, p. 425-521.
3. Collins, C. J.; Hagaman, E. W.; Jones, R. M.; Raaen, V. F., Fuel 1981, 60, 359.
4. For discussion of the effects of ultrasonic irradiation on the dissolution of coal, see Kessler, T.; Friedel, R. A.; Sharkey, A. G. Jr., J. Appl. Chem. 1970, 20, 245.
5. Schweighardt, F. K.; Retcofsky, H. L., private communication to F. K. Schweighardt, as quoted on page 199 of Sharkey, A. G., Jr.; McCartney, J. T., "Physical Properties of Coal and its Products," in Chemistry of Coal Utilization, Second Supplementary Volume, Elliott, M. A., ed., Wiley, New York, 1981.
6. Stahl, E.; Schilz, W.; Shutz, E.; Willing, E., Angew. Chem. Int. Ed. Engl. 1978, 17, 731.
7. Zosel, K., Angew. Chem. Int. Ed. Engl. 1978, 17, 702.
8. Hubert, P.; Vitzthum, O.G., Angew. Chem. Int. Ed. Engl. 1978, 17, 710.

REACTION-INDUCED TEMPERATURE DEVIATIONS DURING
COAL DEVOLATILIZATION IN A HEATED GRID

J. D. Freihaut, M. F. Zabielski and D. J. Seery

United Technologies Research Center
East Hartford, CT 06118

INTRODUCTION

Previous investigations in this laboratory using a heated grid apparatus have indicated:

1. Tar yields and the thermal sensitivity of tar yields obtained in primary (pressure $\leq 10^{-2}$ torr, disperse phase of particles $\leq 100 \mu\text{m}$) devolatilization conditions are distinguishing characteristics of the devolatilization behavior of coal (1).
2. The evolution of coal nitrogen reflects the evolution of coal mass as char, tar or light gas during primary devolatilization. Via coupling to the tar yield, the evolution of coal nitrogen becomes a distinguishing feature of primary devolatilization (2).
3. Increasing the thermal drive (simultaneously varying apparent heating rate and final temperature) did little to alter the total volatile yield but did alter the distribution of volatiles. The most significant changes observed with variations in apparent heating rates from 10^2 C/sec to 10^3 /sec and final temperatures of 600 C and above related to the tar fraction of the volatiles yield (1,2).

A major limitation of the experimental design of these previous experiments was the coupling between the heating rate and final temperature. In addition, no effort was made to determine if the devolatilization process itself significantly influences the temperature history of the sample. To gain further insight into the primary devolatilization process, particularly with respect to the tar yields, a new control circuit was designed to permit any heating rate from 800 C/sec to 4×10^3 C/sec to any final temperature in the 300 to 1100 C range. With this circuit, the effects of sample characteristics on local heating of the grid were examined to assess the influence of devolatilization on programmed heating rates.

In addition to gaining further insight into the tar evolution process it is desirable to address such questions as:

1. Can the primary devolatilization process significantly alter the temperature history of the devolatilizing coal mass?
2. Do coals of varying rank characteristics show the same thermal requirement characteristics when subjected to the same rapid heating conditions?

EXPERIMENTAL DESIGN

Reactor-Analysis System

Figures 1 and 2 display the reactor-analysis system. Provisions are made to monitor one to three thermocouples, a pressure transducer, and the IR active light gases evolved during a devolatilization experiment. The temperature, total pressure and light gas data generated are real time data.

Power to the grid is provided by a programmable power supply (Harrison Model 6269A) operated in one of two modes. In the voltage programmed mode, the voltage delivered to the grid in any instant is determined by a voltage and time selection system (VATS), which will be described in detail elsewhere. Up to five step function increments, both plus and minus, in the grid voltage can be made. The duration of the increments are independently selectable. The response time of the power supply is 20 msec or less.

In the current program mode the screen is forced to conduct a constant current. The voltage across the screen floats to maintain the constant current condition. In the current and time select (CATS) mode, the heating rate and final temperature of the screen are coupled as previously noted (1,2). Figures 3 and 4 display typical temperature vs time plots obtained with each control system.

For synchronization, the FTIR is the master and all other electronic circuits (VATS, CATS, high speed camera, solenoid valve, etc.) are slaves.

Attempts to monitor the real time temperature of the grid by placing small (~75-100 μm dia) thermocouple beads between the folds of the grid produced inconsistent results particularly for heating rates of $\geq 10^3$ C/sec and final temperatures ≥ 800 C. Voltages were frequently induced across the thermocouple bead/leads as were indicated by discontinuities in the temperature-time curves. In the worst case, measured potentials (thermal plus induced) exceeded the maximum allowable for chromel-alumel thermocouples.

Consequently, the temperature of the grid system was monitored by spot welding the beads to the underside of the bottom fold of the grid. Even in this case, care had to be taken to insure a single-spot weld, as it was observed that welds with two or more contact points again produced spurious voltages across the bead. One to three thermocouples attached at different points to the grid could be monitored. Although sampling rates of 2 kHz are possible with the data acquisition system, thermocouple sampling rates of 500 Hz were commonly used. Figures 3 and 4 show typical temperature versus time plots for blank screen runs with the VATS and CATS system respectively.

The pressure was monitored in the devolatilization system with a capacitance manometer. The real time sampling rate of this device is limited to 125 Hz. This was found adequate to track the overall light gas evolution in real time.

The light gas evolution was monitored in real time by a Nicolet FTIR in the rapid scan mode. The rapid scan feature of this device allow collection of data over the complete wavenumber range of the detector as fast as every 120 msec at

8 cm^{-1} resolution. The amounts of identified gaseous species are determined by high resolution (0.5 cm^{-1}) scanning of the cell immediately following the devolatilization process.

Transfer rates between the devolatilization cell and IR cell were determined by slightly pressurizing the devolatilization cell with gas standards and activating the solenoid valve (Fig. 2). The rate of gas transfer from the devolatilization chamber to the IR cell was determined to be fast compared to the rate of evolution at the heating rates used in this study.

High speed films (2 msec/frame) were made of the devolatilization process for some runs. In these cases the camera was focused either upon the glass walls of the grid chamber or upon a KBr disk suspended about 0.4 cm above part of the coal sample within the grid. The purpose of the film was to monitor the real time evolution of the tar species released by following the visible condensation and buildup of the tars on a transparent surface. Under low ambient pressure conditions ($\ll 1$ torr) the tar molecular species are propelled in a line of sight path away from the devolatilizing coal and immediately condense upon striking a cool surface.

Procedure

325 mesh stainless steel screen (~ 7.5 cm long) is folded such that a screen sandwich (~ 1.00 cm wide) is formed. A fine chromel-alumel thermocouple (75-100 μm) bead is spot-welded to the underside of the bottom fold at the center of the screen. For some runs second or third beads are welded approximately 1.5 cm off of screen center, again to the underside of the bottom fold of the grid. The screens are prefired for the following reasons: (1) to obtain a constant tare weight; (2) to obtain nearly constant resistivity and emissivity; (3) to determine the exact control settings needed to produce a given blank screen heating rate, final temperature, and time at a final temperature.

After the prefiring, the screen is loaded with 10-25 mg of -100+325 mesh coal. The coal is vacuum dried at 105 C overnight. The sample is placed in approximately 2 cm length of the strip using the center thermocouple as the marker for the sample center. In the case of the two thermocouple runs the outer thermocouple resides about 0.5 cm from the bulk of the sample area. The "loaded" screen is repositioned in the reactor. The reactor is evacuated and the devolatilization experiment is performed.

The manner of applying power to the grid as well as the temperature monitoring differ significantly from other recent studies using heated grid techniques for rapid heating (3,4,5). For example, although other studies report spot welding a thermocouple to the grid, the weld is such that the bead is apparently positioned between the folds of the grid (5). Upon power application, the thermocouple is forced to follow programmed temperature trajectory by a monitoring-feedback system. In addition, little work has been reported for vacuum conditions despite the fact that it is well established that devolatilization under ambient pressure results in numerous secondary reactions for tar species formed in the primary, thermal devolatilization of the coal (1,6,7).

RESULTS AND OBSERVATIONS

Sample-Induced Temperature Deviations

Figure 5 displays a series of center thermocouple temperature profiles obtained with samples of an Appalachian province, high volatile bituminous coal using the VATS control circuit. In comparing the profiles to corresponding blank screen reference runs (Fig. 3) the deviations in the temperature-time path of the thermocouple are obvious.

Figure 6 displays a series of center thermocouple temperature profiles obtained with samples of a Rocky Mt. province, high volatile bituminous coal using the CATS control circuit. Again the sample-induced temperature deviations become obvious when comparing the profiles to the corresponding blank screen references (Fig. 4).

The Local Nature of the Temperature Deviations

Figure 7 displays temperature profiles for center and edge thermocouples in blank and sample loaded screens, respectively. The curves indicate that the "thermal loading" of the screen by the sample is a local effect. Runs performed with no sample over the center thermocouple but with 5-10 mg of sample placed around the edge thermocouple positions gave similar results but for opposite thermocouples, i.e., the center thermocouple with no sample load reproduced the blank screen temperature-time plot while the edge thermocouple produced a plot similar to the previous, loaded center thermocouple plot. The results indicate that the sample introduces a significant thermal load in the immediate area of the screen such that the local, sample-loaded screen cannot follow the programmed screen temperature.

Physical Loading of the Local Screen

Several types of experiments were performed to ascertain the influence of the physical characteristics of the sample on the programmed temperature profile. In these tests, samples with low volatile matter contents were employed. Figure 8 displays several blank and sample loaded temperature profiles for an anthracite coal. Figure 9 shows blank, coal loaded and resultant char loaded temperature profiles for a high volatile, Appalachian province bituminous coal. The curves obtained with samples of low volatile matter content indicate that the physical properties of the sample such as heat capacity and emissivity do indeed contribute to the local thermal loading of the screen. This perturbation of the physical state of the screen is manifested by a gradual deviation from the programmed heating rate and lower final temperatures achieved. In no case did tests with low volatile matter content produce temperature profiles such as those shown in Fig. 5 and 6. The temperature-time paths observed with coals of appreciable volatile matter are different in character than these observed with nonvolatile samples. The drop in edge thermocouple temperature (Fig. 7) indicates the screen is attempting to reach thermal equilibrium by thermal conduction under pseudo-steady state conditions.

Devolatilization-Induced Temperature Deviations

While Fig. 5 shows variations with programmed final temperature for a particular coal, Fig. 10 shows center thermocouple temperature plots for coals of varying rank using the VATS system. The high volatile bituminous coals appear to have a greater loading effect than coals of lower or higher rank. As noted above, the dip in the thermocouple temperature occurs as the VATS system switches the power output of the supply from the high output (temperature ramping state) to the lower output, temperature hold state. The temperature at the time of the switching is lower and the resultant dip is greater for the high volatile bituminous coals. Similar behavior occurs for lower final temperature runs with the VATS system (see Fig. 5). In these cases however the "warp" in the temperature path is not as severe. As noted above, such thermocouple behavior is not observed for non-volatile samples.

Figure 11 shows center thermocouple plots for 900 C final temperatures runs for coals of varying rank using the CATS system. Due to constant current programming in the CATS system, the instantaneous thermal power generation is different from the VATS system during the main phase of devolatilization process. Consequently, the characters of the temperature plots are different than the corresponding VATS plots for the same final temperatures (See Figs. 10 and 11). The high volatile bituminous coals again display a greater loading effect on the screen than lower or higher rank coals. However, the warp in the temperature plots are not as severe as those observed in the VATS system.

Figure 6 displays temperature curves obtained with a Rocky Mt. province, high volatile bituminous coal for different final temperature runs using the CATS system. The variation in the character of the temperature profile with programmed heating characteristics is apparent. It is to be noted that the product distribution varied significantly with heating conditions although total yield does not, as previously reported (1,2,6,7).

It is apparent from the character of the curves presented that the devolatilization process has a significant effect on the temperature history of the local screen complex. The actual temperature-time path followed is highly dependent on the devolatilization characteristics of the coal sample as well as the programmed, resistive heating of the screen. That is the observed thermocouple temperature path is the resultant of the coupled resistive heating and devolatilization process.

Tar and Light Gas Release Relative to the Thermocouple Temperature History

Figures 6 and 12 indicate the tar and light hydrocarbon (aliphatics) release relative to the thermocouple temperature history. In Fig. 12 the tar yields obtained for various power-on times were obtained by six independent runs for the times shown. The data indicate that the temperature and species evolution profiles are reproducible and that the temperature deviations are induced by the devolatilization process.

The data for the high volatile bituminous coals shown in Figs. 6 and 12 indicate that the tar and light hydrocarbon gases do not evolve simultaneously as has been previously assumed (8). The onset of the tar release precedes the

hydrocarbon light gas evolution for high volatile bituminous coals. For example, the data of Fig. 12 show that at 1.5 sec into a run nearly 50% of the potential tar yield has evolved while only 14% of the total CH₄ yield has evolved. Since the tar yield represents ~ 39% (dry basis) of the parent coal, the devolatilization process is nearly 40% complete before significant CH₄ evolution occurs.

To verify in real time the relative release times, high speed films of the tar release process were made in the manner described above. Several Appalachian and Rocky Mt. province high volatile bituminous coals were examined. Frame-by-frame inspection of these films were compared to the rapid scan infrared data and real time pressure and temperature data. For the coals tested:

1. The tar release was more closely associated with the initial temperature deviations.
2. The onset of the tar release precedes the onset of the light hydrocarbon release.
3. The light hydrocarbon gas evolution occurs mainly in the secondary temperature rise.
4. Rocky Mt. province high volatile bituminous coals displayed more overlap in the tar and light gas evolution than the Appalachian province high volatile bituminous coals.

Discussion and Summary

The results clearly demonstrate that the devolatilization process has a considerable influence on the time-temperature history of the local screen in immediate contact with the sample. Physical properties of the sample load (e.g. heat capacity, emissivity) cannot account for the character or magnitude of the non-steady state temperature deviations that are observed with volatile samples. With respect to the coal particles, the direct implication is that the temperature path is the resultant of several components: the resistive heating of the grid, the physical properties of the samples, the devolatilization properties of the sample. Once the range of devolatilization temperatures of a particular coal is achieved, the primary devolatilization process appears to dominate the temperature-time trajectory. Because the heat requirement of the primary devolatilization affects the temperature trajectory of the coal particle, a real time model of primary coal devolatilization must necessarily include a consideration of this requirement. In addition, the data appears to indicate that the heat requirement varies with the rank characteristics of the coal.

For a transient process such as rapid coal devolatilization the absolute magnitude of the heat required to vaporize the volatile components need not be large to result in a significant deviation from a programmed heating rate or a calculated heating rate of a nonvolatile particle. A modest heat requirement coupled to a sufficiently fast primary devolatilization process can cause appreciable changes in the temperature trajectory of a particle (9,10).

The results indicate that the tar release is closely coupled in time to the devolatilization-induced temperature deviations during primary devolatilization.

The onset of the tar release significantly precedes the slower light hydrocarbon gas evolution. Thus the rapid devolatilization heat requirement appears to be associated with the energy required to overcome intermolecular attractive forces (van der Waal, hydrogen bonds, dipole-dipole interactions) that exist among the mix of molecular species present in the coal. Once the devolatilization heat requirement is met, rapidly supplying additional thermal energy can result in thermal cracking of the primary tars, decreasing the tar yield while increasing light gas yields (See Fig. 6 and Ref. 1,2).

A quantitative real time model of coal devolatilization requires a quantitative estimate of the primary devolatilization heat requirement as well as real time data on the primary tar release rates and their susceptibility to thermal cracking. Provisions are being made to monitor the real time power delivered to the grid as well as the real time evolution of primary tars.

ACKNOWLEDGMENTS

The authors gratefully acknowledge the able technical assistance of Dave Santos and Gerald Wagner.

REFERENCES

1. Freihaut, J. D. and Seery, D. J., An Investigation of Yields and Characteristics of Tars Released During the Thermal Decomposition of Coal, ACS Fuel Chem. Preprints, 26, No. 1, 133 (1981).
2. Freihaut, J. D. and Seery, D. J., Evolution of Fuel Nitrogen During the Vacuum Thermal Devolatilization of Coal, ACS Fuel Chem. Preprints, 26, No. 3, 18 (1981).
3. Franklin, H. D., Mineral Matter Effects in Coal Pyrolysis and Hydropyrolysis. Thesis, MIT (1980).
4. Stangely, P. C. and Sears, P.L., Rapid Pyrolysis and Hydropyrolysis of Canadian Coals. Fuel, 60, 131 (1980).
5. Hamilton, L. H., Ayling, A. Bruce, and Shibaska, M., A New Experimental Device for Pyrolysing Coal Under Controlled Conditions Over a Wide Range of Heating Rates. Fuel, 58, 873 (1979).
6. Anthony, D. B., Howard, J. B., Hottel, H. C. and Meisner, H. P., Rapid Devolatilization of Pulverized Coal. 15th Symp. (Int) Combustion, Combustion Institute, Pittsburgh, p. 1303 (1975).
7. Suuberg, E. M., Rapid Pyrolysis and Hydropyrolysis of Coal. Sc. D. Thesis, MIT, 1977.
8. Solomon, P. R. and Colket, M. B., Coal Devolatilization. 17th Symp. (Int.) Combustion, Combustion Institute Pittsburgh, p. 131 (1979).
9. Freihaut, J. D. and Vastola, F. J., A Computational Examination of the Effect of Coupled Heat Transport and Chemical Kinetics Upon Single Particle Coal Pyrolysis. Presented at Eastern States Combustion Institute Mtg., Miami, Fla. (1978).
10. Freihaut, J. D., A Numerical and Experimental Investigation of Rapid Coal Pyrolysis. Thesis, Penn State Univ. (1980).

EXPERIMENTAL NETWORK

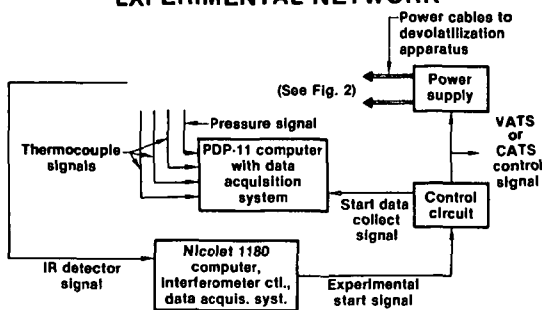


Fig. 1

HEATED-GRID DEVOLATILIZATION APPARATUS

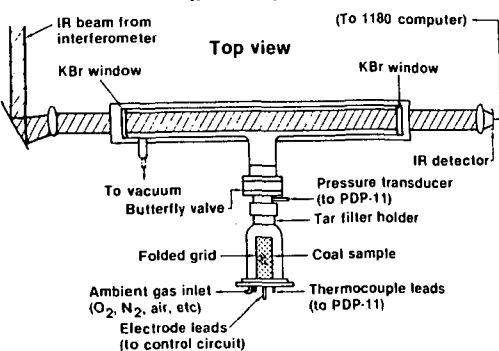


Fig. 2

BLANK SCREEN TEMPERATURE — TIME

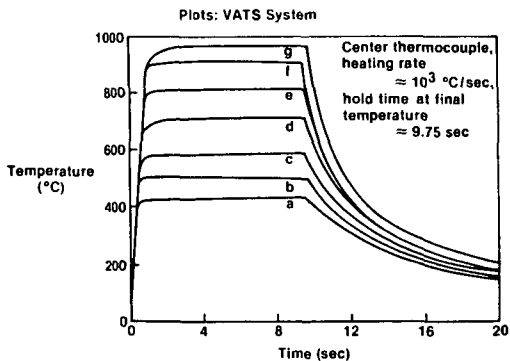


Fig. 3

TEMPERATURE — TIME PLOTS

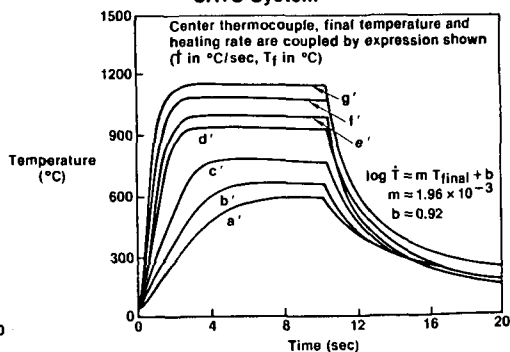


Fig. 4

CENTER THERMOCOUPLE TEMPERATURE — TIME

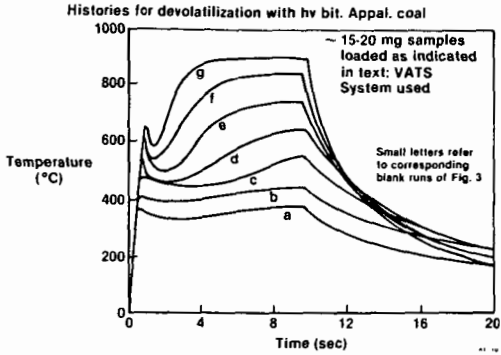


Fig. 5

CENTER THERMOCOUPLE TEMPERATURE — TIME

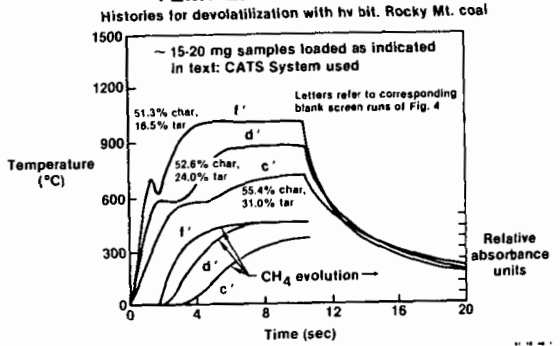


Fig. 6

CENTER AND EDGE THERMOCOUPLE TEMPERATURE HISTORIES

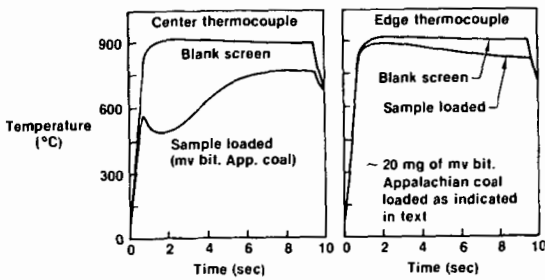


Fig. 7

BLANK AND SAMPLE-LOADED THERMOCOUPLE PLOTS: ANTHRACITE

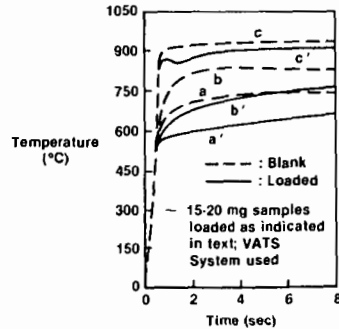


Fig. 8

COAL VS CHAR LOADING OF SCREEN

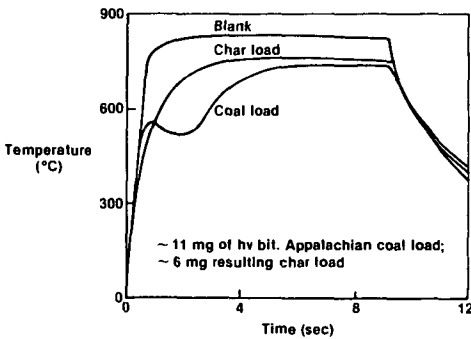


Fig. 9

VARIATION OF THERMAL LOADING WITH RANK-VATS SYSTEM

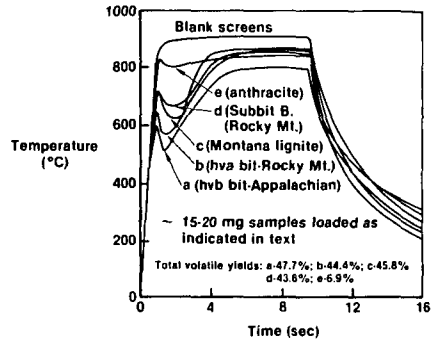


Fig. 10

VARIATION OF THERMAL LOADING WITH RANK - CATS SYSTEM

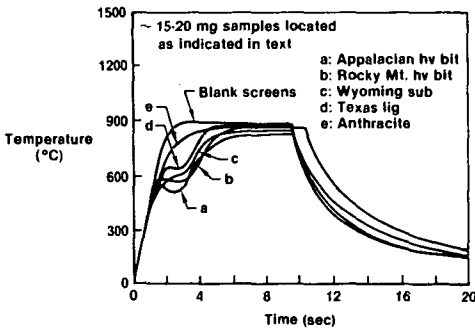


Fig. 11

TAR AND LIGHT HYDROCARBON YIELDS

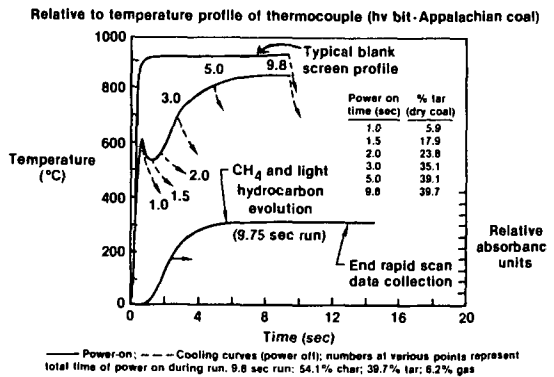


Fig. 12

TRACE ELEMENT DISTRIBUTION IN THE THREE TON PER DAY H-COAL PROCESS DEVELOPMENT UNIT

H. B. Booher, J. W. Adkins, A. W. Wells, and H. Schultz

U. S. Department of Energy
Pittsburgh Energy Technology Center
P. O. Box 10940
Pittsburgh, PA 15236

Introduction

Current research in coal conversion has identified a number of processes that potentially could produce clean burning fuel from coal. The shifting of combustion sources from oil to coal has accentuated the need for a clean burning fuel oil derived from coal. Scientists have studied possible degradation of the environment by tracking trace elements in coal burning power plants, in coal liquefaction pilot plants of various sizes, and in bench scale units (1,2,3,4,5). A study made of the Savannah River coal-fired power plant has given insight into trace element buildup in the environment surrounding the plant (1). The Synthane (coal gasification) process was studied, utilizing isotope dilution Spark Source Mass Spectrometry (SSMS) (2). Determination of trace metals in Solvent Refined Coal by means of INAA (Instrumental Neutron Activation Analysis) revealed much lower elemental concentrations in the SRC product than in the feed coal (3,4). The trace element studies of the Synthoil 1/2 ton per day coal liquefaction Process Development Unit also showed that trace element concentrations are lower in the product oil (CLP) than in the feed coal (5,6). In order to further our knowledge of the fate of the trace metals in coal hydro-liquefaction processes, a study was conducted of the H-Coal Process Development Unit (PDU) located in Trenton, N.J.

Experimental

In the H-Coal process, dried pulverized coal, clean oil tank material, and hydroclone overflow are reacted with hydrogen at pressures up to 3500 psig and temperatures up to 850°F (7). The PDU is unique in that a substantial amount of the liquid products are recycled to the slurry mix tank so equilibrium conditions can be maintained. The products of the process are the atmospheric overhead, which is a light distillate material, and the vacuum still bottoms. The vacuum still bottoms is a viscous material that becomes a semiliquid upon cooling. The severity of the reactor conditions determines the relative amounts of the individual products made (7). The reactor design uses the fluidized bed concept (8). Since the catalyst is in constant motion, spent catalyst may be extracted and fresh catalyst injected into the reactor while the PDU is in operation. Figure 1 shows the flow diagram of the HRI PDU #130 unit.

A sampling exercise was conducted at the H-Coal PDU in Trenton, N.J., the goal of which was to obtain representative, uncontaminated samples for trace element characterization. Factors considered in planning the sampling of the plant included transportation of the trace clean containers to the sampling site, transportation of the samples back to PETC, environmental conditions at the plant, and the PDU design. The flow rates and process streams sampled are listed in Table 1. The feed coal for the run sampled was Burning Star Illinois No. 6.

All liquid samples were collected in soft glass containers with teflon lid spacers where required. Coal samples were taken in polyethylene bags whose tops were sealed with rubber bands. The coal filled bags were placed in tared one-gallon paint cans that were then sealed. Cleaning the soft glass containers was accomplished by detergent washing, rinsing with distilled water, soaking in dilute hydrochloric acid, rinsing with deionized distilled water, and air drying. All liquid samples were drawn directly into the heated clean soft glass containers. Sample temperatures of up to 500oF were encountered when taking some of the liquid samples; so the containers had to be heated to prevent cracking. The head spaces of the precleaned sample containers were purged with nitrogen to prevent exposure of the bulk samples to air after the samples were taken.

Elemental analyses performed on a wide variety of coals has shown the presence of over half the elements in the periodic table (10). Sample inhomogeneity (5) and complex coal matrices (2) play an important role in the precision of analysis. Atomic absorption spectroscopy, both flame and flameless, has been employed successfully for the analyses of coal and coal by-products (11,12) and was therefore selected for this study. To obviate possible matrix effects, the method of standard additions was used, along with deuterium arc background correction. Small amounts of standard solutions of the elements of interest were added to separate aliquots of the sample for each element. The total concentration of each element after the addition was in no case more than three times the concentration in the original solution. Absorbance readings obtained for the sample and the three additions were entered into a desk top calculator programmed to calculate a correlation coefficient, an intercept, and a slope by the method of linear least squares. Concentration levels in the original sample were calculated using these values plus the sample weights, volumes, etc. This method was used with all samples. Method blanks were carried through all steps of the sample preparation with each set of samples.

Analysis of 19 coals in one study (10) and 11 coals in another (13) showed trace element concentrations varied widely between coals from the western and the eastern United States. Details of sample preparation in the determination of trace elements in coal and coal-derived materials have been previously described (9). Briefly the sample is ashed and extracted with dilute hydrochloric acid or dilute nitric acid. Remaining residues are dissolved using a fusion procedure. The dissolved ash is then combined with the acid extract. Four aliquots of the combined solution are taken, standard solution is added to three of the aliquots, and the solutions are analyzed as described above.

Experience has shown that the concentration of chromium, copper, manganese, and nickel in coal is usually greater than one part per million. The exact concentration of each of these elements in a specific coal depends largely on the geographic origin and the type of coal.

Cadmium is usually present in coal at concentration levels below one part per million (9). Lead concentrations are normally much higher. Although flame AA is quite sensitive to cadmium (0.025 $\mu\text{g/ml}$ for 1% absorption), the sensitivity for lead is only 0.5 $\mu\text{g/ml}$ for 1% absorption. Solvent extraction was used to increase the sensitivity of the Pb determination by increasing its concentration. Iodide complexes of Pb and Cd were formed in ascorbic acid media,

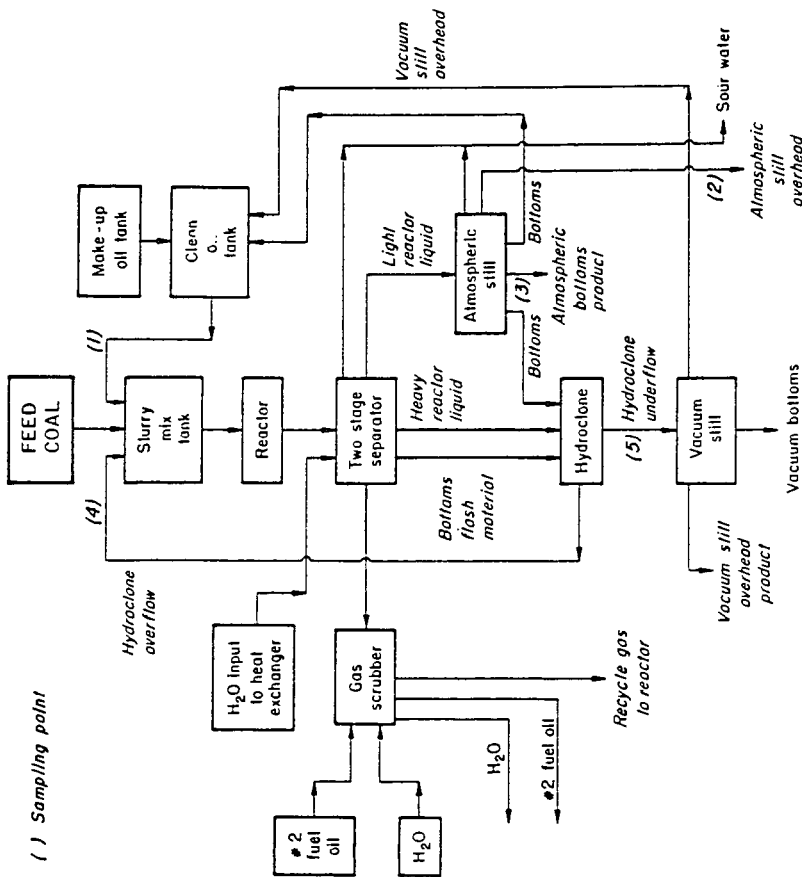


Figure 1. HRI PDU #130 FLOW DIAGRAM

followed by extraction into MIBK (Methyl Isobutyl Ketone). Acidified MIBK was used to establish the instrumental base line. Blank solutions were carried through all steps of the analytical procedure.

Discussion

The recoveries of the determined trace elements, as indicated by the material balances around the slurry mix tank and the product separation unit, demonstrate the success of the sampling procedures and analytical methods employed in this study. The trace elements entering the PDU are accounted for within the precision of the data presented. Material balances (i.e., total input versus total output) ranged from 69% to 137% and are shown in Table II. Incomplete recoveries of Cu, Cr, Mn, and Pb may be indicative of an elemental buildup in the process streams analyzed. Statistical analysis of the available data do not indicate such a buildup, although further work may need to be done in this area.

Table I. HRI PDU #130 PROCESS STREAMS AND FLOW RATES

PERIOD 14A

<u>Process Streams</u>	<u>Lb/Hr*</u>	<u>Kg/Hr</u>	<u>Nature of Samples</u>
Feed Coal	335.2	152.0	Plant grind (98% through -50 mesh)
Hydroclone Overflow	359.3	163.0	Viscous oil held at 500°F (ash = 9.3%)
Clean Oil Tank Material	321.7	145.9	Comb. of vacuum still overhead & atmospheric still bottoms
Slurry Mix	1,016	460.9	Mixture of feed coal, atmospheric still bottoms, vacuum still overhead, & hydroclone overhead (ash = 7.2%)
Hydroclone Underflow	278.3	126.2	Viscous oil held at 500°F (ash = 13.7%)
Atmospheric Still Overhead	49.9	22.6	Light oil
Atmospheric Still Bottoms (COT)	250.7	113.7	Liquid feed to the clean oil tank
Injected Feed Water	2.3	1.0	Tap water
Sour Water	33.1	15.0	Comb. of feed water and water generated in the PDU
Vacuum Still Overhead (COT)	44.8	20.3	Liquid feed to the clean oil tank
Atmospheric Still Bottoms (product)	8.5	3.9	Sample stream outlet used for continuous sampling
Vacuum Still Overhead (product)	1.0	0.5	Sample stream outlet used for continuous sampling
Vacuum Still Bottoms	234.1	106.2	Product of run 130-88 period 14A
Atmospheric Still Bottoms (hydroclone)	60.0	27.2	Liquid feed to the hydroclone
Overhead Flash Material	89.8	40.8	Very light oil
Makeup Oil	34.8	15.8	Oil used when the PDU is not at equilibrium

*Feed Rates as supplied by plant personnel.

Table II. RECOVERIES OF TRACE ELEMENTS IN THE H-COAL PDU.

#130 RUN 130-88 PERIOD 14A

	(Weight in mg)					
	<u>Cu</u>	<u>Cr</u>	<u>Mn</u>	<u>Ni</u>	<u>Pb</u>	<u>Cd</u>
Slurry Mix Tank						
Inputs	2,900	6,100	17,200	3,500	3,300	40
Outputs	2,900	6,600	21,000	3,500	3,200	46
% Recovery	102	109	120	100	98	113
Product Separation Unit						
Inputs	2,900	6,600	21,000	3,500	3,200	46
Outputs	2,900	5,900	19,700	3,500	2,900	56
% Recovery	97	89	94	101	90	122
Complete Plant						
Inputs	1,400	2,900	9,300	1,600	1,700	27
Outputs	1,000	2,300	9,800	1,400	1,200	36
% Recovery	76	81	105	85	69	137

Appendix

TRACE ELEMENT ANALYSIS OF PROCESS STREAMS

From HRI PDU #130 PERIOD 14A

<u>PROCESS STREAMS:</u>	ug/gm					
	<u>Cu</u>	<u>Cr</u>	<u>Mn</u>	<u>Ni</u>	<u>Pb</u>	<u>Cd</u>
Feed Coal	8.9	19	61	11	11	0.18
Hydroclone Overflow	8.4	20	48	12	9.6	0.08
Clean Oil Tank Material	0.6	0.2	0.9	0.1	0.1	0.002
Slurry Mix	6.2	14	45	7.7	7.0	0.10
Hydroclone Underflow	9.9	22	92	13	11	0.34
Atmospheric Still Overhead	0.036	0.022	0.015	0.017	0.003	0.04 ⁻²
Atmospheric Still Bottoms	1.1	0.2	0.8	0.1	0.068	≤0.01 ⁻⁴
Vacuum Still Overhead	0.4	0.003	0.01	≤0.01 ⁻²	0.019	≤0.01 ⁻⁴
Injected Feed Water	0.028	≤0.006	0.007	0.001	≤0.001	0.01 ⁻²
Sour Water	1.2	0.029	0.021	0.032	≤0.001	0.004

REFERENCES

1. Horton, J. H., Dorsett, R. S., Cooper, R. E. Trace Elements in the Terrestrial Environment of a Coal-Fired Powerhouse. ERDA/EPA Interagency Agreement, DP-1475, Sept. 1977.
2. Koppenaar, D. W., Lett, R. G., Brown, F. R. Determination of Nickel, Copper, Selenium, Cadmium, Thallium, and Lead in Coal Gasification Products by Isotope Dilution Spark Source Mass Spectrometry. Anal. Chem. No. 52 (1980), pp. 44-49.
3. Filby, R. H., Shah, K. R., Sautter, C. A. A Study of Trace Element Distribution in the Solvent Refined Coal (SRC) Process Using Neutron Activation Analysis. Journal of Radioanalytical Chemistry, Vol. 37 (1977), pp. 693-704.
4. Filby, R. H., Shah, K. R., Sautter, C. A. Trace Elements in the Solvent Refined Coal Process. Symposium Proceedings: Environmental Aspects of Fuel Conversion Technology III, Hollywood, Florida, Sept. 1977.
5. Lett, R. G., Adkins, J. W., DeSantis, R. R., Brown, F. R. Trace and Minor Elemental Analysis of Coal Liquefaction Products. PETC/TR-79/3, August 1979.
6. Lett, R. G., Schmidt, C. E., DeSantis, R. R., Sharkey, A. G. Jr., Screening for Hazardous Elements and Compounds in Process Streams of the 1/2 Ton Per Day Synthoil Process Development Unit. PERC/RI-77/12, October 1977.
7. Hoertz, C. D., Swan, J. C. The H-Coal Process. Coal Conversion Technology, ACS Symposium Series, 110, pp. 91-101, 1979.
8. Kang, C. C., Johanson, E. S. Deactivation of Co-MO Catalyst During H-Coal Operations. Preprints, Division Fuel Chemistry, ACS, Vol. 21, No. 5, p. 32, 1976.
9. Schultz, H., Gibbon, G. A., Hattman, E. A., Booher, H. B., and Adkins, J. W. The Distribution of Some Trace Elements in the 1/2 Ton Per Day Synthoil Process Development Unit. PERC/RI-77/2, February 1977.
10. Ruch, R. R., Gluskoter, H. J., and Shimp, N. F. Occurrence and Distribution of Potentially Volatile Trace Elements in Coal. Environmental Geology Notes. Illinois State Geological Survey, No. 72, August 1974.
11. Schultz, H., Hattman, E. A., Booher, H. B. The Fate of Some Trace Elements During Coal Pretreatment and Combustion. In Trace Elements in Fuel, Babu, S. P., ed. Advances in Chemistry Series 141, ACS, Washington, D.C., 1975.
12. Coleman, W. M., Perfetti, P., Dorn, H. D., Taylor, L. T. Trace-element Distribution in Various Solvent Refined-Coal Fractions as a Function of the Feed Coal. Fuel, Vol. 57, pp. 612-616, October 1978.
13. Cavallaro, J. A., Deurbrouck, A. W., Schultz, H., Gibbon, G. A., Hattman, E. A. A Washability and Analytical Evaluation of Potential Pollution from Trace Elements in Coal. Environmental Protection Agency, EPA-600/7-78-038, March 1978.

AN ANALYSIS OF KEROGEN DISTRIBUTION IN GREEN RIVER OIL SHALE

John F. Patzer, II

Chemicals and Minerals Division
Gulf Research & Development Company
Pittsburgh, Pennsylvania 15230

ABSTRACT

The classification of Green River oil shales through density separation techniques reveals some new insights into the naturally occurring distribution of kerogen in shale. Twelve Colorado shales and one Utah shale, covering a range of sources and grades, were classified into fractions of varying kerogen content through heavy-media density separation. Analysis of the separation data reveals that the shales all have a linear relationship between the enriched grade kerogen content and the weight fraction of total kerogen recovered in the enriched grade. The slope of the linear relationship correlates with the original shale kerogen content. The correlation provides a powerful tool for a priori prediction of the results for any classification process which operates on density separation. The existence of such a linear relationship implies that the naturally occurring differential mass distribution function for kerogen in shale is an inverse relation between weight fraction of shale and kerogen content of the fraction, i.e., kerogen-lean fractions are present in much greater quantity than kerogen-rich fractions. Another aspect of the distribution function is the existence of clearly defined, sharp cut-points which contain the entire distribution within a range of kerogen content dependent upon the original shale grade.

The Green River oil shale formation comprises one of the largest fossil fuel energy reserves in the world. Commercial development of this source is very likely to become a reality within the next five to ten years. Initial development will almost certainly use current retorting technology. However, full scale development will probably occur only after second generation technology, now in development in many research labs, reaches commercial viability. Knowledge and understanding about how kerogen is distributed within the shale formation will aid in developing more selective, viable processes for recovery of the energy contained in the kerogen.

Gulf has been interested for several years in the potential possibility of selectively discarding very lean shales prior to retorting. If the economic cost of such selective rejection were low enough, the reduction in shale volume retorted for equivalent oil production could yield potential benefits through lowered capital and operating costs for a retort and, possibly, through lessened environmental impact because less shale would be processed.

The correlation between shale density and Fischer Assay yield has been known for many years.^{1,2} Figure 1, due to Smith,¹ shows the expected Fischer Assay as a function of density. The existence of such a correlation results from the wide separation between kerogen and mineral matter density in shale, about 1070 kg/m³ and 2720 kg/m³, respectively, and the narrowness of the mineral matter density range. Smith² developed the relations

$$(GPT) = (31.563 \cdot 10^{-6}) (D_T)^2 - 0.205998 (D_T) + 326.624 \quad (1)$$

$$x_w^o = \frac{D_o}{D_m - D_o} \left(\frac{D_s}{D_T} - 1 \right), \quad (2)$$

$$x_w^m = 1 - x_w^o = \frac{D_m}{D_m - D_o} \left(1 - \frac{D_o}{D_T} \right), \quad (3)$$

$$x_V^O = \frac{1}{D_m - D_o} (D_m - D_T), \quad (4)$$

$$x_V^m = 1 - x_V^O = \frac{1}{D_m - D_o} (D_T - D_o), \quad (5)$$

to describe the interrelationships between the shale density and shale organic content. Equation (1) is the least-squares representation of the correlation shown in Figure 1. Equations (2) to (5) are derived from simple material balance considerations. A best fit to numerous data requires the mineral matter density, $D_m = 2720 \text{ kg/m}^3$, and the organic density, $D_o = 1050$ to 1070 kg/m^3 .

Heavy-Media Separation

The relation between density and organic content provides the basis for a separations scheme based upon density differences.^{3,4} Twelve Colorado shales and one Utah shale, as shown in Table 1, were separated by heavy-media techniques at the Institute of Mineral Research, Michigan Technological University. The shales represent a variety of grades, ranging from 16.5 to 44.2 GPT, and a variety of particle sizes.

The separations were performed in both batch and continuous circuit operations as schematically depicted in Figure 2. The shale sample was immersed in a bath of given density and separated into sink-and-float fractions. The sink fraction was collected. The float fraction was immersed in a bath of lower density and split into sink-and-float fractions. The procedure was performed at least twice, and as many as five times, on the various shales. An air pycnometer was used to determine the density of each separate fraction produced by the sink/float operation. The original sample density was then back-calculated from the individual fraction densities. The heavy-media separations experiments provide cumulative weight fraction distribution curves as a function of specific gravity, as depicted in Figure 3 for shales D

and I. The relatively lean shale D and relatively rich shale I have distinctly different cumulative distribution curves. As is expected from the relation between Fischer Assay and density, the richer shale contains considerably more lower density material than the leaner shale.

The heavy-media separations were analyzed on the basis of splitting the original sample into two fractions, a rich shale fraction and a lean shale fraction, as depicted in Figure 4. The weight fraction organic, (X_w^0) , for each split was determined by calculating the density of each split and using Equation (2).

A measure of the efficiency of the separation process, i.e., the ability to selectively separate rich from lean shales, is obtained by plotting $(X_w^0)_1$, versus the organic recovery in the rich fraction,

$$R = (X_w^0)_1 (w_1) / (\bar{X}_w^0), \quad (6)$$

as shown in Figure 5. An enrichment plot, such as Figure 5, is a concise statement about the ability to perform a separation and the economic benefit of doing so. When the separations operating parameter, in this case, density, is a continuous variable, it is possible to draw a continuous performance curve which describes the separations potential for the mineral. The shape and properties of the performance curve will be determined solely by the distribution of the variable under consideration. Clearly, a very steep slope in the $R > 0.90$ range is desirable for a truly efficient separation process.

The results of the heavy-media separation experiments are shown in Figure 6. Four separate panels are shown only for clarity. The experimental data points are indicated by open symbols. The lines are the result of linear least-squares regression of the data. The most remarkable feature of Figure 6 is that all of the data can be adequately represented by the linear representation

$$(X_w^0)_1 = mR + b \quad (7)$$

Table II provides the calculated values for the slopes and the correlation coefficient for the regression. The goodness of the linear fit is indicated by the range of correlation coefficients, 0.95 to 0.99.

The ability to make an a priori prediction of the slope based only upon knowledge of the feed shale organic concentration, or equivalently, density, would allow prediction of heavy-media separation results. It would also provide a method for heavy-media process control. Figure 7 shows a relation between the slope and feed shale weight fraction organic, given by

$$m = 0.671 - 10.21 (\bar{x}_w^0) + 28.423 (\bar{x}_w^0)^2 \quad (8)$$

The equation, obtained from a quadratic least-squares regression, is only a marginal fit to the data. However, it provides a reasonable estimate for engineering purposes.

With a priori knowledge of the slope, it is possible to predict density separations results. The intercept, b , is obtained from

$$b = (\bar{x}_w^0 - m) \quad \text{at } R = 1 \quad (9)$$

Figure 8 depicts a comparison between the actual and predicted separations results for shales D and I. The linear fit correlation using the coefficients predicted by (8) and (9) reproduce the experimental least-squares relations within an average error of 9% and a maximum deviation of 19%. Thus, it is possible to make reasonable a priori predictions of heavy-media results.

Kerogen Distribution in Shale

The linear relation between weight fraction organic in the enriched shale and kerogen recovery can be used to obtain some basic information about the distribution of kerogen in oil shale. Assuming that the weight fraction

organic can be represented as a continuous variable, a differential weight fraction distribution function can be defined by

$$\int_{\tilde{X}_w^0}^{\tilde{X}_w^0} f(\tilde{X}_w^0) d\tilde{X}_w^0 = 1 \quad (\text{normalization}) \quad (10)$$

$$\int_{\tilde{X}_w^0}^{\tilde{X}_w^0} \tilde{X}_w^0 f(\tilde{X}_w^0) d\tilde{X}_w^0 = \tilde{X}_w^0 \quad (\text{expected value}) \quad (11)$$

where $f(\tilde{X}_w^0) d\tilde{X}_w^0$ represents the differential shale mass between organic content \tilde{X}_w^0 and $\tilde{X}_w^0 + d\tilde{X}_w^0$. The upper limit on \tilde{X}_w^0 is readily obtainable from the linear relation (7) as $(\tilde{X}_w^0)_{\max} = b$ at $R = 0$.

The functional form of the differential shale mass distribution function can be obtained by back-calculating f_j as a function of $(\tilde{X}_w^0)_i$ from (7) by incrementing R in even steps, as

$$(\tilde{X}_w^0)_{1,i} = mR_i + b = \frac{\sum_{j=1}^i f_j (\tilde{X}_w^0)_j}{\sum_{j=1}^i f_j} \quad (12)$$

$$w_{1,i} = \frac{R_i (\tilde{X}_w^0)_i}{(\tilde{X}_w^0)_{1,i}} = \frac{i}{\sum_{j=1}^i f_j} \quad (13)$$

to obtain

$$f_j = w_{1,i} - \sum_{j=1}^{i-1} f_j \quad (14)$$

$$(\bar{X}_w^0)_i = \frac{(\bar{X}_w^0)_{1,i} w_{1,i} - \sum_{j=1}^{i-1} f_j (\bar{X}_w^0)_j}{f_i} \quad (15)$$

The average kerogen concentration of the sample, (\bar{X}_w^0) , is a known and the values of m and b are prescribed through the linear correlation. In the limit as $i \rightarrow \infty$, one obtains the continuous differential shale mass distribution function

$$f(\bar{X}_w^0) = A/(\bar{X}_w^0) \quad (16)$$

by this procedure.

The final two unknowns for the differential distribution function, A and $(\bar{X}_w^0)_{\min}$, are obtained through application of the normalization and expected value properties of the distribution function,

$$\int_{(\bar{X}_w^0)_{\min}}^{(\bar{X}_w^0)_{\max}} f(\bar{X}_w^0) d\bar{X}_w^0 = A \ln [(\bar{X}_w^0)_{\max} / (\bar{X}_w^0)_{\min}] = 1 \quad (17)$$

$$\int_{(\bar{X}_w^0)_{\min}}^{(\bar{X}_w^0)_{\max}} (\bar{X}_w^0) f(\bar{X}_w^0) d\bar{X}_w^0 = A [(\bar{X}_w^0)_{\max} - (\bar{X}_w^0)_{\min}] = \bar{X}_w^0 \quad (18)$$

Note that the normalization property implies that there also exists a practicable minimum naturally occurring grade of shale present in any given deposit. Figure 9 shows the differential weight fraction distribution function for 20 GPT and 35 GPT shales based upon the predictive correlation of

equations (8) and (9). Although Figure 9 shows very sharp cut-off points in the distribution, naturally occurring distributions are likely to have some tailing effects.

Although a straight-line relation between weight fraction kerogen content and weight fraction kerogen recovery has the unique representation in differential shale mass distribution function space given by Equation (16), the actual distribution of kerogen in shale might differ somewhat from the inverse proportional relationship. This results because the straight-line relation is an inference from least-squares regression of the data and because the least-squares regressions are not perfect, i.e., correlation coefficient equal to one. In order to validate the differential distribution function, it is important to examine the cumulative weight fraction data of the heavy-media separations experiments in differential manner. Because of the small number of data points available per sample, such differential distributions are only crude representations of the actual distribution.

Figure 10 presents the histogram of weight fraction kerogen for shale D normalized so that the area under the bars equals one. Such a histogram is an approximation to the differential distribution function. The plotted histogram is similar to the derived inverse proportional distribution function. However, some tailing which is evident at the leaner grades of shale indicates that a rival distribution function, the log normal distribution function given by

$$f(\tilde{x}_w^0) = \frac{1}{\sqrt{2\pi} \sigma} \cdot \frac{1}{(\tilde{x}_w^0)} \exp \left[-\frac{(\ln \tilde{x}_w^0 - \xi)^2}{2\sigma^2} \right] \quad (19)$$

could also approximate the distribution.

The inverse proportional distribution function is described by the parameters A, $(\tilde{x}_w^0)_{\max}$ and $(\tilde{x}_w^0)_{\min}$ which are directly determinable and related in a fundamental, physical manner to the shale. The log normal distribution has two parameters, ξ and σ which have no readily determinable

physical relation to shale. They can be determined in a reasonable manner, however, by assuming that 95% of the shale has kerogen content less than the $(\bar{X}_w^0)_{\max}$ predicted by the a priori method, Equations (7), (8) and (9). Figure 11 contrasts the predicted inverse proportional and log normal differential distribution functions for a 20.6 GPT shale. The two distributions are similar, with rapid rise to a maximum in kerogen content and tailing off toward richer shales. The log normal distribution is more diffuse, with greater tailing at both the rich and lean ends of the distribution.

Figure 12 shows the predicted enrichment plot for a 20.6 GPT shale with the inverse proportional and log normal differential distribution functions as parameters. A heavy vertical bar is drawn at $R=0.20$ to emphasize that this was the smallest value on the abscissa which was obtained in the experimental study. The salient feature of Figure 12 is that for values of $R < 0.20$, both distributions could easily give least-squares representations as straight lines; significant curvature in the log normal distribution occurs at values of $R < 0.20$. Thus, it is doubtful that the experimental data can readily distinguish between the two distributions.

The inverse proportional distribution is, however, the recommended distribution function for describing a shale resource for three reasons. First, the parameters which define the distribution have real, physical meaning which readily define what is present in a shale deposit. Second, the functional form of the inverse proportional distribution is more easily worked with in analytical equations than is the functional form of the log normal distribution. Finally as demonstrated in Figure 13, the inverse proportional distribution function provides excellent agreement with experimental observations.

ACKNOWLEDGMENT

The author is indebted to O. A. Larson of GR&DC who conceived of and directed the experimental program which provided the data necessary for this analysis and to C. W. Schultz and E. L. Michaels who performed the experiments at the Institute of Mineral Research, Michigan Technological University.

NOMENCLATURE

b	intercept in linear relation
D_o	kerogen (organic) density, kg/m^3
D_m	mineral density, kg/m^3
D_T	oil shale density, kg/m^3
GPT	oil shale Fischer Assay, gal/ton
m	slope in linear relation
R	weight fraction organic recovery
x_v^o	volume fraction kerogen (organic) in shale
x_v^m	volume fraction mineral in shale
x_w^o	weight fraction kerogen (organic) in shale
x_w^m	weight fraction mineral in shale
\bar{x}_w^o	average weight fraction kerogen (organic)
\tilde{x}_w^o	point weight fraction kerogen (organic)
w	weight fraction of shale

subscripts

1	riched fraction from heavy-media separation
2	lean fraction from heavy-media separation
i	increment index
j	increment index

REFERENCES

1. Smith, John Ward, "Specific Gravity-Oil Yield Relationship of Two Colorado Oil Shale Cores," Ind. Eng. Chem., 48 (3), 441 (1956).
2. Smith, John Ward, "Theoretical Relationship Between Density and Oil Yield for Oil Shales," USBM ROI 7248, 1976.
3. O. A. Larson, to appear in ACS Symposium Series.
4. J. F. Patzer, manuscript submitted to Fuel.

TABLE I
OIL SHALES USED FOR HEAVY MEDIA SEPARATION

<u>SHALE</u>	<u>GPT</u>	<u>SIZE, CM</u>	<u>SOURCE</u>
A	16.5	0.20-0.64	C-8 TRACT, MAHOGANY ZONE
B	19.2	0.64-5.08	ANVIL POINTS MINE, 0 TO +20 FT, MAHOGANY MARKER
C	19.3	0.64-5.08	C-8 TRACT, MAHOGANY ZONE
D	22.0	0.64-7.62	RIFLE MINE, COMPOSITE BEDS A, B, C, E, F, G, H, I, J
E	22.2	0.64-1.91	RIFLE MINE, COMPOSITE BEDS A, B, C, E, F, G, H, I, J
F	22.6	0.64-7.62	RIFLE MINE, BEDS A, B, C
G	26.7	0.64-5.08	ANVIL POINTS MINE, -20 TO -40 FT, MAHOGANY MARKER
H	29.8	0.64-7.62	RIFLE MINE, BEDS E, F
I	30.9	0.64-5.08	ANVIL POINTS MINE, 0 TO -20 FT, MAHOGANY MARKER
J	32.1	0.64-7.62	RIFLE MINE, BEDS G, H, I, J
K	36.1	0.64-5.08	HELL'S COLE CANYON, UTAH, MAHOGANY ZONE
L	38.7	0.64-15.2	HORSE DRAW CREEK, R-3 ZONE, USBM 96" SHAFT
M	44.2	0.64-15.2	HORSE DRAW CREEK, R-4 ZONE, USBM 96" SHAFT

TABLE II

LINEAR REGRESSION OF HEAVY MEDIA SEPARATION RESULTS

$$(X_w^0)_1 = mR + b$$

<u>SHALE</u>	<u>SLOPE, m</u>	<u>CORRELATION COEFFICIENT</u>
A	-0.116	-1.000
B	-0.157	-0.977
C	-0.083	-0.995
D	-0.174	-0.995
E	-0.151	-0.997
F	-0.105	-0.997
G	-0.250	-0.996
H	-0.274	-0.987
I	-0.301	-0.969
J	-0.268	-0.982
K	-0.262	-0.993
L	-0.083	-0.949
M	-0.132	-0.986

Figure 1

SHALE GRADE AS A FUNCTION OF DENSITY

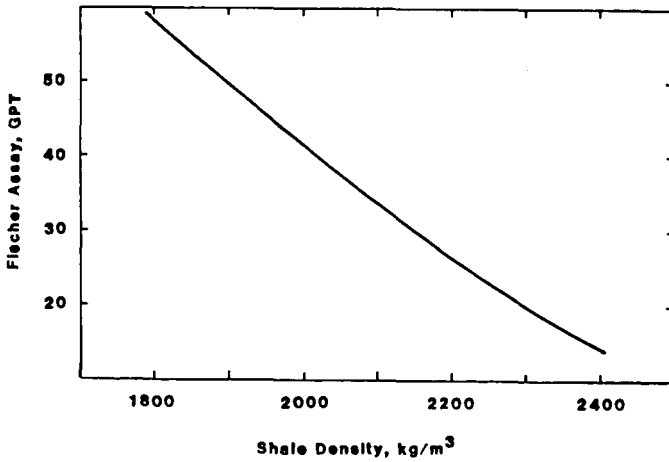


Figure 2
HEAVY MEDIA OIL SHALE SEPARATIONS

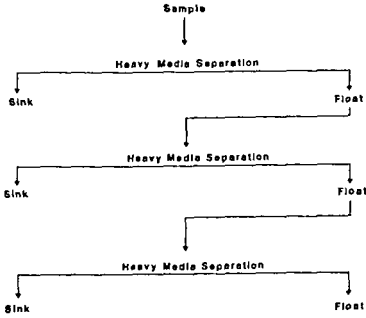


Figure 4
OIL SHALE BENEFICIATION ANALYSIS

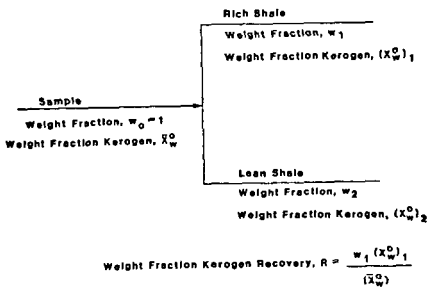


Figure 3
CUMULATIVE WEIGHT FRACTION DISTRIBUTION CURVE FOR HEAVY-MEDIA SEPARATION OF OIL SHALE AS A FUNCTION OF SPECIFIC GRAVITY

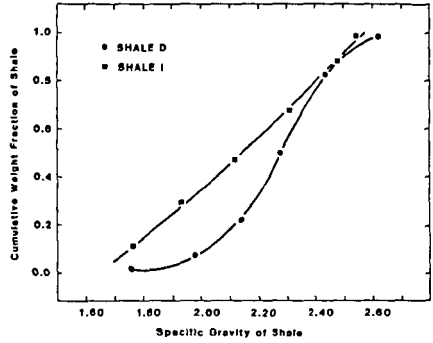


Figure 5
TYPICAL ENRICHMENT PLOT FOR OIL SHALE BENEFICIATION

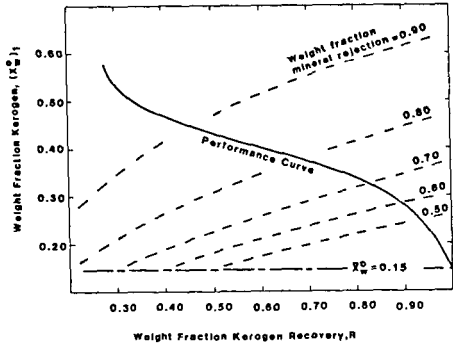


Figure 6
HEAVY MEDIA SEPARATIONS RESULTS

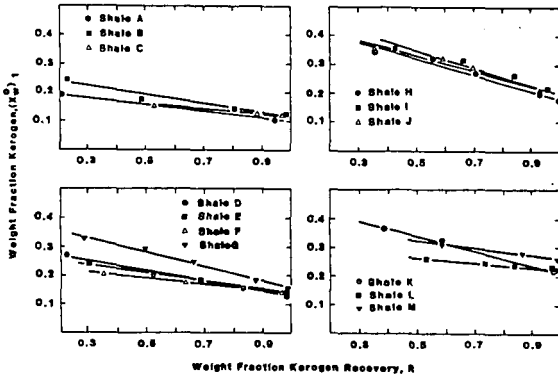


Figure 7
SLOPE OF LINEAR BENEFICIATION EQUATION
AS A FUNCTION OF FEED SHALE KERODEN CONTENT

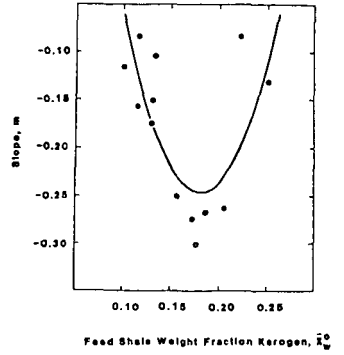


Figure 8
COMPARISON BETWEEN ACTUAL AND PREDICTED RESULTS
FOR HEAVY MEDIA SEPARATION OF SHALE

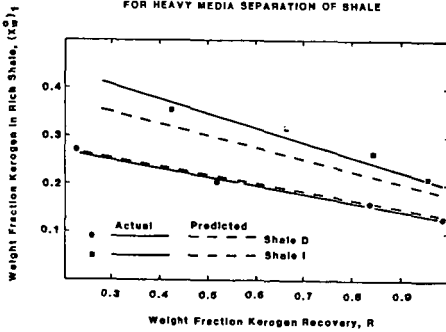


Figure 9
DIFFERENTIAL DISTRIBUTION FUNCTION

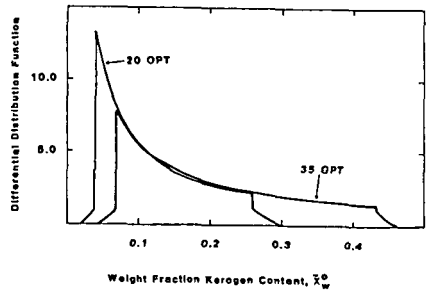


Figure 10
AREA NORMALIZED HISTOGRAM OF
WEIGHT FRACTION KEROGEN FOR SHALE D

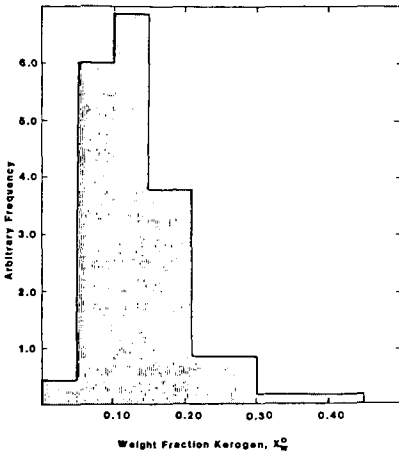


Figure 11
PREDICTED DIFFERENTIAL DISTRIBUTION
FOR 20.6 GPT ($\bar{x}_w^0 = 0.12$) SHALE

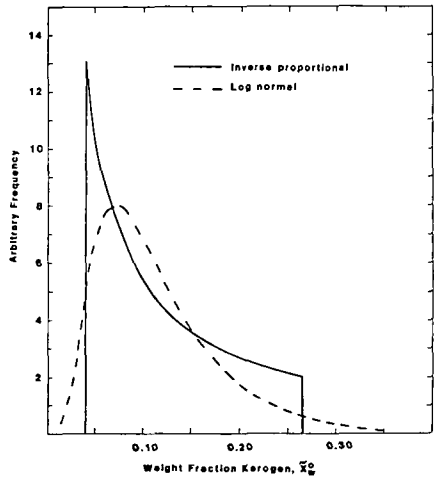


Figure 12
PREDICTED ENRICHMENT PLOT FOR 20.6 GPT ($\bar{x}_w^0 = 0.12$) SHALE

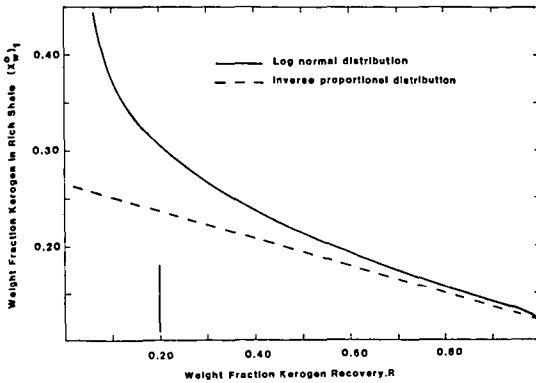


Figure 13
CUMULATIVE WEIGHT FRACTION DISTRIBUTION
CURVE FOR SHALE AS A FUNCTION OF WEIGHT
FRACTION KEROGEN

